

# Film Formation of Multiphase Latex Particles

**Elvis Lopes Brito**

Supervisor: Dr. Nicholas Ballard

Chemical Engineering Group

Applied Chemistry Department

University of the Basque Country (UPV/EHU)

Donostia-San Sebastián

(2023)





## Acknowledgements

I would like to express my sincere gratitude to my supervisor Nicholas Ballard for his patience and guidance. Working under your supervision was a great opportunity for to grow as a chemist and person.

I would like to extend my gratitude to the professors of the Polymerisation Processes Group, especially to Professors José R. Leiza, María Paulis, and Radmila Tomovska, for their support and kind remarks. I would also like to give a special thanks to Inés Plaza for her help and kindness.

I would like to gratefully thank Dr. Vincent Bodart and Dr. Frédéric Boschet who provided me with the opportunity to join their team as an intern and for their support during these three months in INOVYN Manufacturing Belgium S/A. I would like to particularly thank Dr Bertrand Willocq for his endless support in synthesis and kind remarks. Being part of your research team was an excellent experience.

I would like to acknowledge the financial support of Industrial Liaison Program in Polymerization in Dispersed Media.



Amaia, thank you so much for your help in the lab with the GPC and DSC samples. I want to extend my gratitude to Merche and Itxaso from the Rheology group, for all the support with the DMTA measurements.

Mehdi, it has been a long road but we are finally at the end. Thank you very much for all your help with the synthesis of my ASRs, you are very good friend. Nerea, it was amazing to share the lab with you, we made reactor 2.2 the best one to work on. Sayrunga, I still laugh remembering your jokes. Adrián Pérez, muchísimas gracias por tantas veces que me ayudó en el laboratorio. Además, tenemos que jugar el football otra vez, eres un crack. Hesham, I am still waiting for your simulations. Alessandra, muito obrigado pela ajuda com as correções da tese. Meu inglês esta melhorando e o seu português? Juan Felipe, Muchísimas gracias por ayudarme con el español, nos vemos en iguana. Finally, thank you to all the PhD students of the Polymerization Processes Group, it was a great pleasure.

## **Declaration**

The work contained within this thesis is my own, except where acknowledged as for following collaborations: (I) the simulations in CHAPTER 5 and CHAPTER 6 were performed by Dr. Nicholas Ballard. (II) the TEM images of the latexes and films throughout this work were performed by Dr. Ana Martínez Amesti and Ms. Maite Miranda. (III) the AFM images were performed by Dr. Loli Martín Alberdi. (IV) The FTIR measurements in Appendix 5 were performed by Dr. Bertrand Willocq.



## Contents

<b>CHAPTER 1. Introduction and objectives</b>	<b>1</b>
1.1. Motivation	1
1.2. Synthesis of multiphase latex particles	2
1.2.1. Emulsion polymerization	3
1.3. Multiphase latexes	7
1.4. Film formation of polymer latexes	10
1.4.1. Film formation of heterogeneous polymer particles	12
1.5. Objectives	19
1.6. Outline of the thesis	20
1.7. References	21

<b>CHAPTER 2. Film formation of alkali soluble resin stabilized latexes</b>	<b>29</b>
2.1. Introduction	29
2.2. Experimental	30
2.2.1 Materials	30
2.2.2 Preparation of structured ASR stabilized latexes.	30
2.2.3 Characterization	34
2.3. Results	34
2.3.1 Synthesis of ASR and ASR stabilized latexes	34
2.3.2 Drying of ASR containing latexes	37
2.3.3 Film formation of ASR containing latexes	40
2.3.4 Film formation of ASR stabilized latexes and blends	46
2.4. Conclusions	51
2.5. References	53



<b>CHAPTER 3. Film formation of latexes with hydroplasticizable domains</b>	<b>55</b>
3.1. Introduction	55
3.2. Experimental	57
3.2.1. Materials	57
3.2.2. Synthesis of MMA/BA latex	57
3.2.3. Synthesis of core/shell MMA-BA/MMA-BA-MAA particles	58
3.2.4. Synthesis of hydroplasticizable latexes	59
3.2.5. Preparation of latex blends	60
3.2.6. Characterization	61
3.3. Results and discussion	61
3.3.1. Film formation	66
3.3.2. Mechanical properties	70
3.3.3. Water sensitivity of films with hydroplasticizable domains	79
3.4. Conclusions	81
3.5. References	82

<b>CHAPTER 4. Film formation of hard-core/soft-shell latex particles</b>	<b>83</b>
4.1. Introduction	83
4.2. Experimental	84
4.2.1 Materials	84
4.2.2 Latex synthesis	84
4.2.3 Characterizations	88
4.3. Results and discussion	88
4.3.1 Synthesis of core/shell and conventional latexes.	88
4.3.2 Film formation behaviour of hard-core/soft-shell particles	92
4.3.3 Mechanical properties of hard-core/soft-shell systems	95
4.3.4 Effect of hard phase packing on the minimum film formation temperature	100
4.4. Conclusions	104
4.5. References	105

**CHAPTER 5. Film formation of high poly(vinyl chloride) content latex particles** **107**

5.1.	Introduction	107
5.2.	Experimental	108
5.2.1	Materials	108
5.2.2	Latex synthesis	109
5.2.3	Characterization	111
5.3.	Results and discussion	111
5.3.1	Limits on the PVC content in simple latex blends	111
5.3.2	Synthesis of PVC/acrylic hybrid latexes.	112
5.3.3	Film formation of PVC/acrylic hybrid latexes.	117
5.3.4	Film formation of blends of PVC/acrylic hybrid latexes.	122
5.3.5	Mechanical properties of films cast from PVC/acrylic hybrid latexes.	126
5.4.	Conclusions	130
5.5.	References	130

**CHAPTER 6. Film formation of two-stage acrylic latexes: towards soft-core/hard-shell systems** **133**

---

6.1.	Introduction	133
6.2.	Experimental	134
6.2.1	Materials	134
6.2.2	Synthesis of seed latexes	135
6.2.3	Synthesis of two-stage latex particles	136
6.2.4	Characterization	138
6.3.	Results and discussion	139
6.3.1	Latex synthesis	139
6.4.	Film formation	146
6.4.1	Effect of particle size of the seed	146
6.4.2	Effect of second stage monomer composition	151
6.4.3	Effect of first stage monomer composition	155
6.5.	Conclusions	160
6.6.	References	162

**CHAPTER 7. Conclusions** **163**

---

**List of publications and conference presentations** **173**

---

---

**Resumen y conclusiones** **175**

---

**Appendix i. Characterization methods** **181**

I.I.	Solid content and monomer conversion	181
I.II.	Particle size and particle size distribution	182
I.III.	Differential scanning calorimetry	182
I.IV.	Determination of Acid values of Alkali-soluble resins	183
I.V.	Gel content	183
I.VI.	Gel permeation chromatography	184
I.VII.	Microscopic techniques	184
I.VIII.	Critical micellar concentration (CMC)	185
I.IX.	Determining the amount of ASR adsorbed on the latexes surface	185
I.X.	Film casting	186
I.XI.	Weight loss measurements	186
I.XII.	Adaptive speckle imaging interferometry measurements	186
I.XIII.	Minimum film Formation Temperature (MFFT).	187
I.XIV.	Water uptake	187
I.XV.	Tensile Tests	188
I.XVI.	Dynamic Mechanical Thermal Analysis (DMTA)	188
I.XVII.	Simulations of packing of binary particles	188

**Appendix ii. Supporting information for Chapter 2** **191**

II.I.	Amount of ASR in the water phase	191
II.II.	Surface tension of ASRs	192
II.III.	Images of the drying process of ASR films using different bases.	193
II.IV.	Drying process of ASR with different bases	194

**APPENDIX III. Supporting information for Chapter 3** **195**

III.I.	Weight loss measurements	195
III.II.	Tensile properties of blends containing hydroplasticizable polymer with different molecular weights.	196
III.III.	Tensile properties of films made of core/shell particles and Nano Blend 1.	197

**APPENDIX IV. Supporting information for Chapter 5** **199**

IV.I.	Characteristics of the soft polymers used to prepare the blends	199
IV.II.	Phase separation in dried film containing PBA as film forming polymer.	200
IV.III.	Critical film formation thickness of the Core/shell latex blends	202

<b>APPENDIX V. Supporting information for Chapter 6</b>	<b>203</b>
V.I. Images of two-stage latex particles obtained using crosslinked and non-crosslinked cores.	203
V.II. Mechanical properties of samples S <sub>a</sub> 4-30 and L <sub>a</sub> 4-30.	204
V.III. Thermomechanical behaviour of the two-stage latex films with different seed composition.	205
V.IV. Tensile properties and morphology of two-stage latex films with different seed composition.	206
<b>List of acronyms and abbreviations</b>	<b>207</b>





# Chapter 1. Introduction and objectives

## 1.1. Motivation

The presence of volatile organic compounds (VOCs) in conventional solvent-based polymer coatings and their associated negative environmental impact has resulted in the increased use of waterborne alternatives.<sup>1</sup> However, in many cases matching the application properties of solvent-based polymers has proven challenging for waterborne systems due to the unique mechanism of film formation, which requires polymers with relatively low glass transition temperatures ( $T_g$ s). This issue can potentially be overcome by the production of latexes containing multiple phases. In this case, the presence of a high  $T_g$  “hard phase” reinforces the mechanical properties in the dry state, while the presence of a low  $T_g$  “soft phase” aids film formation.<sup>2-4</sup>

Although there has been a significant amount of work investigating the relationship between particle morphology of multiphase systems and the resulting effects on the mechanical properties of the final film, relatively little is known about the processes and parameters affecting

the film formation process itself. This is an issue of growing importance as government mandated reductions in VOC of coatings have become increasingly strict, making formulation of low temperature film forming systems even harder. The main goal of this PhD thesis is to explore the influence of the morphology of multiphase latex particles on the film formation process and the resulting mechanical properties of the final film. In this introductory chapter, an overview of the main synthetic techniques that are used throughout the work is provided, followed by a more detailed discussion of the film formation behaviour of homogeneous and multiphase latex systems.

## **1.2. Synthesis of multiphase latex particles**

Multiphase latexes are polymer dispersions or emulsions in which the particles are composed of two or more phases. These systems are conventionally produced by emulsion polymerization and find widespread industrial application in products including coatings and adhesives. Two distinct and separate polymerization stages are needed to obtain these latexes. The first stage leads to a conventional homogeneous latex, typically via semi-batch or batch emulsion polymerization. Under controlled conditions, the second stage (co)polymer can be synthesized in the presence of the first-stage latex (often referred to as seed particles). Due to the immiscibility of the polymer pairs, the polymers tend to migrate within the particle, giving rise to multiphase-structured particles<sup>5</sup>. Although multiple techniques can potentially be used to produce structured particles, emulsion polymerization is used throughout this thesis and therefore a brief explanation of the generic emulsion polymerization process is provided below.

### 1.2.1. Emulsion polymerization

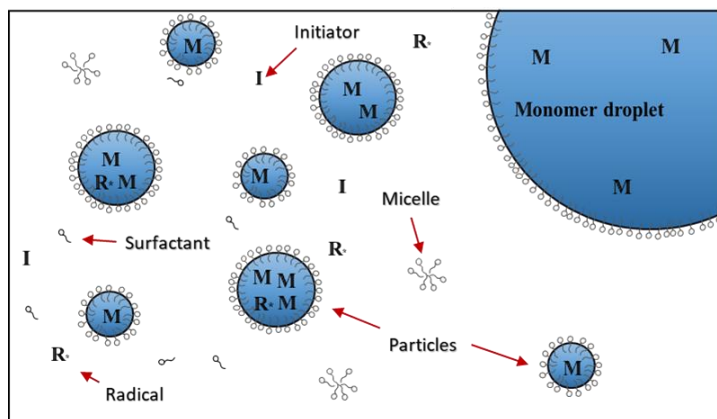
Emulsion polymerization is a heterogeneous process in which monomers are dispersed in a continuous phase, normally water, by the addition of a surfactant and polymerized by free radicals that come from the decomposition of a soluble or partially soluble initiator in the continuous phase. The emulsion polymerization produces stable colloidal polymer particles dispersed in an aqueous medium, which is conventionally called latex<sup>6</sup>. This process can be carried out either in batch or, more commonly, in semi-batch by continuous feeding of the monomer to the reactor.

#### 1.2.1.1. Batch emulsion polymerization

Batch emulsion polymerization is a conventional method to synthesize polymers in which most of the reagents (except the initiator) are added into the reactor as an initial charge. Under continuous stirring, the reactor is heated up to the reaction temperature. The polymerization is started by adding the initiator into the reactor, which can be a solution of thermal initiator (added as a shot) or a redox initiator. At this point, three phases can be simultaneously present during emulsion polymerization: the aqueous phase (containing initiator, emulsifier, micelles and dissolved monomer), monomer droplets dispersed in the aqueous phase and stabilized by the emulsifier, and latex particles (containing polymer and monomer) stabilized by an emulsifier<sup>7,8</sup>.

Batch emulsion polymerization is generally considered to occur in three distinct kinetic intervals. **Figure 1-1** shows an illustrative scheme of Interval I. This step corresponds to the beginning of emulsion polymerization, known as the particle nucleation step. It is a transient and

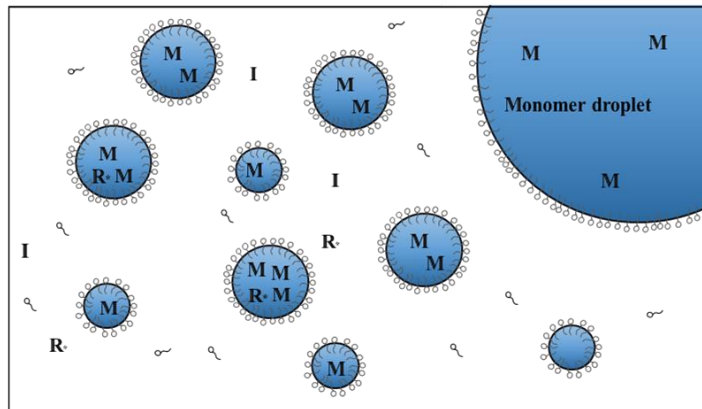
fast stage where the small particles are formed and rapidly swollen by the monomer. The conversion of monomer to polymer is usually around 2-10% and the system shows huge changes. In this interval, the nucleation of the particles occurs and the polymerization rate increases until the number of particles is defined. It may be noted that although nucleation is generally considered to be over at the end of Interval I, for monomers that are relatively soluble in water and under certain conditions, the formation of secondary particles is observed throughout the polymerization.



**Figure 1-1** - Representative scheme of the particle nucleation interval I in emulsion polymerization.

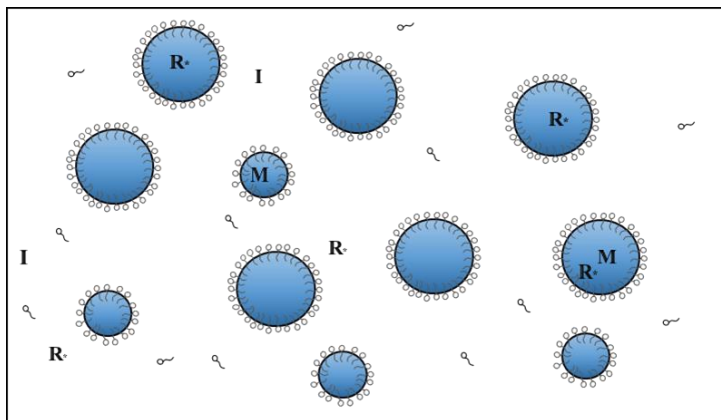
Interval II is generally known as the growth step, where the conversion varies from 10 to 40%. **Figure 1-2** shows a representative scheme of interval II. During this stage, the particle size increases while the monomer droplets are constantly depleted as monomer is transported through the aqueous phase to the polymer particle where monomer is consumed by

polymerization. The transition between interval II and III happens when the monomer droplets disappear. This transition is affected by the solubility of the monomer, where the higher the solubility of monomer in the aqueous phase, the faster the transition occurs.



**Figure 1-2** - Representative scheme of the particle growing during interval II of emulsion polymerization.

In Interval III, all the monomer has migrated to the polymer phase and the system consists of polymer particles swollen by monomer (see **Figure 1-3**). In this interval, the polymerization rate progressively decreases as a result of the reduction of concentration of monomer remaining inside the particles. At high conversion, the mobility of the radicals can be highly affected by the increase in the viscosity inside the particles. This phenomenon is known as the gel effect and might result in a considerable increase in the polymerization rate at the end of the polymerization.



**Figure 1-3** - Representative scheme of the particle nucleation interval II in an emulsion polymerization.

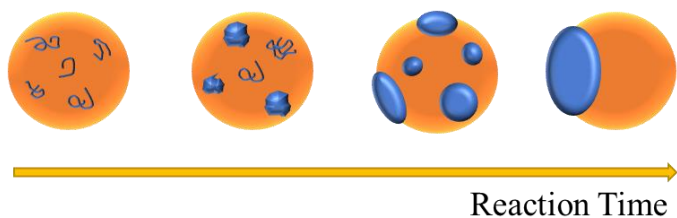
### 1.2.1.2. Semi-batch emulsion polymerization

In contrast to batch emulsion polymerization, in semi-batch (or semi-continuous) emulsion polymerization monomer is added continuously to the reactor, often with other ingredients such as initiator, surfactant and chain transfer agents. The main advantage of semi-batch reactions is that the rate of monomer addition can be used to control the rate of polymerization<sup>8,9</sup>, which is necessary in large industrial reactors where removal of the heat released by polymerization is a major issue. Generally speaking, the instantaneous conversion in a semi-batch reaction is high such that the system is similar to that represented by Interval III of a batch emulsion polymerization system (**Figure 1-3**).

### 1.3. Multiphase latexes

Waterborne polymer particles are widely applied in many areas such as coatings, adhesives, paper, impact-modified plastic, water treatment and many biomedical applications. The use of homogeneous polymer particles can provide the material with good performance for many of these applications. However, for more demanding applications the use of multiphase polymer particles is often necessary. The main characteristic that makes multiphase latexes attractive is the capacity to combine the properties of two or more polymer phases in single material. However, in multiphase systems obtaining synergetic effects from multiple polymer phases requires control over the particle morphology<sup>5,10,11</sup>.

Structured latexes can be synthesized by a sequential emulsion polymerization process in which different monomer feeds are used. For example, **Figure 1-4** shows an illustration of particle morphology development over time in a representative seeded emulsion polymerization, in which phase 1 is the seed and phase 2 is the second stage polymer being synthesized. The system initially consists of particles of polymer 1 swollen by monomers of phase 2. When the reaction begins chains of polymer 2 are generated with a matrix of polymer 1. The incompatibility between the polymers leads to phase separation and the formation of clusters of phase 2 inside the particles. These clusters continue to grow, eventually merging into bigger clusters. The growth of clusters can occur for different reasons, such as the polymerization of monomers inside the clusters, the diffusion of the polymer chains into the clusters and the coagulation with other clusters. The reaction proceeds and the clusters migrate toward a final particle morphology that gives the lowest interfacial tension to the system, known as the equilibrium morphology<sup>12-15</sup>.

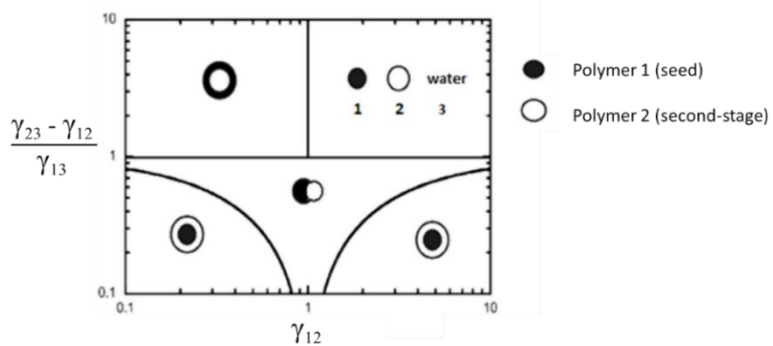


**Figure 1-4** – Representative scheme of polymer particle development for polymer-polymer systems.

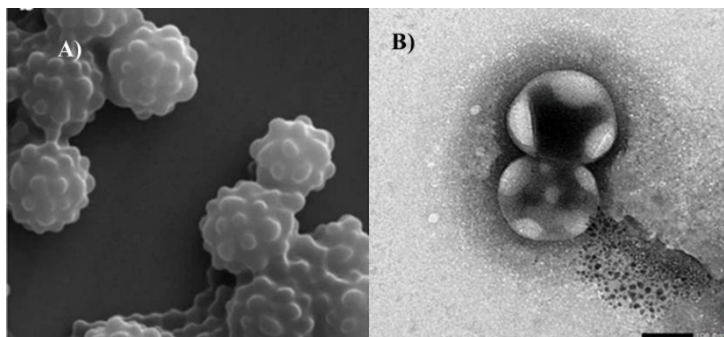
The equilibrium morphology that is formed is determined by the interfacial areas, and the interfacial tension ( $\gamma_{12}$ ) between the two polymer phases as well as that between the polymers and the aqueous phase ( $\gamma_{13}, \gamma_{23}$ )<sup>13,16</sup>. **Figure 1-5** shows a diagram with examples of the different equilibrium particle morphologies of two phase polymer latexes. Considering polymer 1 as a non-cross-linked system, an inverted core/shell morphology can be achieved when polymer 2 has higher hydrophobicity than polymer 1<sup>17</sup>. If the hydrophilicity of both polymer phases does not differ significantly, the system may lead to a final hemispherical morphology.

As mentioned above, a variety of particle morphologies can occur during the polymerization process. When the phase migration is not hindered, the final equilibrium morphology can be achieved given enough reaction time. Otherwise, the internal viscosity of the polymer matrix can compromise phase migration, resulting in non-equilibrium particle morphologies. In this case more complex structures, such as the raspberry and occluded morphologies shown in **Figure 1-6**, can be formed.





**Figure 1-5** – Diagram of thermodynamic equilibrium morphologies for polymer-polymer hybrids.<sup>15</sup> Reproduced with permission of the American Chemical Society.

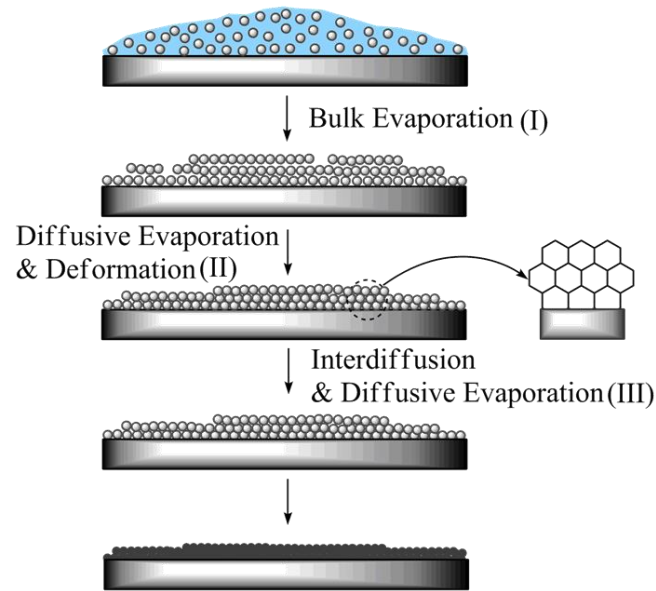


**Figure 1-6** – Illustrative examples of a raspberry like structure<sup>18</sup> (A) and occluded<sup>19</sup> (B). Reproduced with permission from American Chemical Society (A) and John Wiley and Sons (B).

## 1.4. Film formation of polymer latexes

Emulsion polymers are widely used in coatings formulations and are increasingly being developed as an alternative to solvent-based coating systems which have well-known issues related to their high VOC content.<sup>20,21</sup> In order to use latexes in coatings applications, it is necessary to transform the initial aqueous polymer dispersion into a dry polymer film<sup>22</sup>. The process of film formation of latex particles is considered to occur in three stages<sup>23</sup> as can be seen in **Figure 1-7**. In the first stage, bulk water evaporation occurs at a constant rate. The second stage begins when the particle concentration increases to the point where the particles become closely packed. In this stage, water evaporation continues from the interstitial voids at a reduced rate and latex particle deformation occurs. The third stage begins once the film is macroscopically dry. In this stage polymer diffuses across the residual particle boundaries as the film is aged<sup>20,23–25</sup>.

Based on the idea that deformation during the second stage of film formation is driven by surface tension effects, there is an upper limit of the modulus of the polymer of around  $1 \times 10^7$  Pa, above which the resistance to deformation prevents film formation. As a result, films can only be cast at temperatures above the  $T_g$  of the polymer, leading to significant limitations in the mechanical properties of films cast from aqueous dispersions. In effect, the viscoelastic properties of the polymer that are required for use in physically demanding coatings applications (e.g. high modulus, long terminal relaxation times)<sup>26,27</sup> are precisely the properties that prevent the formation of a homogeneous film at reasonable temperatures.<sup>22,28–30</sup>



**Figure 1-7** - Illustration of film formation stages for latexes dispersions.

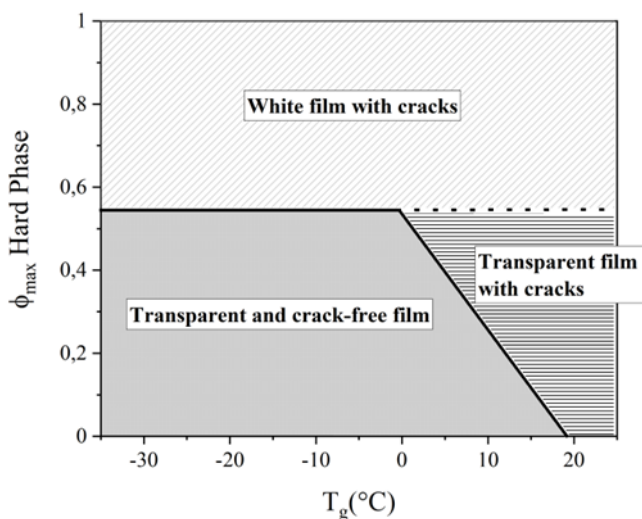
One way to improve the mechanical properties of films cast from waterborne latexes is through the use of multiphase systems that contain a “hard” phase to boost mechanical performance and a “soft” phase to promote film formation.<sup>2,3,31</sup> In the context of emulsion polymers, the “hard” phase is typically a polymer that has a  $T_g$  higher than the standard application temperature (i.e.  $> 25\text{ }^\circ\text{C}$ ), while the “soft” phase has a  $T_g$  lower than the temperature at which the film is cast (i.e.  $< 25\text{ }^\circ\text{C}$ ). Unfortunately, while the presence of a hard phase may be expected to improve mechanical properties, it would also be expected to result in worse film formation behaviour. Unlike the influence of composite structure on mechanical properties, which is a fundamental problem in engineering and has been widely studied, the influence of particle morphology on film formation behaviour requires further investigation and is the major focus of

this thesis. In the following section, the previous work that has been performed that looks at film formation of multiphase latexes, and in particular the influence of particle morphology, will be discussed.

### **1.4.1. Film formation of heterogeneous polymer particles**

#### **1.4.1.1. Latex Blends**

In terms of film formation of multiphase systems, one of the most studied cases is that of hard/soft latex blends. In latex blends, the relative particle size and volume fraction dictate the film formation behaviour as well as the structure and properties of the final film.<sup>2,32-36</sup> For example, Lepizzera et al<sup>37</sup> synthesized a series of “soft” latexes with different  $T_g$ s and blended them with a high  $T_g$  latex at different volume fractions. Based on the properties of the film they determined the maximum volume fraction of the hard phase ( $\phi_{max}$ ) that could be used to obtain a homogeneous film at ambient temperature. They observed two different situations as shown in **Figure 1-8**. When the  $T_g$  of the soft phase was below 0 °C,  $\phi_{max}$  was constant ( $\phi_{max} = 0.55$ ). When the  $T_g$  of the soft phase was above 0 °C  $\phi_{max}$  decreased gradually from 0.55 to 0 for 0 °C <  $T_g(\text{soft})$  < 17°C.



**Figure 1-8** - Film formation behaviour of latex blends as a function of the fraction of hard phase in the blend and the soft phase  $T_g$ . The hard phase polymer was a poly(methyl methacrylate) homopolymer with  $T_g = 105$   $^{\circ}\text{C}$ . Adapted based Ref. <sup>37</sup> with permission from John Wiley and Sons.

As an alternative to latex blends, biphasic latex particles, in which both polymer phases are present in the same particle, can be used to ensure a more homogenous distribution throughout the film structure.<sup>38</sup> In such systems, the film formation behaviour strongly depends on the particle structure and dramatic differences can be observed depending on the initial particle morphology.

### 1.4.1.2. Hard-core/soft-shell particles

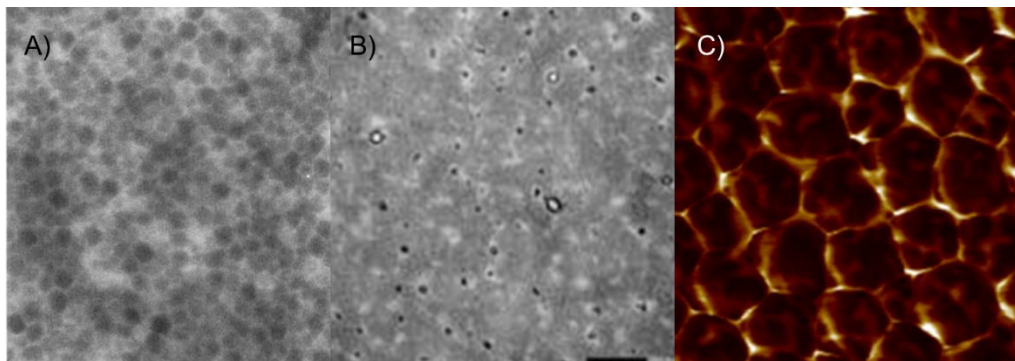
Similar to the blends between hard and soft latexes, in hard-core/soft-shell systems the hard phase content can be relatively high before the MFFT begins to be affected.<sup>3,39-41</sup> For example, Devon et al explored the effect of soft-shell thickness on the MFFT of hard-core/soft-shell latexes, showing that even at 50 wt% hard phase, MFFTs below room temperatures were observed. They concluded that when thinner soft-shells on hard-cores are used, higher drying temperatures are required than with thicker shells with similar composition because more deformation is required to form a void-free film.<sup>40</sup> While this work provides important insights about the limits in which a coherent film can be formed, the contribution of polymer phases to the mechanical properties of the film also depends on events happening during the interdiffusion stage.

Juhué and Lang<sup>42</sup> used a fluorescent nonradiative energy transfer technique to monitor the extent of mixing between the two phases of a core/shell latex compared to a single-phase latex of poly(butyl methacrylate). The glass transition of the core (butyl methacrylate) was higher than the shell (butyl methacrylate – butyl acrylate). They found that the rate of chain migration across the interface was larger for the core-shell system than the homopolymer particles, which is due to the high rates of diffusion of the low  $T_g$  polymer in the shell. They also showed that the rate of interdiffusion in the core-shell latex could be faster than for a plasticized single-phase latex, thus opening up opportunities in systems where plasticizing solvents need to be removed.

### 1.4.1.3. Soft-core/hard-shell particles

In contrast to the hard-core/soft-shell structures discussed in the previous section, soft-core/hard-shell latexes do not have a low  $T_g$ , deformable layer located at the surface of the particles. The presence a high  $T_g$  shell can have tremendous contribution to the mechanical properties of the film, however, it also affects the film formation behaviour. For example, Dos Santos et al<sup>43</sup> have reported the synthesis of core/shell particles of poly(*n*-butyl acrylate) (core) and poly(methyl methacrylate) (shell). When the fraction of shell polymer was low (*ca.* 20wt%) film formation of these films was possible at ambient temperature, leading to ductile films with a relative high yield stress of 2 MPa. They attributed the unique mechanical behaviour to the formation of a continuous network of the hard phase.

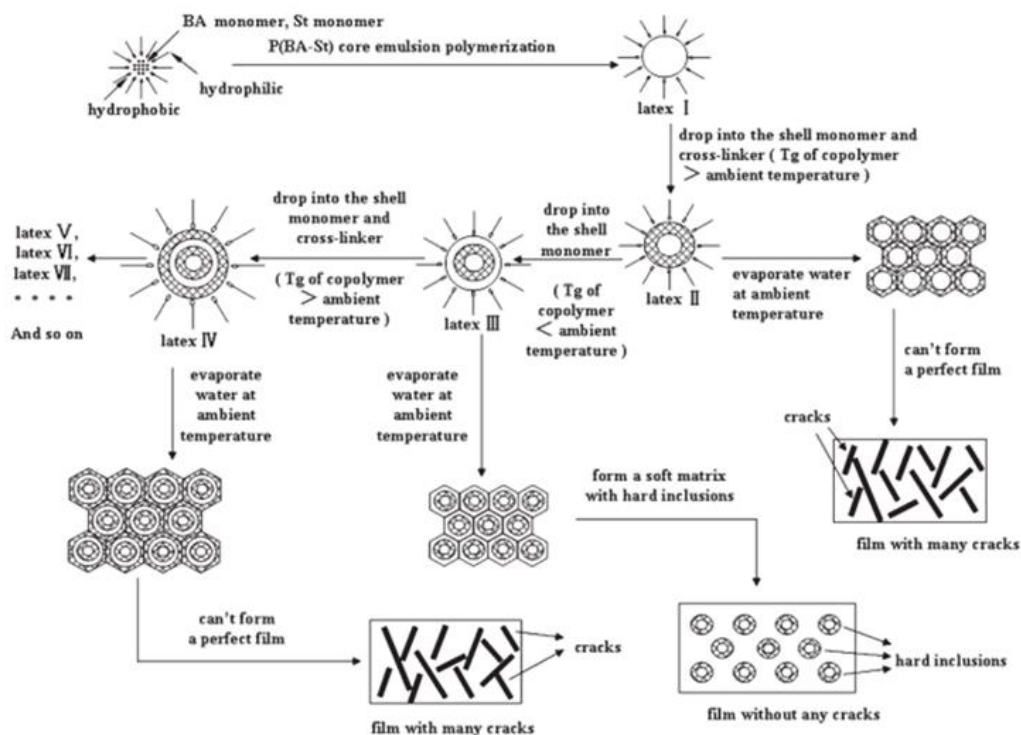
Although the mechanical properties of soft-core/hard-shell latexes are very promising, the way in which they can form a cohesive film is not well understood. Dos Santos et al<sup>43</sup> reported that the morphology was a true core-shell structure as evidenced by the honeycomb structure of the final film as observed by TEM (see **Figure 1-9 (A)**). Later work by Asua and coworkers<sup>19,44</sup> has demonstrated that a remarkably similar system leads to a kinetically frozen morphology in which the second-stage polymer does not form a true shell but is present in patches at the surface (see **Figure 1-9 (B) and (C)**). In this case, film formation can be understood to occur by deformation and interdiffusion of the soft phase. In both cases the amount of hard phase that can be incorporated before the MFFT becomes higher than ambient temperature was significantly lower than in comparative hard-core/soft-shell systems.



**Figure 1-9** – Structural features of film obtained using soft core/hard shell latex particles. (A) TEM image of film cast from soft core/hard shell particles<sup>45</sup>. (B) TEM image of film cast from soft latex particles with patches of hard phase on the surface<sup>19</sup>. (C) AFM image of film cast from soft latex particles with patches of hard phase on the surface<sup>44</sup>. Reproduced with permission of American chemical society and John Wiley and Sons.

In addition to simple binary systems, more complex multishell latexes have also been reported. For example, Mu et al. investigated the film formation behaviour of multilayer core-shell particles as illustrated in **Figure 1-10**.<sup>46</sup> The layer-by-layer growth on the latex core (soft) was demonstrated by the alternating changes in the film-formation behavior at room temperature, which corresponded to the  $T_g$  of the outermost polymer layer. They found that the deformation of the latex particles is largely dependent on the nature of the polymer in the outermost layer of the latex particles, although some effects of the molecular redistribution and the interlayer structures were observed.





**Figure 1-10** – Schematic illustration of the preparation of multilayer core-shell particles.

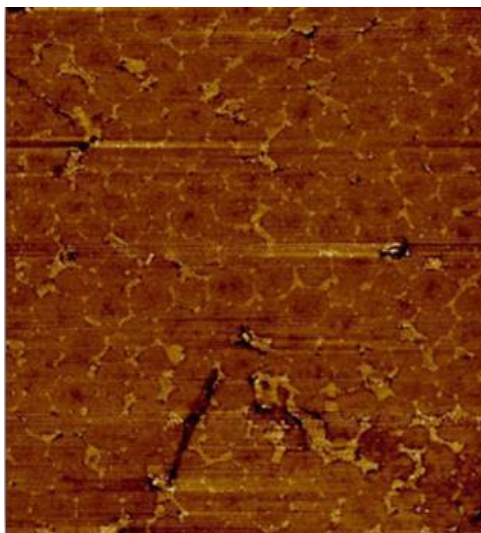
Reproduced with permission of American Chemical Society.<sup>46</sup>

#### 1.4.1.4. Alkali soluble resin stabilized latexes.

In addition to simple hard/soft systems, there are a number of multiphase latex systems, such as alkali soluble resin (ASR) stabilized latexes, that are used commercially which have less well defined structures. Although ARSs are often employed for their rheological characteristics in the wet state,<sup>47,48</sup> they can also be used to reinforce the mechanical properties of the dried film. For example, Wu et al. reported that the addition of 20% of a neutralized, high  $T_g$  ASR ( $T_g$

= 110 °C) to a low  $T_g$  acrylic latex ( $T_g = -5$  °C) led to an increase of 5 times the tensile strength.<sup>58</sup> ASRs are conventionally produced either by solution polymerization,<sup>49–51</sup> bulk high-temperature polymerization<sup>52</sup> or emulsion polymerization.<sup>53–56</sup> They can then be used either by blending with a preformed latex<sup>57,58</sup> or by using the ASRs as a surfactant in emulsion polymerization.<sup>56,59–62</sup>

While commonly used in film-forming systems, little is known about how the ASR influences the film formation process itself. The ASR and the main emulsion polymer are immiscible and therefore the resulting film has a nanostructure consisting of distinct ASR and emulsion polymer domains.<sup>63,64</sup> Park *et al.* used Atomic Force Microscopy (AFM) to study the morphology of ASR-based latex films.<sup>57</sup> They used a surfactant-free poly (butyl methacrylate) latex and added known amounts of resin with different  $T_g$ s before casting the films. They noticed that using a high  $T_g$  resin the process of film formation is hindered and high annealing temperatures were required to ensure film formation. Similarly, the coalescence and interdiffusion of waterborne polymers stabilized by commercial high  $T_g$  ASRs were evaluated by Gonzalez *et al.*, through environmental scanning microscopy (ESEM) and fluorescence resonance energy transfer (FRET).<sup>65</sup> They observed that the coalescence temperature was higher in the presence of high  $T_g$  ASRs and the films of ASR stabilized latexes were stiffer than the ones stabilized with conventional ionic surfactants. **Figure 1-11** shows a cross-section AFM image of a film cast from an ASR stabilized latex. It can be seen that the latex particles are dispersed in a continuous hard phase of ASR. The authors attributed this structure to the presence of a barrier that hindered the interdiffusion of the latex polymer, which was confirmed by FRET measurements. For ASR containing systems, a high drying temperature was needed and led to the formation of brittle films.



**Figure 1-11** - AFM phase image of the cross-sectioned film formed from the latex stabilized by ASR. Film annealed at 60°C for 2 days<sup>65</sup>. Image reproduced with permission from Springer.

### 1.5. Objectives

While many publications have addressed the synthesis of structured particles and the films produced by those systems, comparatively little has been done to investigate how the initial latex structure translates into the morphology of the dried film and how particle morphology influences the film formation process itself. As the control of film properties depends on understanding the processes involved in film formation, further research must be conducted in this area in order to be able to overcome the current limitations that are preventing more widespread use of waterborne polymers in demanding coatings applications. Therefore, in this work, a series of multiphase latexes with specific particle morphologies are synthesized in order

to study the effect of morphology on film formation behaviour. The information acquired throughout the investigation is used to target VOC-free hybrid films with low MFFT and good mechanical properties, which is the central objective of the work.

## 1.6. Outline of the thesis

In **Chapter 2** and **Chapter 3**, the film formation of latexes containing hydroplasticizable species are explored. In **Chapter 2** alkali-soluble resins (ASRs) are used in two configurations, either as a stabilizer for latexes or in the preparation of ASR/latex blends. A series of ASRs are synthesized with a wide range of  $T_g$ s and the film formation behaviour of these systems is explored using a combination of MFFT measurements, adaptive speckle imaging interferometry and weight loss measurements to gain an understanding of the underlying physical processes that occur during film formation of these multiphase systems. In **Chapter 3**, the film formation behaviour of the hydroplasticizable systems is extended to study latexes containing hydroplasticizable domains. A series of latex systems that contain hydrophilic comonomers are synthesized and the effect of the initial colloidal morphology on the film formation properties and the film structure of each is explored.

In **Chapter 4** and **Chapter 5**, the film formation of hard core/soft shell latex particles is investigated. In **Chapter 4**, the synthesis and film formation behaviour of a series of poly(styrene) core/acrylic shell latexes with varying compositions is described. This series of latexes is used to study the influence of the hard-core content and the packing fraction of hard phase on the MFFT. In **Chapter 5**, the influence of packing fraction of hard phase and the MFFT is further investigated using a series of PVC/acrylic latexes with a core-shell structure.

In **Chapter 6**, the film formation behaviour of an inverted system, in which the core is a low  $T_g$  “soft” polymer and the second-stage polymer is a high  $T_g$  acrylic copolymer, is studied. This work focuses on investigating the different film formation behaviour of soft-core/hard-shell latex structures that contain a discontinuous polymer layer forming the shell.

Finally, in **Chapter 7**, the most relevant conclusions of this thesis are summarized and the various morphologies used throughout the thesis are contrasted. In order to avoid repetition characterization, a detailed description of the characterization methods part is given in Appendix I.

## 1.7. References

- (1) Jiang, S.; Van Dyk, A.; Maurice, A.; Bohling, J.; Fasano, D.; Brownell, S. Design Colloidal Particle Morphology and Self-Assembly for Coating Applications. *Chem. Soc. Rev.* **2017**, *46* (12), 3792–3807. <https://doi.org/10.1039/C6CS00807K>.
- (2) Eckersley, S. T.; Helmer, B. J. Mechanistic Considerations of Particle Size Effects on Film Properties of Hard/Soft Latex Blends. *J. Coatings Technol.* **1997**, *69* (864), 97–107. <https://doi.org/10.1007/BF02696096>.
- (3) Limousin, E.; Ballard, N.; Asua, J. M. The Influence of Particle Morphology on the Structure and Mechanical Properties of Films Cast from Hybrid Latexes. *Prog. Org. Coatings* **2019**, *129*, 69–76. <https://doi.org/10.1016/j.porgcoat.2019.01.015>.
- (4) Mehravar, S.; Ballard, N.; Tomovska, R.; Asua, J. M. Polyurethane/Acrylic Hybrid Waterborne Dispersions: Synthesis, Properties and Applications. *Ind. Eng. Chem. Res.* **2019**, *58* (46), 20902–20922. <https://doi.org/10.1021/acs.iecr.9b02324>.
- (5) Sundberg, D. C.; Durant, Y. G. Latex Particle Morphology, Fundamental Aspects: A Review. *Polym. React. Eng.* **2003**, *11* (3), 379–432. <https://doi.org/10.1081/PRE-120024420>.

- (6) Urban, D., Takamura, K. *Polymer Dispersions and Their Industrial Applications*; Eds.; Wiley, 2002. <https://doi.org/10.1002/3527600582>.
- (7) Warson, H. Emulsion Polymerization, a Mechanistic Approach. *Polym. Int.* **2003**, *41* (3), 352–352. <https://doi.org/10.1002/pi.1996.210410321>.
- (8) Lovell, P. A.; Schork, F. J. Fundamentals of Emulsion Polymerization. *Biomacromolecules* **2020**, *21* (11), 4396–4441. <https://doi.org/10.1021/acs.biomac.0c00769>.
- (9) Chern, C. S. Emulsion Polymerization Mechanisms and Kinetics. *Progress in Polymer Science (Oxford)*. 2006. <https://doi.org/10.1016/j.progpolymsci.2006.02.001>.
- (10) Guyot, A.; Landfester, K.; Joseph Schork, F.; Wang, C. Hybrid Polymer Latexes. *Prog. Polym. Sci.* **2007**, *32* (12), 1439–1461. <https://doi.org/10.1016/j.progpolymsci.2007.07.003>.
- (11) Hamzehlou, S.; Leiza, J. R.; Asua, J. M. A New Approach for Mathematical Modeling of the Dynamic Development of Particle Morphology. *Chem. Eng. J.* **2016**, *304*, 655–666. <https://doi.org/https://doi.org/10.1016/j.cej.2016.06.127>.
- (12) Asua, J. M. *Polymer Reaction Engineering*; 2008. <https://doi.org/10.1002/9780470692134>.
- (13) Gonzalez-Ortiz, L. J.; Asua, J. M. Development of Particle Morphology in Emulsion Polymerization. 1. Cluster Dynamics. *Macromolecules* **1995**, *28* (9), 3135–3145. <https://doi.org/10.1021/ma00113a016>.
- (14) González-Ortiz, L. J.; Asua, J. M. Development of Particle Morphology in Emulsion Polymerization. 2. Cluster Dynamics in Reacting Systems. *Macromolecules* **1996**, *29* (1), 383–389. <https://doi.org/10.1021/ma950512b>.
- (15) González-Ortiz, L. J.; Asua, J. M. Development of Particle Morphology in Emulsion Polymerization. 3. Cluster Nucleation and Dynamics in Polymerizing Systems. *Macromolecules* **1996**, *29* (13), 4520–4527. <https://doi.org/10.1021/ma960022z>.
- (16) Torza, S.; Mason, S. . Three-Phase Interactions in Shear and Electrical Fields. *J. Colloid Interface Sci.* **1970**, *33* (1), 67–83. [https://doi.org/10.1016/0021-9797\(70\)90073-1](https://doi.org/10.1016/0021-9797(70)90073-1).
- (17) Kirsch, S.; Doerk, A.; Bartsch, E.; Sillescu, H.; Landfester, K.; Spiess, H. W.; Maechtler, W. Synthesis and Characterization of Highly Cross-Linked, Monodisperse Core–Shell and Inverted Core–Shell Colloidal Particles. Polystyrene/Poly( Tert -Butyl Acrylate)

- Core-Shell and Inverse Core-Shell Particles. *Macromolecules* **1999**, *32* (14), 4508–4518. <https://doi.org/10.1021/ma980916e>.
- (18) Ostovar, M.; Eslami, H. Synthesis of Nanostructured Confetti-like and Mace-like Particles via Dispersion Polymerization of Alkyl Methacrylates on Polystyrene Seeds. *Colloid Polym. Sci.* **2016**, *294* (10), 1633–1642. <https://doi.org/10.1007/s00396-016-3923-6>.
- (19) Limousin, E.; Ballard, N.; Asua, J. M. Soft Core-Hard Shell Latex Particles for Mechanically Strong VOC-Free Polymer Films. *J. Appl. Polym. Sci.* **2019**, *136* (23), 47608. <https://doi.org/10.1002/app.47608>.
- (20) Jiang, S.; Van Dyk, A.; Maurice, A.; Bohling, J.; Fasano, D.; Brownell, S. Design Colloidal Particle Morphology and Self-Assembly for Coating Applications. *Chem. Soc. Rev.* **2017**, *46* (12), 3792–3807. <https://doi.org/10.1039/C6CS00807K>.
- (21) Swartz, N. A.; Clare, T. L. Understanding the Differences in Film Formation Mechanisms of Two Comparable Solvent Based and Water-Borne Coatings on Bronze Substrates by Electrochemical Impedance Spectroscopy. *Electrochim. Acta* **2012**, *62*, 199–206. <https://doi.org/10.1016/j.electacta.2011.12.015>.
- (22) Routh, A. F.; Russel, W. B. A Process Model for Latex Film Formation: Limiting Regimes for Individual Driving Forces. *Langmuir* **1999**, *15* (22), 7762–7773. <https://doi.org/10.1021/la9903090>.
- (23) KEDDIE, J. Film Formation of Latex. *Mater. Sci. Eng. R Reports* **1997**, *21* (3), 101–170. [https://doi.org/10.1016/S0927-796X\(97\)00011-9](https://doi.org/10.1016/S0927-796X(97)00011-9).
- (24) Casier, R.; Gauthier, M.; Duhamel, J. Using Pyrene Excimer Fluorescence To Probe Polymer Diffusion in Latex Films. *Macromolecules* **2017**, *50* (4), 1635–1644. <https://doi.org/10.1021/acs.macromol.6b02726>.
- (25) Wu, J.; Tomba, J. P.; Winnik, M. A.; Farwaha, R.; Rademacher, J. Temperature Dependence of Polymer Diffusion in Poly(Vinyl Acetate- c o -Dibutyl Maleate) Latex Films. *Macromolecules* **2004**, *37* (6), 2299–2306. <https://doi.org/10.1021/ma030569v>.
- (26) Zosel, A. Mechanical Properties of Films from Polymer Latices. *Polymers for Advanced Technologies*. 1995. <https://doi.org/10.1002/pat.1995.220060502>.
- (27) Schuler, B.; Baumstark, R.; Kirsch, S.; Pfau, A.; Sandor, M.; Zosel, A. Structure and Properties of Multiphase Particles and Their Impact on the Performance of Architectural Coatings. *Prog. Org. Coatings* **2000**. [https://doi.org/10.1016/S0300-9440\(00\)00136-3](https://doi.org/10.1016/S0300-9440(00)00136-3).
- (28) Keddie, J. L.; Routh, A. F. *Fundamentals of Latex Film Formation: Processes and*

*Properties*; Springer, 2010.

- (29) Eckersley, S. T.; Rudin, A. *Film Formation in Waterborne Coatings*; Provdor, T., Winnik, M. A., Urban, M. W., Eds.; ACS Symposium Series; American Chemical Society: Washington, DC, 1996; Vol. 648. <https://doi.org/10.1021/bk-1996-0648>.
- (30) Overbeek, A. Polymer Heterogeneity in Waterborne Coatings. *J. Coatings Technol. Res.* **2010**. <https://doi.org/10.1007/s11998-009-9201-5>.
- (31) Overbeek, A. Polymer Heterogeneity in Waterborne Coatings. *J. Coatings Technol. Res.* **2010**, 7 (1), 1–21. <https://doi.org/10.1007/s11998-009-9201-5>.
- (32) Geurts, J.; Bouman, J.; Overbeek, A. New Waterborne Acrylic Binders for Zero VOC Paints. *J. Coatings Technol. Res.* **2008**, 5 (1), 57–63. <https://doi.org/10.1007/s11998-007-9036-x>.
- (33) Colombini, D.; Hassander, H.; Karlsson, O. J.; Maurer, F. H. J. Influence of the Particle Size and Particle Size Ratio on the Morphology and Viscoelastic Properties of Bimodal Hard/Soft Latex Blends. *Macromolecules* **2004**, 37 (18), 6865–6873. <https://doi.org/10.1021/ma030455j>.
- (34) Tzitzinou, A.; Keddie, J. L.; Geurts, J. M.; Peters, A. C. I. A.; Satguru, R. Film Formation of Latex Blends with Bimodal Particle Size Distributions: Consideration of Particle Deformability and Continuity of the Dispersed Phase. *Macromolecules* **2000**, 33 (7), 2695–2708. <https://doi.org/10.1021/ma991372z>.
- (35) Overbeek, A.; Bückmann, F.; Martin, E.; Steenwinkel, P.; Annable, T. New Generation Decorative Paint Technology. In *Progress in Organic Coatings*; Elsevier, 2003; Vol. 48, pp 125–139. [https://doi.org/10.1016/S0300-9440\(03\)00101-2](https://doi.org/10.1016/S0300-9440(03)00101-2).
- (36) Limousin, E.; Ballard, N.; Asua, J. M. Synthesis of Cellulose Nanocrystal Armored Latex Particles for Mechanically Strong Nanocomposite Films. *Polym. Chem.* **2019**, 10, 1823–1831. <https://doi.org/10.1039/c8py01785a>.
- (37) Lepizzera, S.; Lhommeau, C.; Dilger, G.; Pith, T.; Lambla, M. Film-Forming Ability and Mechanical Properties of Coalesced Latex Blends. *J. Polym. Sci. Part B Polym. Phys.* **1997**, 35 (13), 2093–2101. [https://doi.org/10.1002/\(SICI\)1099-0488\(19970930\)35:13<2093::AID-POLB10>3.0.CO;2-](https://doi.org/10.1002/(SICI)1099-0488(19970930)35:13<2093::AID-POLB10>3.0.CO;2-).
- (38) Chevalier, Y.; Hidalgo, M.; Cavaillé, J. Y.; Cabane, B. Small Angle Neutron Scattering Studies of Composite Latex Film Structure. *Prog. Org. Coatings* **1997**, 32 (1–4), 35–41. [https://doi.org/10.1016/S0300-9440\(97\)00072-6](https://doi.org/10.1016/S0300-9440(97)00072-6).



- (39) Hasanzadeh, I.; Mahdavian, A. R.; Salehi-Mobarakeh, H. Particle Size and Shell Composition as Effective Parameters on MFFT for Acrylic Core-Shell Particles Prepared via Seeded Emulsion Polymerization. *Prog. Org. Coatings* **2014**, *77* (11), 1874–1882. <https://doi.org/10.1016/j.porgcoat.2014.06.018>.
- (40) Devon, M. J.; Gardon, J. L.; Roberts, G.; Rudin, A. Effects of Core-shell Latex Morphology on Film Forming Behavior. *J. Appl. Polym. Sci.* **1990**, *39* (10), 2119–2128. <https://doi.org/10.1002/app.1990.070391007>.
- (41) Heuts, M. P. J.; le Fèvre, R. A.; van Hilst, J. L. M.; Overbeek, G. C. Influence of Morphology on Film Formation of Acrylic Dispersions. **1996**, 271–285. <https://doi.org/10.1021/BK-1996-0648.CH018>.
- (42) Juhue, D.; Lang, J. Film Formation from Dispersion of Core-Shell Latex Particles. *Macromolecules* **2002**, *28* (4), 1306–1308. <https://doi.org/10.1021/MA00108A070>.
- (43) Domingues Dos Santos, F.; Fabre, P.; Drujon, X.; Meunier, G.; Leibler, L. Films from Soft-Core/Hard-Shell Hydrophobic Latexes: Structure and Thermomechanical Properties. *J. Polym. Sci. Part B Polym. Phys.* **2000**, *38* (23), 2989–3000. [https://doi.org/10.1002/1099-0488\(20001201\)38:23<2989::AID-POLB10>3.0.CO;2-D](https://doi.org/10.1002/1099-0488(20001201)38:23<2989::AID-POLB10>3.0.CO;2-D).
- (44) Abdeldaim, H.; Reck, B.; Roschmann, K. J.; Asua, J. M. Cracking in Films Cast from Soft Core/Hard Shell Waterborne Polymer Dispersions. *Macromolecules* **2023**, *56* (9), 3304–3315. <https://doi.org/10.1021/acs.macromol.3c00321>.
- (45) Domingues Dos Santos, F.; Fabre, P.; Drujon, X.; Meunier, G.; Leibler, L. Films from Soft-Core/Hard-Shell Hydrophobic Latexes: Structure and Thermomechanical Properties. *J. Polym. Sci. Part B Polym. Phys.* **2000**, *38* (23), 2989–3000. [https://doi.org/10.1002/1099-0488\(20001201\)38:23<2989::AID-POLB10>3.0.CO;2-D](https://doi.org/10.1002/1099-0488(20001201)38:23<2989::AID-POLB10>3.0.CO;2-D).
- (46) Mu, Y.; Qiu, T.; Li, X.; Guan, Y.; Zhang, S.; Li, X. Layer-by-Layer Synthesis of Multilayer Core-Shell Latex and the Film Formation Properties. *Langmuir* **2011**, *27* (8), 4968–4978. <https://doi.org/10.1021/la104862h>.
- (47) Siddiq, M.; Tam, K. C.; Jenkins, R. D. Dissolution Behaviour of Model Alkali-Soluble Emulsion Polymers: Effects of Molecular Weights and Ionic Strength. *Colloid Polym. Sci.* **1999**, *277* (12), 1172–1178. <https://doi.org/10.1007/s003960050506>.
- (48) Wu, W.; Shay, G. D. Tailoring HASE Rheology through Polymer Design: Effects of Hydrophobe Size, Acid Content, and Molecular Weight. *J. Coatings Technol. Res.* **2005**, *2* (6), 423–433. <https://doi.org/10.1007/BF02733885>.
- (49) Wu, W.; Severtson, S.; Miller, C. Alkali-Soluble Resins (ASR) and Acrylic Blends:

- Influence of ASR Distribution on Latex Film and Paint Properties. *J. Coatings Technol. Res.* **2016**, *13* (4), 655–665. <https://doi.org/10.1007/s11998-016-9792-6>.
- (50) Alkali-Soluble Resins and Method of Preparing the Same. 1968. <https://lens.org/039-381-001-353-56X>.
- (51) Chang, S.; Zhang, Z.; Wang, X.; Tang, C. Alkali-Soluble Resin and Method for Preparing the Same, 2016. <https://patents.google.com/patent/US20160002381>.
- (52) Kim, H. S.; Park, H. K.; Lee, K. Y.; Kwak, S. K.; Heo, Y. H.; Lee, C. S.; Cho, C. H.; Kim, S. H.; Won Jin Chung. Alkali Soluble Resin Polymer and Negative-Type Photosensitive Resin Composition Including the Same, 2012. <https://lens.org/191-676-494-990-506>.
- (53) Andrist, K. M.; Campbell, J. D.; Chylla, R.; Debling, J. A.; Deyoung, D. J.; Kaai, M.; Kimura, T.; Wilson, D. M. Process for Producing Polymers by Free Radical Polymerization and Condensation Reaction, and Apparatus and Products Related Thereto, 2000. <https://lens.org/096-068-869-505-51X>.
- (54) Kiehlbauch, R. A.; Volk, V. S.; Morgan, L. W.; Esser, R. J.; Jensen, D. P. Process for Producing a Stabilized Latex Emulsion Adhesive, 1992. <https://lens.org/148-336-965-944-216>.
- (55) Paula, M. D. E.; Mart, H.; Rob, A. Process For Preparing Aqueous Vinyl Polymer Dispersions. <https://lens.org/087-264-417-505-975>.
- (56) Morgan, L. W.; Esser, R. J.; Jensen, D. P. Stable Emulsion Polymers and Methods of Preparing Same, 1990. <https://lens.org/090-824-298-904-80X>.
- (57) Bandiera, M.; Balk, R.; Barandiaran, M. J. One-Pot Synthesis of Waterborne Polymeric Dispersions Stabilized with Alkali-Soluble Resins. *Polymers (Basel)*. **2018**. <https://doi.org/10.3390/polym10010088>.
- (58) Park, Y.-J.; Lee, D.-Y.; Khew, M.-C.; Ho, C.-C.; Kim, J.-H. Effects of Alkali-Soluble Resin on Latex Film Morphology of Poly( n -Butyl Methacrylate) Studied by Atomic Force Microscopy. *Langmuir* **1998**, *14* (19), 5419–5424. <https://doi.org/10.1021/la971105r>.
- (59) Caballero, S.; de la Cal, J. C.; Asua, J. M. Radical Entry Mechanisms in Alkali-Soluble-Resin-Stabilized Latexes. *Macromolecules* **2009**, *42* (6), 1913–1919. <https://doi.org/10.1021/ma802642w>.
- (60) Hwu, H.-D.; Lee, Y.-D. Studies of Alkali Soluble Resin as a Surfactant in Emulsion Polymerization. *Polymer (Guildf)*. **2000**, *41* (15), 5695–5705.

[https://doi.org/10.1016/S0032-3861\(99\)00762-4](https://doi.org/10.1016/S0032-3861(99)00762-4).

- (61) Lee, D.; Kim, J. Preparation of Small-sized Carboxylated Latexes by Emulsion Polymerization Using Alkali-soluble Random Copolymer. *J. Appl. Polym. Sci.* **1998**, *69* (3), 543–550. [https://doi.org/10.1002/\(SICI\)1097-4628\(19980718\)69:3<543::AID-APP14>3.3.CO;2-D](https://doi.org/10.1002/(SICI)1097-4628(19980718)69:3<543::AID-APP14>3.3.CO;2-D).
- (62) Kato, S.; Sato, K.; Maeda, D.; Nomura, M. A Kinetic Investigation of Styrene Emulsion Polymerization with Surface Active Polyelectrolytes as the Emulsifier. II: Effects of Molecular Weight and Composition. *Colloids Surfaces A Physicochem. Eng. Asp.* **1999**, *153* (1–3), 127–131. [https://doi.org/10.1016/S0927-7757\(98\)00433-6](https://doi.org/10.1016/S0927-7757(98)00433-6).
- (63) Choi, H.-Y.; Lee, D.-Y.; Lee, J.-Y.; Kim, J.-H. Miscibility Behavior of Poly(*n*-Butyl Methacrylate) Latex Films Containing Alkali-Soluble Resin. *J. Appl. Polym. Sci.* **2000**, *78* (3), 639–649. [https://doi.org/10.1002/1097-4628\(20001017\)78:3<639::AID-APP200>3.0.CO;2-D](https://doi.org/10.1002/1097-4628(20001017)78:3<639::AID-APP200>3.0.CO;2-D).
- (64) Lee, D.-Y.; Choi, H.-Y.; Park, Y.-J.; Khew, M.-C.; Ho, C.-C.; Kim, J.-H. Kinetics of Film Formation of Poly(*n*-Butyl Methacrylate) Latex in the Presence of Poly(Styrene/ $\alpha$ -Methylstyrene/Acrylic Acid) by Atomic Force Microscopy. *Langmuir* **1999**, *15* (23), 8252–8258. <https://doi.org/10.1021/la990306n>.
- (65) Gonzalez, E.; Tollan, C.; Chuvilin, A.; Paulis, M.; Barandiaran, M. J. Effect of Alkali-Soluble Resin Emulsifiers on Coalescence and Interdiffusion between Latex Polymer Particles. *Colloid Polym. Sci.* **2015**, *293* (8), 2419–2427. <https://doi.org/10.1007/s00396-015-3635-3>.



## **Chapter 2. Film formation of alkali soluble resin stabilized latexes**

### **2.1. Introduction**

The first approach to understand the film formation of structured latex particles was focused on investigating the influence of systems containing alkali-soluble resins as stabilizer for conventional acrylic particles. As discussed in Chapter 1, alkali-soluble resins are a form of polymeric surfactant that contain both hydrophobic moieties and carboxylic acid groups.<sup>1</sup> Above the pKa of the carboxylic acid, the acid groups are neutralized, allowing for the dissolution of the polymer and leading to surface-activity. Although there has been a significant amount of work investigating the synthesis of ASR stabilized latexes and ASR/latex blends, relatively little is known about the conditions under which low MFFT films containing high  $T_g$  ASRs can be obtained with these systems. In this chapter, the synthesis of a series of ASR stabilized latexes and ASR/latex blends with a wide range of  $T_g$ s is reported. The film formation behavior of these systems is explored using a combination of MFFT measurements, adaptive speckle imaging interferometry and weight loss measurements to gain an understanding of the underlying physical processes that occur during film formation of these multiphase systems.

## **2.2. Experimental**

### **2.2.1. Materials**

Methyl methacrylate (MMA, technical grade, Quimidroga), ethyl acrylate (EA, >99%, Sigma Aldrich), styrene (S, technical grade, Quimidroga), butyl acrylate (BA, technical grade, Quimidroga) and methacrylic acid (MAA, >99% Sigma Aldrich) were used without any further purification. Sodium persulfate (NaPS, >98%, Sigma Aldrich,) and sodium dodecyl sulfate (SDS, >98%, Sigma Aldrich), 2-ethylhexyl thioglycolate (EHTG,>95%, Sigma Aldrich), ammonium hydroxide (25% solution in water, Merck) and potassium hydroxide (NaOH, >85%, Scharlau) were used as supplied. Deionized water was used throughout the work.

### **2.2.2. Preparation of structured ASR stabilized latexes.**

In the present work, two different methods were used to synthesize latexes stabilized by ASRs. The first group of samples, the in-situ systems, were performed using an ASR generated in situ as a stabilizer in a semi-batch emulsion polymerization as previously reported by Bandiera et al.<sup>2</sup> Briefly, the reactor was loaded with the initial charge and the temperature was raised to 80 °C under nitrogen flux. After the temperature was equilibrated, the initiator solution was added. The resultant solution was agitated for 5 minutes at 250 rpm, then the feeding of the first-stage pre-emulsion was started and completed in 40 min. The system was held at the reaction temperature for an additional 10 min. Thereafter ammonium hydroxide was added as a shot, followed by 10 min of agitation whereby the ASR was completely dissolved and a homogeneous, transparent aqueous mixture was obtained. Then, the second-stage pre-emulsion was fed over

90 min. The reaction mixture was then kept at 80 °C for an additional 60 min before cooling to room temperature. The ratio ASR:monomer was set to 30:70 and the final solids content of the dispersions was 40 wt%. The composition of ASR stabilized latexes prepared via the in-situ method are presented in **Table 2.1**.

**Table 2-1.** Composition of ASR stabilized latexes prepared in-situ.

	Component	ASR/Latex 1 (g)	ASR/Latex 2 (g)
<b>Initial Charge</b>	Water	258	258
	SDS	0.6	0.6
<b>Initiator solution</b>	Water	20	20
	NaPS	1.5	1.5
<b>First stage pre-emulsion</b>	Water	60	60
	SDS	0.6	0.6
	MMA	80	40
	S	5	5
	EA	-	40
	MAA	15	15
	EHTG	4.0	4.0
<b>Base</b>	Ammonium hydroxide (25%)	10.9	10.9
<b>Second stage pre-emulsion</b>	Water	111	111
	SDS	0.6	0.6
	MMA	105	105
	BA	105	105

The second group of samples were prepared by blending neutralized ASR solutions with conventional, electrostatically stabilized latexes. Semi-batch emulsion polymerizations were used to synthesize both the ASRs and the conventional latexes. For the ASR latexes, the reactor was charged with the initial charge, then the temperature was raised to 80 °C under nitrogen flux. After the temperature was equilibrated, the initiator solution was added as a shot. The

resultant solution was agitated for 5 minutes at 250 rpm, then the feeding of the pre-emulsion was started and completed in 40 min. The system was held at the reaction temperature for an additional 60 min for post polymerization. The composition for the ASRs can be seen in **Table 2-2**. The different ASR formulations are labeled as ASR XX with XX describing the theoretical glass transition temperature of the polymer in degrees Celsius as determined by the Fox equation.

Similarly, for the conventional latexes the reactor was charged with the initial charge, then the temperature was raised to 80 °C under nitrogen flux. After the temperature was equilibrated, the initiator solution was added as a shot. The resultant solution was agitated for 5 minutes at 250 rpm, then the feeding of the pre-emulsion was started and completed in 120 min. The system was held at the reaction temperature for an additional 60 min. The different latex formulations are labeled as Latex XX with XX describing the theoretical glass transition temperature in degrees Celsius of the polymer determined by the Fox equation.

In order to investigate the effect of the particle size of conventional latexes/ASR blends, conventional latexes with different particle size were prepared through seeded semi-batch emulsion polymerization using the same method as for the conventional latex, using the recipes shown in **Table 2-2**. In Latex 68<sub>235</sub>, Latex 68 was used as seed. In Latex 68<sub>450</sub>, Latex 68<sub>235</sub> was used as seed.



**Table 2-2.** Composition of ASRs and conventional latexes used in the blends

Stages	Component	ASR	ASR	ASR	ASR	ASR	Latex	Latex	Latex	Latex	Latex
		127	90	60	36	14	68	5	-21	68 <sub>235</sub>	68 <sub>450</sub>
Initial Charge	Water (g)	258	258	258	258	258	320	320	320	348	348
	SDS (g)	0.6	0.6	0.6	0.6	0.6	1.2	1.2	1.2	-	-
	Latex 68 (g)	-	-	-	-	-	-	-	-	63.5	-
	Latex 68 <sub>235</sub> (g)	-	-	-	-	-	-	-	-	-	63.5
Initiator solution	Water (g)	20	20	20	20	20	20	20	20	20	20
	NaPS (g)	1.5	1.5	1.5	1.5	1.5	1.5	1.5	1.5	1.5	1.5
Pre-emulsion	Water (g)	60	60	60	60	60	111	111	111	111	111
	SDS (g)	0.6	0.6	0.6	0.6	0.6	4.6	4.6	4.6	4.6	4.6
	MMA (g)	80	60	40	20	0	260	153	92	260	260
	S (g)	5	5	5	5	5	-	-	-	-	-
	EA (g)	-	20	40	60	80	-	-	-	-	-
	MAA (g)	15	15	15	15	15	-	-	-	-	-
	EHTG (g)	4	4	4	4	4	-	-	-	-	-
	BA (g)	-	-	-	-	-	46	153	214	46	46
Calculated	-	127	90	60	36	14	68	5	-21	68	68
T <sub>g</sub> (°C) <sup>a</sup>											

<sup>a</sup> Calculated using the Fox equation.

The blends were prepared by raising the pH until the ASR was soluble at 65°C using aqueous ammonium hydroxide, then blending it with the corresponding proportion of conventional latex under continuous agitation by magnetic stirring. The solid content of the ASRs

and conventional latexes were 23% and 40%, respectively. For all the blends prepared in the present work, the solid content was around 30%.

### **2.2.3 Characterization**

The detailed characterization techniques used to measure the properties of the latexes and films cast from the latexes are provided in Appendix I.

## **2.3. Results**

### **2.3.1 Synthesis of ASR and ASR stabilized latexes**

Two sets of ASR based systems were synthesized. In the first case, the emulsion polymerization of a 50:50 wt/wt MMA/BA mixture was conducted in the presence of a neutralized ASR synthesized in-situ with either MMA/S/MAA 80/5/15 (ASR/Latex 1) or MMA/S/EA/MAA 40/5/40/15 (ASR/Latex 2) (see **Table 2-1**). Both the samples were obtained as stable dispersions with high conversion (> 99%). The characteristics of the in-situ ASR stabilized latexes are presented in **Table 2-3**. In both cases the molecular weights of the ASR were similar as they were controlled by the presence of 2-ethylhexyl thioglycolate in the monomer feed. The particle size distribution as determined by the PDI of the latexes is relatively broad for both samples, which is likely indicating that the nucleation process is continuous in these systems.

**Table 2-3** – Characteristics of in-situ ASR stabilized latexes

Samples	Particle size (nm)	PDI	ASR Mw (g.mol <sup>-1</sup> )	Latex Mw (g.mol <sup>-1</sup> )	Gel content (%)
ASR/Latex 1	126	0.12	$9.5 \times 10^3$	$6.5 \times 10^5$	<5
ASR/Latex 2	108	0.25	$9.5 \times 10^3$	$5.8 \times 10^5$	<5

A second set of latexes was made by blends of ASRs and conventional surfactant stabilized latexes with varying  $T_g$ s (see **Table 2-2**). The particle size, molecular weight and gel content are presented in **Table 2-4**. Note that in the case of the ASRs the particle size refers to the particle size of the latex *before* neutralization, where the ASR exists as a colloiddally stable latex. As can be seen, the PDI indicates a narrow particle size distribution in all cases. The molecular weight is in the predicted range for the ASR latexes given the amount of chain transfer agent used in the formulation and essentially no gel content was observed in any sample. In addition, the acid values as well as the pKa were also determined for the ASR latexes and the respective results are in good agreement with the amount of acid used in the formulation. The pKa is notably higher than that of the homopolymer of methacrylic acid, in agreement with previous studies.<sup>3</sup>

**Table 2-4.** Features of ASRs and latexes used to prepare the blends

<b>Samples</b>	<b>Particle size (nm)</b>	<b>PDI</b>	<b>M<sub>w</sub> (g.mol<sup>-1</sup>)</b>	<b>Đ</b>	<b>Gel content (%)</b>	<b>Acid Value (Ac)</b>	<b>pKa</b>
<b>ASR 127</b>	108	0.08	1.1 × 10 <sup>4</sup>	1.9	<5	99 (±2)	8.6 (±0.3)
<b>ASR 90</b>	88	0.01	1.0 × 10 <sup>4</sup>	2.0	<5	100 (±2)	8.6 (±0.3)
<b>ASRS 60</b>	111	0.02	1.1 × 10 <sup>4</sup>	2.0	<5	103 (±2)	8.6 (±0.3)
<b>ASR 36</b>	87	0.03	1.0 × 10 <sup>4</sup>	2.1	<5	107 (±2)	8.5 (±0.3)
<b>ASR 14</b>	99	0.04	1.0 × 10 <sup>4</sup>	2.2	<5	110 (±2)	8.5(±0.3)
<b>Latex 68</b>	67	0.07	1.2 × 10 <sup>5</sup>	2.3	<5	-	-
<b>Latex 5</b>	89	0.03	1.0 × 10 <sup>5</sup>	2.4	<5	-	-
<b>Latex-21</b>	71	0.05	1.3 × 10 <sup>5</sup>	2.7	<5	-	-

The weight fraction of ASR present in the water phase of the blends and ASR/Latex systems was determined via ultracentrifugation and gravimetric measurements (see **Figure S2-1 - Appendix 2**). The results obtained for the neutralized ASR/latex blends show that in most cases around 70 % of the ASR remains in the water phase, with approximately 30 % adsorbed to the latex surface. Thus, in all cases the ASR/latex systems should be considered as a complex system in which a fraction of the ASR is adsorbed to the latex surface, generating a “hairy” latex, and a fraction remains free in the aqueous phase. In the systems in which the neutralized ASR was used as stabilizer during the emulsion polymerization the water soluble content was significantly lower and dropped from approximately 50% (ASR/Latex 1) to nearly 15% (ASR/Latex 2). The cause of this decrease is chain transfer reactions that occur during the polymerization that lead to grafting of the ASR to the emulsion polymer.<sup>4</sup> This is more prominent

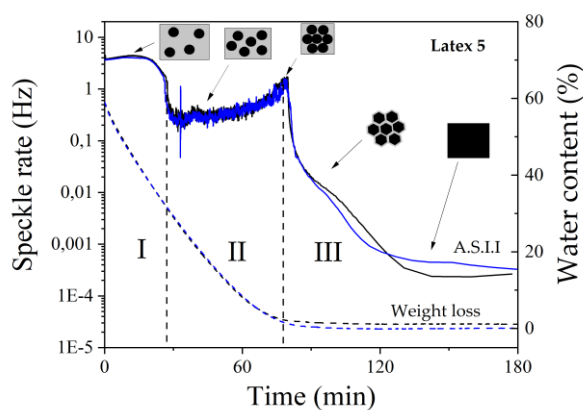
in ASR/Latex 2 due to the presence of a high fraction of ethyl acrylate in the ASR composition, which has a more readily abstractable hydrogen in the polymer backbone.<sup>5</sup>

The aggregation behavior of the neutralized ASRs in solution was also determined by measuring the surface tension across a wide concentration range using the Du Noüy ring method. The results are shown in **Figure S2-2 – Appendix 2**. In all cases the surface tension ( $\gamma$ ) decreased with the concentration of ASRs up to around 0.2 g/L before beginning to plateau as the critical micelle concentration was reached. The shape of the curves is almost identical for all the ASRs synthesized indicating that they have similar aggregation behavior. It should be noted that the measured CMC and the measured aqueous phase ASR concentration indicates that the majority of the neutralized ASR in the aqueous phase is in the micellar form at the concentrations used in the rest of this work.

### 2.3.2 Drying of ASR containing latexes

The different stages of water evaporation during film formation were investigated by simultaneous adaptive speckle imaging interferometry (ASII) and mass loss measurements. It is important to highlight that due to the experimental setup the weight loss is the global weight loss across a film occupying a surface area of  $\sim 200 \text{ cm}^2$  while the ASII measurement is a local measurement performed at two points along the film. **Figure 2-1** shows the ASII kinetics and weight loss measurement for the regular surfactant stabilized latex (Latex 5) prepared in this work for two independent measurements. As mentioned in the introduction, the drying process for a conventional latex occurs in three main stages. In **Figure 2-1** all the stages are clearly defined and the typical ASII drying profile of a latex is obtained.<sup>6</sup> It can be seen that the first stage

was reached after 27 minutes at which point the water content was approximately 30 %. This stage is closely correlated with the “open time” of latex systems.<sup>6</sup> After this event, the particles are in close contact and begin to pack (II). In the case of Latex 5 this stage took 50 minutes and proceeded until effectively all water had evaporated. In the final phase the speckle rate decreased sharply indicating a drastic reduction of the average motion speed of scatterers inside the sample. At the beginning of phase III it can be assumed that the water content (around 3 wt.%) corresponds only to interstitial water remaining in the film and water adsorbed within the polymer particles themselves.

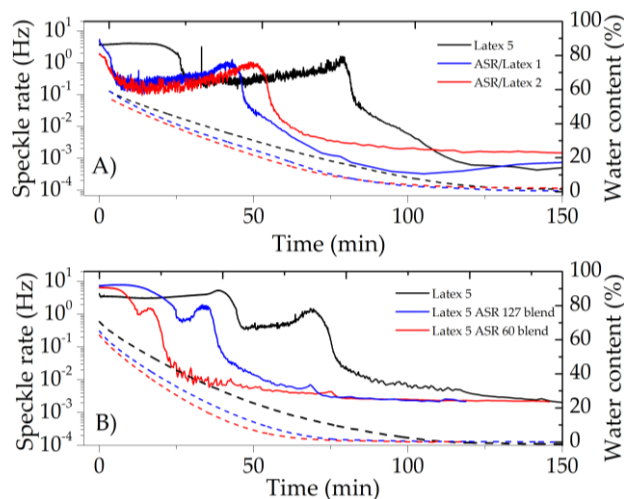


**Figure 2-1.** Different phases of the drying process and weight loss observed for Latex 5. The full lines show the change in speckle rate over time obtained from adaptive speckle imaging interferometry and the dashed line shows the weight loss due to evaporation.

In order to compare the drying process of ASR stabilized latexes and a conventional latex, the drying kinetics for ASR stabilized latexes and for the neutralized ASR/latex blends using a

latex phase with  $T_g=5$  °C are shown in **Figure 2-2**. Note that due to differences in the synthetic procedure the film formation of the blends is conducted at 30 wt% while the in-situ samples are conducted at 40 wt%.

Starting with the ASR stabilized latexes, it can be seen that just as in the case of Latex 5 the three conventional stages are observed (**Figure 2-2A**). However, the value of water content and respective time for the onset of stages I and II are significantly different from that of Latex 5. In addition, in the final stage a slightly higher residual water content is observed for the in-situ ASR stabilized latexes when compared to Latex 5 at long times. These results are attributed to the presence of water absorbed by the ASR. During the early stages of drying this absorbed water leads to an increase in the effective volume fraction and therefore particle packing occurs at higher water content/shorter time. This results in the packing and deformation stages occurring at higher water content. During the latter stages, when the majority of the bulk water has evaporated and polymer particles are packed, the water that is adsorbed in the ASR itself leads to a higher water content being retained. In the latexes formed from blending (**Figure 2-2B**), similar behavior was observed, although because the latex blends were cast at lower solid contents, the initial drying period is extended.



**Figure 2-2.** Different phases of the drying process and weight loss observed using ASR stabilized latexes (solid content = 40 wt%) and neutralized ASR/latex blends (solid content = 30 wt%). For comparative purposes Latex 5 diluted to the same solid content is shown. The full lines show the change in speckle rate over time obtained from adaptive speckle imaging interferometry and the dashed line shows the weight loss due to evaporation.

### 2.3.3 Film formation of ASR containing latexes

The ASII and water evaporation experiments above show that the ASR influences the drying process, but it can also play a major role in the coalescence/interdiffusion stages that occur in the final stages of film formation.<sup>7,8</sup> Understanding these processes is particularly important to establish the limits to which ASRs can be used to reinforce the mechanical properties of the film whilst maintaining a relatively low MFFT. As a first step to understanding the influence of the ASR on coalescence and interdiffusion, films of conventional latexes and



ASRs of different  $T_g$ s were cast separately and the MFFT was measured. In the case of the ASRs, films were prepared with the ASR in the acidic, latex form as well as in the soluble, neutralized form following addition of either potassium hydroxide (a non-volatile base) or ammonia (a volatile base). **Table 2-5** shows the MFFT values for all the ASRs and conventional latexes synthesized in the present work.

In the case of the conventional latexes the MFFT was in reasonable agreement with the  $T_g$  of the polymer estimated by the Fox equation as expected. Similar behaviour is seen in the ASR systems in the non-soluble, acid form and the MFFT decreases as the dry  $T_g$  of the polymer is reduced due to increasing the fraction of EA in the copolymer. An even more interesting aspect that is demonstrated by these results is that for neutralized, high  $T_g$  ASRs, even when the system appears to be effectively water soluble, a coherent film is not formed at room temperature. This is in contrast to what would be expected for a true polymer solution but is more similar in nature to colloidal systems in which there is a close relation between the MFFT and the  $T_g$  of the polymer.

**Table 2-5.** MFFT of conventional latexes and neutralized and non-neutralized ASRs.

<b>Samples</b>	<b>MFFT(°C) (Acid)<sup>a</sup></b>	<b>MFFT(°C) (NH<sub>4</sub>OH)</b>	<b>MFFT(°C) (KOH)</b>
<b>Latex 68</b>	85	-	-
<b>Latex 5</b>	7	-	-
<b>Latex -21</b>	<5 <sup>b</sup>	-	-
<b>ASR 127</b>	>90 <sup>c</sup>	74	65
<b>ASR 90</b>	55	44	37
<b>ASR 60</b>	27	18	14
<b>ASR 36</b>	22	<5 <sup>b</sup>	<5 <sup>b</sup>
<b>ASR 14</b>	<5 <sup>b</sup>	<5 <sup>b</sup>	<5 <sup>b</sup>

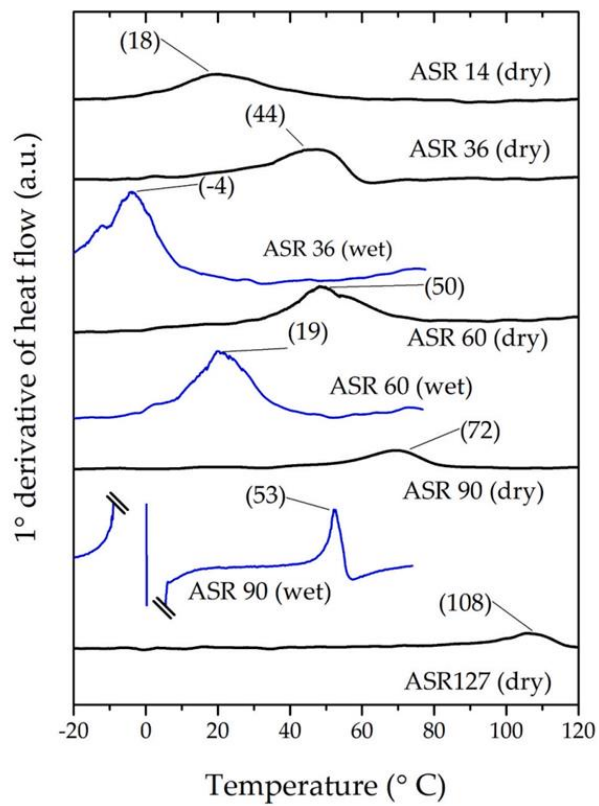
<sup>a</sup> The pH of the latex without additives is around 4 in all cases.

<sup>b</sup> The system forms a coherent film up to the point at which the latex is frozen at low temperatures

<sup>c</sup> Film formation did not occur up to the limit of measurement.

In order to explore this idea further, DSC was performed on the ASR resins in the dry state, and in the wet state by drying a neutralized ASR to around 30% water content. It is important to point out that due the overlapping events between the glass transition and the melting/freezing processes of water as well as the limitation of boiling point of water, it was not possible to determine the wet T<sub>g</sub>s of all samples by this method. This can be seen for example in the DSC of ASR 90 in the wet state where a large peak arising from the melting of free water can be clearly observed, although in this case it does not interfere with the T<sub>g</sub> of the hydroplasticized polymer which is at higher temperatures.

The DSC thermograms are shown in **Figure 2-3** while **Table 2-6** gives a summary of the difference in  $T_g$  between samples. In **Table 2-6** the experimental values are also compared with theoretical values calculated using the Fox equation for the dry  $T_g$  and a model that takes into account hydroplasticization effects for the wet  $T_g$ . Comparing first the dry  $T_g$ s and those measured in the wet state, it is clear that the presence of water leads to the hydroplasticization of the polymer, resulting in a decrease in  $T_g$ . Looking at the values of the  $T_g$  in comparison to those of the MFFT shown in **Table 2-5** shows that the  $T_g$  of the ASR in the wet state is closer to the MFFT, showing that it is the hydroplasticized ASR that is of more importance during film formation. This is in agreement with recent work from Voogt *et al.* who reported that the adsorption of water in methacrylic acid rich latexes led to hydroplasticization, thus lowering substantially the  $T_g$  of the polymer in the wet state.<sup>9,10</sup>



**Figure 2-3.** Comparison between DSC results in wet and dry conditions for the ASRs. The labelled values above the thermograms are the T<sub>g</sub> values in °C.

**Table 2-6.** Theoretical and Experimental  $T_g$  of ASRs.

Samples	Theoretical		Experimental	
	$T_g$ -Dry <sup>a</sup> (°C)	Wet $T_g$ -acid <sup>b</sup> (°C)	$T_g$ -Dry (°C)	Wet $T_g$ -acid (°C)
<b>ASR 127</b>	127	78	108	<sup>c</sup>
<b>ASR 90</b>	91	51	72	53
<b>ASR 60</b>	61	28	50	19
<b>ASR 36</b>	36	-8	44	-4
<b>ASR 14</b>	14	-9	18	<sup>d</sup>

<sup>a</sup> Theoretical dry  $T_g$ s are calculated using the Fox equation.

<sup>b</sup> Theoretical wet  $T_g$ s are calculated using the model developed by Tsavalas and Sundberg.<sup>3</sup>

<sup>c</sup> Not possible to measure in wet conditions due to the high temperature required.

<sup>d</sup> Not possible to measure in wet conditions due to the low temperatures required.

The extent of hydroplasticization is also expected to be dependent on the ionization state of the polymer which may explain the lower MFFT when KOH was used to neutralize the ASRs (see **Table 2-5**). This discrepancy is particularly important because typically ammonia, a volatile base, is used for neutralization. This means that the ionization state can change during the drying of the latex, further complicating the film formation behavior. To evaluate the effect of the volatility of the base, a volatile ( $\text{NH}_3$ ) and a non-volatile (KOH) base were used to neutralize ASR 60 in presence of an indicator that exhibits a color change from blue to yellow at pH 7 (bromothymol blue). As reported before (see **Table 2-4**) the pKa of ASRs were determined by titration and the values were around 8.5 and therefore a color change indicates evaporation of the base and protonation of the methacrylic acid.

As can be seen in **Figure S2-3 – Appendix 2**, in the film prepared with ammonium hydroxide, the pH of the system was reduced to 7 within 10 minutes, while the film neutralized with KOH remained at high pH. Therefore, in comparison with the drying curves shown in **Figure 2-1** this experiment demonstrates that the ammonia present evaporates before any coalescence occurs and it is the  $T_g$  of the protonated polymer in the wet state that is important in the film formation process. This result would also explain why the MFFT of the ammonium hydroxide-neutralized ASRs is higher than that of KOH (**Table 2-5**). In the case of the KOH neutralized ASRs the hygroscopic nature of the polymer leads to a higher concentration of water at the onset of stage III and a high concentration of residual water in the film, even after prolonged drying (see **Figure S2-4 – Appendix 2**), which would be undesirable in practical applications.

### **2.3.4 Film formation of ASR stabilized latexes and blends**

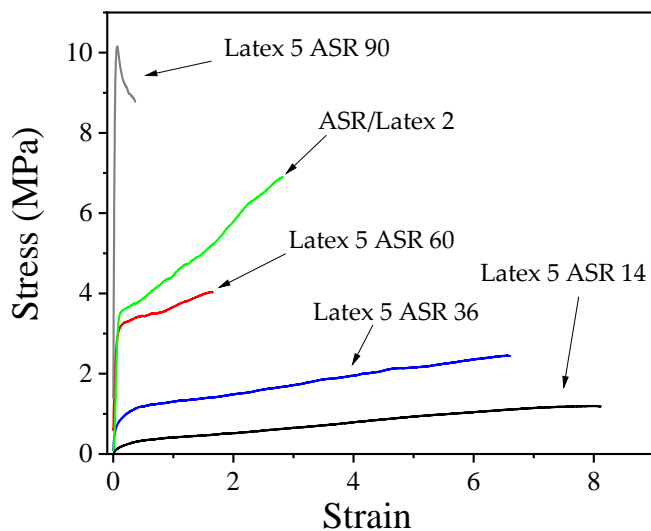
The results above suggest that the ASRs behave in a similar way to conventional colloidal particles with respect to film formation behaviour, with a strong dependency of the MFFT on the wet  $T_g$  of the ASR. In order to further explore how the  $T_g$  of both the ASR phase and the latex phase influence the film formation behaviour, a series of blends of ammonium hydroxide neutralized ASRs with latexes of varying  $T_g$  were prepared and their respective MFFTs were recorded. **Table 2-7** shows the MFFT of the blends.

**Table 2-7.** MFFT of the blends with different ASRs and latexes. In all cases the ratio ASR:Latex is 30:70 wt/wt

	Samples	MFFT (°C)	Samples	MFFT (°C)	Samples	MFFT (°C)
<b>Blends</b>	Latex 68 ASR 127	83	Latex 5 ASR 127	10	Latex -21 ASR 127	<5
	Latex 68 ASR 90	65	Latex 5 ASR 90	8	Latex -21 ASR 90	<5
	Latex 68 ASR 60	50	Latex 5 ASR 60	<5	Latex -21 ASR 60	<5
	Latex 68 ASR 36	44	Latex 5 ASR 36	<5	Latex -21 ASR 36	<5
	Latex 68 ASR 14	40	Latex 5 ASR 14	<5	Latex -21 ASR 14	<5
			ASR/Latex 1	10	-	-
<b>In situ</b>		ASR/Latex 2	11	-	-	

The results show that for a given latex blend the MFFT decreases with the  $T_g$  of the ASR used as stabilizer. Similarly, keeping the same ASR, the MFFT decreases with  $T_g$  of the latex polymer. However, the effect of the latex was substantially higher. For the highest  $T_g$  latex (Latex 68) the MFFT was greater than room temperature for all cases, even when blending with the softer ASRs that form a cohesive film by themselves at low temperatures. The likely reason for this is that the amount of ASR present in the blend (30% w/w) is not enough to occupy the space between the particles and allow the formation of a coherent film. Thus, these results demonstrate it is possible to form a film with a high  $T_g$  ASR as long as the condition is met that the  $T_g$  of the conventional latex is low enough such that deformation readily occurs to occupy void spaces left by the non-deformable ASR. Note that similar results were observed for the latexes that were producing using ASRs as a surfactant (ASR/Latex 1 and ASR/Latex 2) suggesting that this result can be generalized.

It is important to note that while the addition of ASR to the latex results in only a slight increase in the MFFT, it leads to a huge improvement in the mechanical properties. This can be seen in **Figure 2-4** which shows the tensile test results for a series of blends using Latex 5 and the different ASRs. As  $T_g$  of the ASRs increased, the Young's modulus and yield stress increased, but a reduction in the strain at break was observed. Except when using the highest  $T_g$  ASR (ASR 127), the films were relatively ductile. It may be noted that when the ASR was used as surfactant (ASR/latex 2) there was a substantial improvement in the Young's modulus and tensile strength when compared to the blends of identical formulation (Latex 5 ASR 60) which may be related to the grafting between the two phases. These results highlight that ASRs can lead to low MFFT, high Young's modulus latex systems.



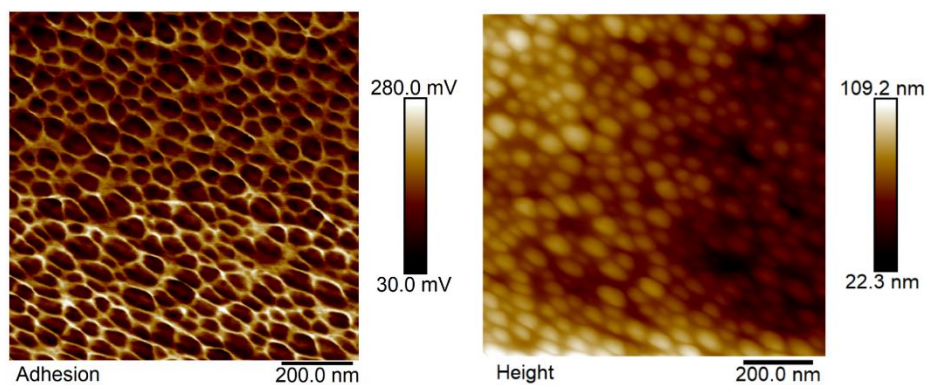
**Figure 2-4.** Tensile properties of the films prepared using blends with different ASRs using Latex

5.



The MFFT results above suggest that ASR/latex systems behave in a similar manner to conventional latex blends in which the relative size of the two colloids and the  $T_g$  of each phase is important.<sup>11-13</sup> The colloidal state of the ASR depends on the extent of neutralization but can be considered to exist as small aggregates on the order of 5-50 nm.<sup>14</sup> Thus, blending with latex particles that are substantially larger tends to lead to a continuous ASR phase, even when it is present at relatively low volume fractions. This can be observed in **Figure 2-5**, which shows the AFM images of a blend of latex 68 and ASR 60. Despite being present in lower volume fraction, it is the ASR phase that forms the continuous phase due to the smaller size of the colloidal aggregates of the ASR.<sup>13</sup> Recent work has suggested that the continuous nature of the high  $T_g$  ASR phase is the main reason for the significant improvement in mechanical properties in these systems.<sup>15</sup>

Given the similarity between the ASR/latex systems and conventional latex blends, it is possible to use the knowledge of film formation of latex blends to try to produce films using the higher  $T_g$  latex (Latex 68) whilst maintaining low MFFT. This would have the advantage that the high  $T_g$  latex would be expected to contribute to mechanical stability even if the ASR phase were plasticized by water.



**Figure 2-5.** AFM phase and height images of the surface of a film formed from the blend Latex 68 ASR 60.

In conventional latex blends there are two main factors that can be manipulated to change film formation behavior: (1) relative volume fraction of the hard/soft phase and (2) relative particle size. Therefore, blends of Latex 68 and ASR 60 were made with various volume fractions of the ammonium hydroxide neutralized ASR 60. It should be recalled from **Table 2-5** that this ASR is film-forming by itself. **Table 2-8** shows the MFFT of blends with increasing ASR fraction. It can be observed that increasing the amount of ASR leads to a decrease in the MFFT, albeit a limited one. A second series of experiments were conducted by comparing the influence of the particle size of the latex, keeping the same ASR fraction. As can be seen, in this case the MFFT of blends is highly affected by affected, and the MFFT dropped substantially as the latex particle size increased. This is to be expected as the increase in particle size relative to the colloidal aggregates of the ASR improves the interconnectivity of the film-forming ASR phase. Combining these two effects (high particle size ratios, high volume fraction of the film-forming ASR phase)

led to a system with MFFT below room temperature. This offers a route to the design of ASR stabilized latexes that are capable of forming a film at ambient temperatures even when the  $T_g$  of both the ASR and the emulsion polymer phase is high.

**Table 2-8.** MFFTs of the blend Latex 68 ASR 60 with different particle size of latex and ASR/Latex fractions.

Size of Latex 68 (nm)	Weight fraction (ASR/Latex)	MFFT (°C)
79	30/70	55
79	40/60	43
79	50/50	40
215	30/70	48
400	30/70	26
400	40/60	26
400	50/50	17

## 2.4. Conclusions

In order to investigate the film formation behavior of alkali soluble resin (ASR) stabilized latexes, ASRs and conventional latex samples were prepared via semi-batch emulsion polymerization. Two different system were studied, in-situ latexes stabilized by ASRs and blended samples. The combination of the experiments discussed within this work allow us to make some general comments on the film formation of alkali soluble resin containing emulsion polymers.

Upon addition of alkali these systems are not true polymer solution but rather undergo assembly into small, water-swollen micelle-like structures. In the presence of additional surface area provided by the latex a portion of the ASR is strongly adsorbed to the surface but a substantial proportion remains in the form of dispersed colloidal aggregates. During drying the adsorbed water inside the ASR leads to higher effective particle volume fraction and therefore the time at which particles begin to pack and deform is significantly reduced. As the neutralized ASRs do not form true polymer solutions but exist as colloidal aggregates, their film formation behavior is more similar to that of conventional latexes and is strongly affected by the  $T_g$  and the extent of hydroplasticization of the ASR phase. As a result of this behavior, in blends with latexes, and when used as stabilizers in emulsion polymerizations, the film formation is more similar to conventional latex blends. As the colloidal aggregates formed by the ASRs are very small and can be deformed in the hydroplasticized state, they tend to form the continuous phase in the dried film, which leads to excellent mechanical properties. Where the latex polymer is soft ( $T_g < T_{\text{Film formation}}$ ), the deformation of the ASR is not necessary and the MFFT is dictated almost entirely by the properties of the latex. When the latex polymer is hard ( $T_g > T_{\text{Film formation}}$ ), unless relatively high-volume fractions of the ASR or large latex particles are used, film formation is not possible regardless of the MFFT of the ASR by itself.

## 2.5. References

- (1) Siddiq, M.; Tam, K. C.; Jenkins, R. D. Dissolution Behaviour of Model Alkali-Soluble Emulsion Polymers: Effects of Molecular Weights and Ionic Strength. *Colloid Polym. Sci.* **1999**, *277* (12), 1172–1178. <https://doi.org/10.1007/s003960050506>.
- (2) Bandiera, M.; Balk, R.; Barandiaran, M. J. One-Pot Synthesis of Waterborne Polymeric Dispersions Stabilized with Alkali-Soluble Resins. *Polymers (Basel)*. **2018**. <https://doi.org/10.3390/polym10010088>.
- (3) Tsavalas, J. G.; Sundberg, D. C. Hydroplasticization of Polymers: Model Predictions and Application to Emulsion Polymers. *Langmuir* **2010**, *26* (10), 6960–6966. <https://doi.org/10.1021/la904211e>.
- (4) Caballero, S.; de la Cal, J. C.; Asua, J. M. Radical Entry Mechanisms in Alkali-Soluble-Resin-Stabilized Latexes. *Macromolecules* **2009**, *42* (6), 1913–1919. <https://doi.org/10.1021/ma802642w>.
- (5) Ballard, N.; Asua, J. M. Radical Polymerization of Acrylic Monomers: An Overview. *Prog. Polym. Sci.* **2017**. <https://doi.org/10.1016/j.progpolymsci.2017.11.002>.
- (6) Brun, A.; Dhang, H.; Brunel, L. Film Formation of Coatings Studied by Diffusing-Wave Spectroscopy. *Prog. Org. Coatings* **2008**, *61* (2), 181–191. <https://doi.org/https://doi.org/10.1016/j.porgcoat.2007.09.041>.
- (7) Park, Y.-J.; Lee, D.-Y.; Khew, M.-C.; Ho, C.-C.; Kim, J.-H. Effects of Alkali-Soluble Resin on Latex Film Morphology of Poly(n-Butyl Methacrylate) Studied by Atomic Force Microscopy. *Langmuir* **1998**, *14* (19), 5419–5424. <https://doi.org/10.1021/la971105r>.
- (8) Gonzalez, E.; Tolan, C.; Chuvilin, A.; Paulis, M.; Barandiaran, M. J. Effect of Alkali-Soluble Resin Emulsifiers on Coalescence and Interdiffusion between Latex Polymer Particles. *Colloid Polym. Sci.* **2015**, *293* (8), 2419–2427. <https://doi.org/10.1007/s00396-015-3635-3>.
- (9) Voogt, B.; Huinink, H. P.; Erich, S. J. F.; Scheerder, J.; Venema, P.; Keddie, J. L.; Adan, O. C. G. Film Formation of High T<sub>g</sub> Latex Using Hydroplasticization: Explanations from NMR Relaxometry. *Langmuir* **2019**, *35* (38), 12418–12427. <https://doi.org/10.1021/acs.langmuir.9b01353>.
- (10) Voogt, B.; Huinink, H.; van de Kamp-Peeters, L.; Erich, B.; Scheerder, J.; Venema, P.; Adan, O. Hydroplasticization of Latex Films with Varying Methacrylic Acid Content. *Polymer (Guildf)*. **2019**, *166*, 206–214. <https://doi.org/10.1016/j.polymer.2019.01.074>.

- (11) Eckersley, S. T.; Helmer, B. J. Mechanistic Considerations of Particle Size Effects on Film Properties of Hard/Soft Latex Blends. *J. Coatings Technol.* **1997**, *69* (864), 97–107. <https://doi.org/10.1007/BF02696096>.
- (12) Colombini, D.; Hassander, H.; Karlsson, O. J.; Maurer, F. H. J. Influence of the Particle Size and Particle Size Ratio on the Morphology and Viscoelastic Properties of Bimodal Hard/Soft Latex Blends. *Macromolecules* **2004**, *37* (18), 6865–6873. <https://doi.org/10.1021/ma030455j>.
- (13) Tzitzinou, A.; Keddie, J. L.; Geurts, J. M.; Peters, A. C. I. A.; Satguru, R. Film Formation of Latex Blends with Bimodal Particle Size Distributions: Consideration of Particle Deformability and Continuity of the Dispersed Phase. *Macromolecules* **2000**, *33* (7), 2695–2708. <https://doi.org/10.1021/ma991372z>.
- (14) Scheerder, J.; Dollekens, R.; Langermans, H. The Colloidal Properties of Alkaline-Soluble Waterborne Polymers. *J. Appl. Polym. Sci.* **2018**, *135* (17), 46168. <https://doi.org/10.1002/app.46168>.
- (15) Pérez, A.; Kynaston, E.; Lindsay, C.; Ballard, N. Mechanical Properties of Films Cast from Alkali Soluble Resin Stabilized Latexes. *Prog. Org. Coatings* **2022**, *168*, 106882. <https://doi.org/https://doi.org/10.1016/j.porgcoat.2022.106882>.

# Chapter 3. Film formation of latexes with hydroplasticizable domains

## 3.1. Introduction

In the previous chapter the film formation behavior of latexes containing alkali-soluble resins was investigated. In this chapter polymers of similar composition are used, but with significantly higher molecular weight so that they are no longer alkali-soluble (as was the case in Chapter 2), but can still be hydroplasticized. In principle this should make subsequent product formulation more flexible as the need for specific pH ranges and the presence of water soluble polymer is avoided. As discussed in the previous chapter, hydroplasticizable systems typically contain a fraction of hydrophilic co-monomer in the latex formulation such that in the presence of water, the latex becomes plasticized and the glass transition temperature drops significantly.<sup>1,2</sup> Thus, during the film formation stage the hydroplasticized polymer is softened and can be readily deformed by the effects of surface tension, yet when dry, the  $T_g$  increases and the polymer becomes stiff. These hydroplasticization systems therefore make use of water to behave as for conventional plasticizers, but do not lead to the release of any VOCs to the environment.

In the literature hydroplasticized polymers have previously been reported in homogeneous latex systems. For example, Voogt et al.<sup>3</sup> synthesized a series of methyl methacrylate/butyl acrylate/methacrylic acid polymer latexes. When the fraction of methacrylic acid was increased to 10 wt%, the wet (hydroplasticized)  $T_g$  was around 19 °C and thus film formation was possible at ambient temperature, yet in the dry state the  $T_g$  was measured as 37 °C. Similarly, Dron and Paulis<sup>4</sup> have shown that the inclusion of as little as 1 wt% of a hydrophilic comonomer in emulsion polymerization can lead to a film with similar mechanical properties in the dry state but significantly reduced MFFT.

In this chapter the focus is on how to make best use of the hydroplasticization effect by tailoring latex systems such that the MFFT is minimized, while the mechanical properties in the dry state are maximized. To probe this question, a series of latex systems involving hydroplasticizable polymers has been designed. First, the synthesis of a series of different latex systems is described. Subsequently the film formation properties and the effect of hydroplasticization depending on the colloidal structure is explored. Finally, the influence of the initial colloidal structure on the final properties when the hydroplasticizable domains are dried is studied. This allows for some conclusions to be drawn on the optimum structure that can lead to low MFFT, high modulus films.



## 3.2. Experimental

### 3.2.1. Materials

The monomers used in this work, methyl methacrylate (MMA, technical grade, Quimidroga), styrene (S, technical grade, Quimidroga), ethyl acrylate (EA, >99%, Sigma Aldrich), butyl acrylate (BA, technical grade, Quimidroga) and methacrylic acid (MAA, >99% Sigma Aldrich) were used without any further purification. Sodium persulfate (NaPS, >98%, Sigma Aldrich) ammonium persulfate (APS, >98%, Sigma Aldrich) sodium dodecyl sulfate (SDS, >98%, Sigma Aldrich), 2-ethylhexyl thioglycolate (EHTG, >95%, Sigma Aldrich) were used as supplied. Deionized water was used throughout the work.

### 3.2.2. Synthesis of MMA/BA latex (L1).

Semi-batch emulsion polymerization was used to synthesize the MMA/BA latex. The composition of the latex can be seen in **Table 3-1**. Briefly, a 1 L jacketed glass reactor equipped with nitrogen inlet, a thermocouple, a condenser and a stainless steel anchor-type stirrer was loaded with the initial charge and the temperature was raised to 80 °C under nitrogen flux with continuous stirring (250 rpm). After the temperature was equilibrated, the initiator solution was added as a shot. The resultant solution was agitated for 5 minutes, and then the feeding of the pre-emulsion was started and completed in 120 minutes. The system was held at the reaction temperature for an additional 60 min.

**Table 3-1.** Composition of MMA-BA latex (L1).

Reagent	Initial Charge		Initiator Solution		pre-emulsion			
	Water	SDS	Water	KPS	Water	SDS	MMA	BA
Amount (g)	320	1.2	20.0	1.50	111	4.60	153	153

### 3.2.3. Synthesis of core/shell MMA-BA/MMA-BA-MAA particles (CS1, CS2)

Two core/shell latex particles were synthesized via seeded semi-batch emulsion polymerization. The core of the particles was composed of a copolymer of MMA and BA while the shell consisted of hydroplasticizable polymer containing 15% methacrylic acid. The compositions of the shell polymers can be found in **Table 3-2**. The reactions were performed by adding the initial charge to the reactor and heating to 80 °C under nitrogen flux and continuous stirring (250 rpm). The initiator solution was added as a shot and the reaction started with the feeding of the pre-emulsion. The pre-emulsion was fed for 40 minutes. To ensure close to full conversion the system was held for an additional 60 minutes before cooling.

**Table 3-2.** Composition of core/shell particles (**CS1, CS2**).

	Reagent	Amount (g)	
<b>Initial Charge</b>	Seed (L1)	583	
<b>Initiator Solution</b>	Water	20	
	KPS	1.50	
<b>Shell composition</b>		<b>CS1</b>	<b>CS2</b>
	Reagent	Amount (g)	Amount (g)
<b>Pre-emulsion</b>	Water	60.0	60.0
	SDS	0.5	0.5
	MMA	80.0	40.0
	S	5.0	5.0
	MAA	15.0	15.0
	EA	0.0	40.0
	EHTG	-	-

### 3.2.4. Synthesis of hydroplasticizable latexes (H1, H2, CTAH1, CTAH2, NanoH1, NanoH2)

A series of hydroplasticizable latexes with different composition (**H1, H2, CTAH1, CTAH2**) and different particle size (**NanoH1, NanoH2**) were synthesized via semi-batch emulsion polymerization. The details of their composition can be found in **Table 3-3**. The preparation started by adding the initial charge into the reactor and raising the temperature to 80 °C under nitrogen flux and continuous stirring (250 rpm). When the temperature stabilized at 80 °C, the initiator solution was added as a shot. The polymerization began with the feeding stage, which was carried out using two different procedures depending on the desired particle size of

the final latex. For latexes H1, H2, CTAH1 and CTAH2 feeding of the pre-emulsion occurred over 40 minutes. Latexes NanoH1 and NanoH2, which targeted a lower particle size, were prepared by feeding a monomer mixture for 180 min. After the feeding stage ended, both systems were held for 60 minutes to allow the polymerization to reach high conversion.

**Table 3-3** - Composition of hydroplasticizable latexes.

Large Latexes						Small Latexes	
Reagent		Amount (g)				Amount (g)	
<b>Initial Charge</b>	Water	255				220	
	SDS	0.6				12	
<b>Initiator Solution</b>	Water	20.00				20	
	NaPS	1.50				-	
	APS	-				0.15	
<b>Samples</b>	H1	H2	CTAH1	CTAH2	NanoH1	NanoH2	
Reagent		Amount (g)				Amount (g)	
<b>Monomer Feed</b>	Water	60.00	60.00	60.00	60.00	-	-
	SDS	0.50	0.50	0.50	0.50	-	-
	MMA	80.0	40.0	40.0	40.0	42.2	21.1
	S	5.00	5.00	5.00	5.00	2.64	2.64
	MAA	15.0	15.0	15.0	15.0	7.92	7.92
	EA	-	40.0	-	40.0	-	21.1
	EHTG	-	-	4.0	4.0	-	-

### 3.2.5. Preparation of latex blends

The blends were prepared by mixing the MMA/BA latex (L1) with a hydroplasticizable latex at room temperature and stirring for 30 min. In most parts of this work, the final polymer

composition was L1:hydroplasticizable latex 70:30 wt:wt on a dry weight basis. The composition of the blends can be found in **Table 3-4**. No additional water was added to the blends, giving a final solid content of 32% for the blends.

**Table 3-4** - Composition of latex blends. All blends have a final composition of L1:hydroplasticizable latex of 70:30 wt:wt.

Sample	Hydroplasticizable latex
Blend 1	H1
Blend 2	H2
Blend CTAH1	CTAH1
Blend CTAH2	CTAH2
Nano blend 1 30%	NanoH1
Nano blend 2 30%	NanoH2

### 3.2.6. Characterization

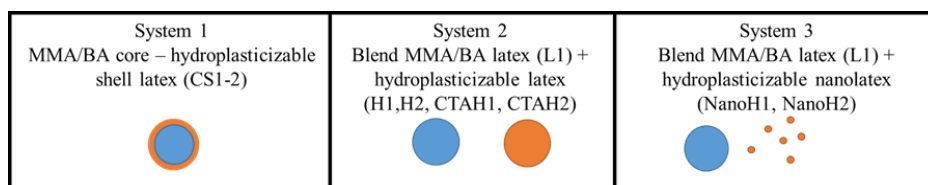
The detailed characterization techniques used to measure the properties of the latexes and films cast from the latexes are provided in Appendix I.

## 3.3. Results and discussion

A series of latexes were synthesized with the aim of generating three distinct colloidal systems that would allow us to investigate the effect of colloidal structure on film formation (see **Scheme 3-1**). In system 1, a core shell structure was targeted in which a conventional acrylic latex formed the core and a hydroplasticizable polymer was in the shell. Systems 2 and 3 corresponded to latex blend systems in which a conventional acrylic latex was blended with a

latex containing a hydroplasticizable polymer. In system 2 the hydroplasticizable latex was of similar size to the conventional acrylic latex, while in system 3 the hydroplasticizable latex was substantially smaller than the conventional acrylic latex.

**Scheme 3-1** – Schematic representation of the three different colloidal systems explored in this work

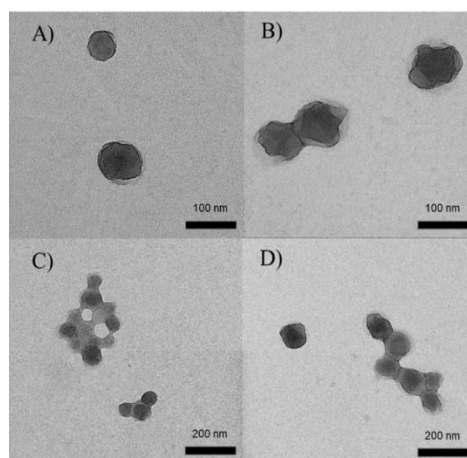


### Latex synthesis

A summary of the most relevant colloidal and macromolecular properties of the latexes synthesized in this work is given in **Table 3-5**. All latexes obtained had high final conversion (>98%) and very low gel content. First, a conventional acrylic latex (L1) was synthesized by semi-batch emulsion polymerization. This latex was used as a seed in the synthesis of a pair of core/shell latexes in which the shell comprised 30% of the total polymeric components and contained a significant fraction of methacrylic acid to promote hydroplasticization. In one latex (CS1) the shell was an MMA/S/MAA 80/5/15 copolymer while the other (CS2) the shell was an MMA/EA/S/MAA 40/40/5/15 copolymer. Evidence for shell formation could be seen in the increase of particle size by DLS following the second stage polymerization, but could also be observed by TEM (see **Figure 3-1**).

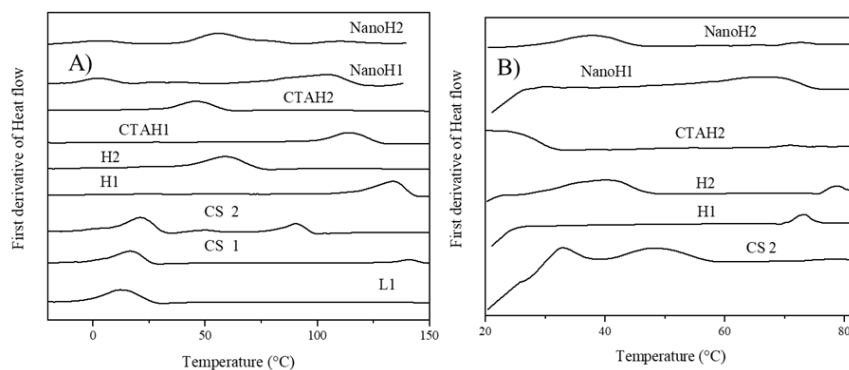
**Table 3-5** – Characteristics of hydroplasticizable and core/shell latex particles

Sample	Particle size (nm)	PDI	$M_w$ (g/mol)	$\bar{D}$	Gel content (%)	Dry $T_g$ (°C)	Wet $T_g$ (°C)
L1	112	0.05	$1.0 \times 10^5$	2.4	<5	13	-
CS1	125	0.02	$5.1 \times 10^4$	8.9	<5	140	-
CS2	123	0.02	$6.7 \times 10^4$	5.8	<5	90	32
H1	156	0.10	$8.1 \times 10^4$	2.2	<5	133	73
H2	84	0.01	$2.5 \times 10^5$	3.5	<5	59	41
CTAH1	108	0.08	$1.1 \times 10^4$	1.9	<5	113	-
CTAH2	111	0.02	$1.1 \times 10^4$	1.9	<5	46	21
NanoH1	22	0.37	$1.4 \times 10^5$	2.6	<5	104	66
NanoH2	36	0.13	$1.6 \times 10^5$	3.8	<5	55	37



**Figure 3-1.** TEM images of the core-shell latex particles, where A) and C) correspond to CS1 and B) and D) correspond to CS2.

The glass transition temperature ( $T_g$ ) of the dried polymers was determined experimentally via DSC (see **Figure 3-2**). The acrylic latex L1 shows a single  $T_g$  around 13°C which is expected based on the MMA/BA composition and the Fox equation. In the core/shell systems CS1 and CS2 two  $T_g$ s can be observed. The first is related to the L1 latex which is the core of the particles ( $T_g \approx 13^\circ\text{C}$ ), while the higher  $T_g$ s represent the  $T_g$  of the outer shell polymer. CS2, which has a large ethyl acrylate fraction in the copolymer has a lower dry  $T_g$  of around 90°C, while for CS1 the shell polymer has a dry  $T_g$  of around 140°C.



**Figure 3-2.** DSC curves of dry (A) and wet (B) samples. Note that the presence of water leads to large peaks related to the melting and freezing of water. To avoid this, only data in the range of 20 °C to 85 °C are shown in **Figure 3-2 (B)**.

A second series of single-phase hydroplasticizable latexes was synthesized in order to make blends with the conventional acrylic latex (L1). In latex H1 the polymer was an MMA/S/MAA 80/5/15 copolymer while H2 was an MMA/EA/S/MAA 40/40/5/15 copolymer. A pair of otherwise identical latexes (CTAH1 and CTAH2) were synthesized in which additional chain transfer agent



was added to reduce the molecular weight of the polymer. Finally, a pair of latexes with substantially smaller particle size (NanoH1 and NanoH2) were synthesized by inclusion of additional surfactant and conducting the polymerization with low feeding rates following the work of De Souza Nunes and Asua.<sup>5,6</sup>

In terms of their thermal properties, the glass transition temperatures of the dry polymers are shown in **Figure 3-2 (A)**. All the latexes that were synthesized using MMA/S/MAA 80/5/15 (H1, CTAH1 and NanoH1) had high  $T_g$ s ( $T_g=100-130$  °C). Although the composition of all these polymers is identical, in the case of reactions with added CTA (CTAH1) and added surfactant (NanoH1) the  $T_g$  was reduced, which may be due to small amounts of residual water that results in hydroplasticization. The latexes that were synthesized using a monomer feed composition of MMA/EA/S/MAA 40/40/5/15 (H2, CTAH2 and NanoH2) had lower  $T_g$ s due to the ethyl acrylate added to the feed. Although the nominal compositions were similar, there were again some variations in  $T_g$ , which may be attributed to small differences in the amounts of residual water.

The dry  $T_g$  values are important when considering mechanical properties of the final dried films but, as discussed in the previous chapter, the  $T_g$  in the wet state is thought to be more influential during the film formation process. The wet  $T_g$ s were measured by performing DSC on latexes that contained approximately 30 wt% water (i.e. highly concentrated dispersions). As shown in **Figure 3-2 (B)**, a significant shift occurs in the  $T_g$  as a result of hydroplasticization. The latexes that were synthesized using MMA/EA/S/MAA 40/40/5/15 (CS2, H2, CTAH2 and NanoH2) had reduced wet  $T_g$ s with broad transitions ranging from around 20 up to 40 °C. This broad transition may be the result of the chemical composition distribution of the chains such that chains containing higher fractions of MAA experience a greater hydroplasticization effect. Based

on estimates from the work of Tsavalas and Sundberg,<sup>1</sup> the wet  $T_g$  of these systems should be around 30 °C, which is in good agreement with the measured values. For the latexes that were synthesized using MMA/S/MAA 80/5/15 (CS1, H1, CTAAH1 and NanoH1), the calculated wet  $T_g$  of is around 80 °C, which is close to the upper limit of what is possible to observe in systems containing significant amounts of water. In the present case, a wet  $T_g$  of around 70 °C could be seen in the case of H1 and NanoH1 but it was not possible to see any transition in the case of CS1.

### 3.3.1 Film formation

Before looking at the film formation behavior of the core/shell and latex blends, the minimum film formation temperature (MFFT) values of the individual latex components was measured and the results can be seen in **Table 3-6**. The MFFT of the samples that contained mainly MMA in their composition (H1, CTAH1 and NanoH1) were greater than 90 °C, while those hydroplasticizable latexes with a significant fraction of EA (H2, CTAH2 and NanoH2) showed much lower values (MFFT $\approx$ 30 °C). Note that in the latter case, the measured MFFTs are substantially lower than the dry  $T_g$ s shown in **Figure 3-2**, and are close to the measured values of the wet  $T_g$ s which suggests that there is a substantial effect of hydroplasticization that lowers MFFT. Despite the clear hydroplasticization effect on the MFFT, no major differences in the drying times were seen for the hydroplasticizable latexes in comparison to L1 (see **Figure S3-1A in Appendix 3**) as measured by the rate of weight loss during film formation.

**Table 3-6** – MFFT of individual latex components.

<b>Sample</b>	<b>MFFT (°C)</b>
<b>L1</b>	7
<b>H1</b>	>90
<b>H2</b>	25
<b>CTAH1</b>	>90
<b>CTAH2</b>	27
<b>NanoH1</b>	>90
<b>NanoH2</b>	31

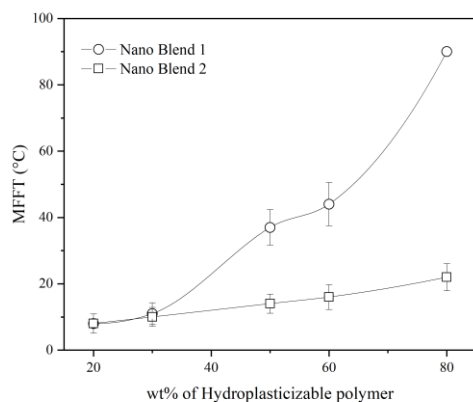
In multiphase latexes particles, the glass transition temperature of each component plays a role in the MFFT of the latexes. However, the structural features of the particles can strongly affect particle deformation during the film formation process. **Table 3-7** shows the MFFT of the core/shell particles and the blends prepared in this work for which the fraction of hydroplasticizable polymer is identical in every case (30 wt%). As can be seen, all the blends have MFFTs around 11°C, independent of the  $T_g$  of hydroplasticizable component used. Comparison of Blend 1 with Blend CTAH1 and Blend 2 with CTAH2 shows that there is also limited effect of the reduction of the molar mass, with the MFFT close to the MFFT of the acrylic latex L1. This is common for latex blends, where the MFFT is largely determined by the MFFT of the majority phase, which in this case is latex L1.

**Table 3-7** – Minimum film formation temperature of core/shell latexes and latex blends.

Samples	MFFT (°C)
CS1	60
CS2	20
Blend 1	10
Blend 2	<5
Blend CTAH1	13
Blend CTAH2	13
Nano blend 1 30%	12
Nano Blend 2 30%	11

To understand the effect of the hydroplasticizable polymer content on the film properties, blends containing different hydroplasticizable polymer ratios were prepared and the MFFTs were analysed for Nano blend 1 and Nano blend 2. **Figure 3-3** shows the MFFT of the blends as a function of hydroplasticizable polymer content. As can be seen, the MFFT of both systems increases with the increase in content of hydroplasticizable polymer in their compositions. At low wt% of hydroplasticizable polymer, both blends show relatively low MFFT values (below ambient temperature). However, as the amount of hydroplasticizable polymer increases the two systems show significant differences; For Nano blend 1 the MFFT increases significantly, reaching the upper limit of the measurement, while for Nano blend 2 even with 80wt% hydroplasticizable polymer the MFFT only increased to 22 °C. This behaviour can be attributed the wet  $T_g$ s of the hydroplasticized polymers, as the higher  $T_g$  of NanoH1 leads to the sharp increase in MFFT. Thus, in blend systems the hydroplasticization effect can be used to form films containing

significantly higher amounts of high  $T_g$  polymer than is possible in conventional systems. Note that the drying profile in these systems was independent of the content of hydroplasticizable polymer, indicating that even at relatively high concentrations of hydroplasticizable polymer, there is only a limited effect on the drying process itself (**Figure S3-1B in Appendix 2**). With respect to the results shown in Chapter 2 the comparatively limited effect on the drying process for these systems may be due to lower amounts of adsorbed water as compared to the soluble resins described in Chapter 2.



**Figure 3-3** – Minimum film formation temperature as a function of hydroplasticizable polymer content for Nano blend 1 and Nano blend 2.

In contrast to the blend systems where even at low hydroplasticizable polymer content the MFFT was not significantly affected, in the case of core/shell particles, the high  $T_g$  of the polymer located on the shell requires a higher temperature to deform into a continuous film. In the case of CS2, hydroplasticization leads to a sufficient reduction of the  $T_g$  in the wet state to

allow film formation to occur close to ambient temperature. In the case of CS1, although the MFFT is clearly reduced compared to the MFFT of the shell layer alone (MFFT of H1 latex is >90 °C), it is not sufficient to reduce the MFFT to a practically useful temperature.

### 3.3.2 Mechanical properties

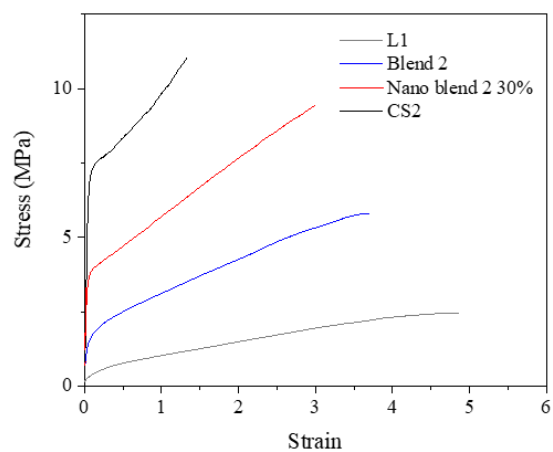
The tensile properties of latexes that were able to form a film at temperatures lower than 22°C (*i.e.* excluding CS1) were analyzed. The results for CS2, Blend 2 and Nano Blend 2 30%, which have identical polymeric components but are present in different initial colloidal states (see **Scheme 3-1**) are shown in **Figure 3-4** and summarized in **Table 3-8**. Looking first at the CS2 system and comparing with the standard acrylic latex L1, it can be seen that the inclusion of the hydroplasticizable polymer in the shell results in a large increase in the Young's modulus, yield stress and stress at break. This effect can be attributed to the presence of a honeycomb structure of the glassy polymer that remains after all water is evaporated from the initially hydroplasticized shell polymer as shown in the TEM images of cross-sections of the film (**Figure 3-5**). AFM images of the film surface also support this idea and show the presence of a honeycomb structure (see **Figure 3-6A**) where only the hard hydroplasticizable polymer that remains after drying can be observed as the soft core is encapsulated.

Turning to the results with the blends, similar to the core shell sample, the presence of the high  $T_g$  polymer that remains following evaporation of water from the hydroplasticizable polymer results in an increase in the Young's modulus, yield stress and stress at break in all cases when compared to the standard latex L1. However, the extent of reinforcement is strongly dependent on the particle size of the hydroplasticizable polymer used. In the case of Blend 2

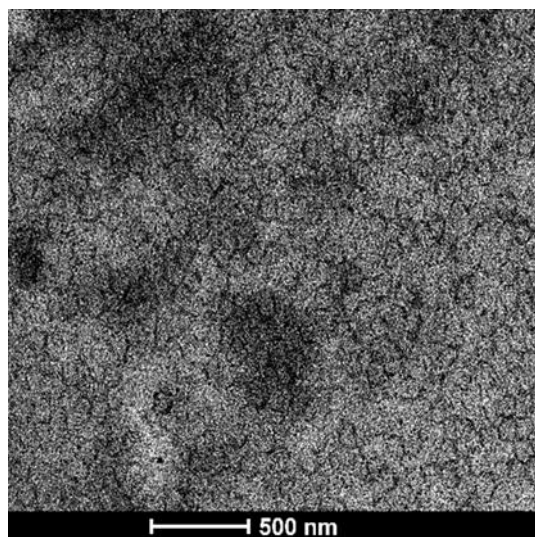
the large particle size of the hydroplasticizable polymer results in a system in which the film structure would be expected to be a continuous matrix of L1 with the hydroplasticizable domains dispersed.<sup>7</sup> Indeed, this structure can be observed by AFM (see **Figure 3-6B**). As a result, the glassy polymer is dispersed and does not increase the mechanical properties to a huge extent. Similar results in terms of mechanical properties were also observed with the corresponding blend samples containing chain transfer agent (see **Figure S3-2 in Appendix 2**). In contrast, as the particle size of the hydroplasticizable polymer for NanoBlend 2 is substantially smaller, the hydroplasticizable latex tends towards a more continuous network structure (see **Figure 3-6C**) and therefore the Young's modulus increases.

**Table 3-8** – Tensile properties of samples presented in **Figure 3-4**.

<b>Samples</b>	<b>Young's Modulus (MPa)</b>	<b>Yield Strength (MPa)</b>	<b>Ultimate tensile Strength (MPa)</b>
<b>CS 2</b>	150 ( $\pm 1$ )	7.4	10.9
<b>Nano Blend 2 30%</b>	98 ( $\pm 2$ )	3.9	9.5
<b>Blend 2</b>	24 ( $\pm 1$ )	1.5	5.8
<b>L1</b>	-	-	2.7

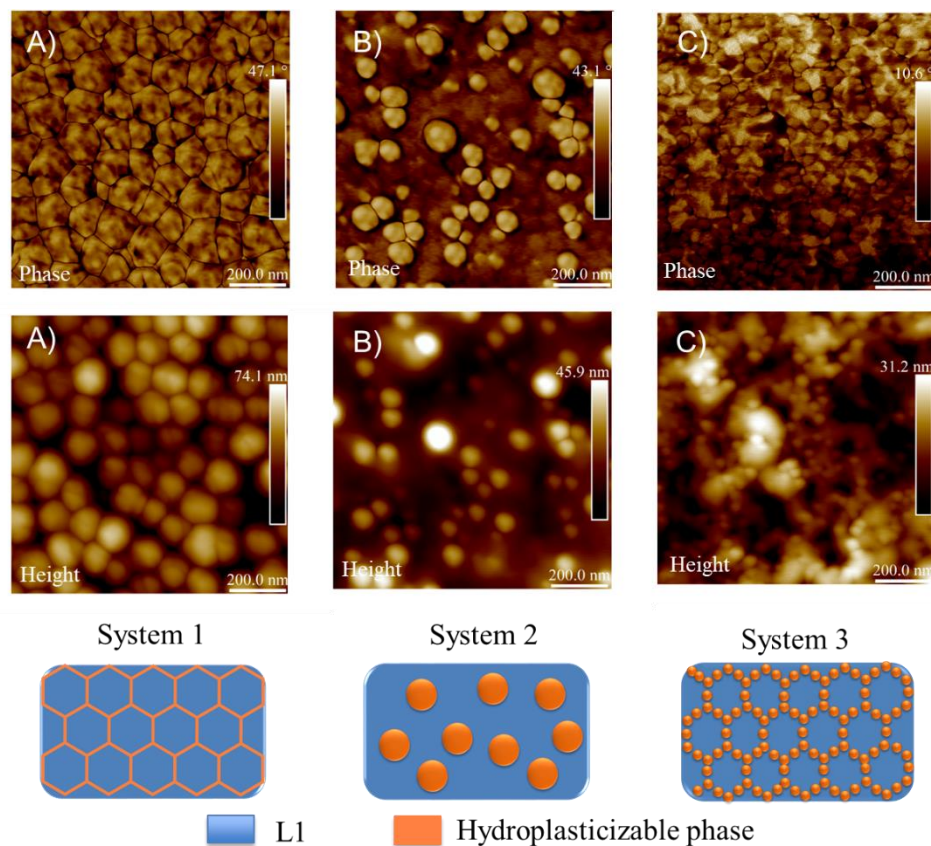


**Figure 3-4** – Tensile properties of core/shell latexes and blends.



**Figure 3-5** – TEM images of the cross-section of film CS2.

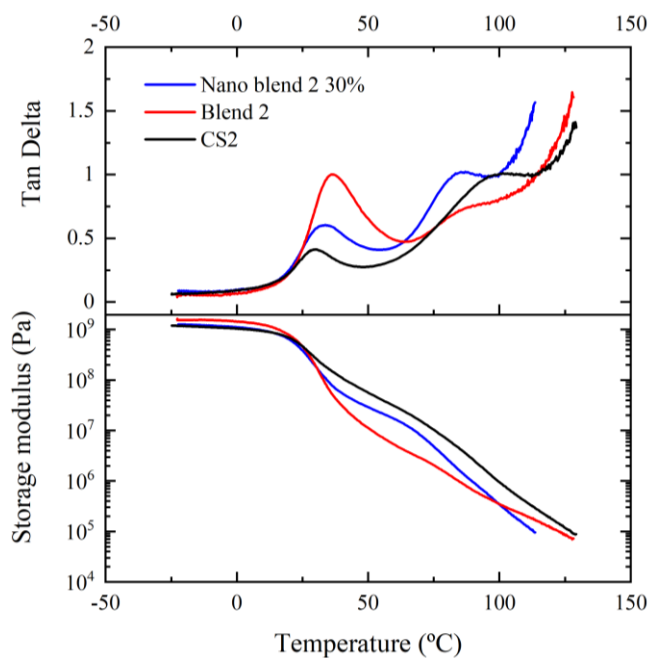




**Figure 3-6** – AFM phase (top) and height (bottom) images of the top surface following film formation of (A) CS2, (B) Blend 2 and (C) Nano Blend 2 30 %.

These differences can also be observed in the thermomechanical properties of Nano Blend 2 30%, Blend 2 and CS2, which were investigated via DMTA as shown in **Figure 3-7**. The  $\tan(\delta)$  curves show two peaks at 25°C and 75°C, which correspond to the  $T_g$ s of the soft (MMA/BA) and hard (MMA/EA/S/MAA) phases, respectively. After the first glass transition

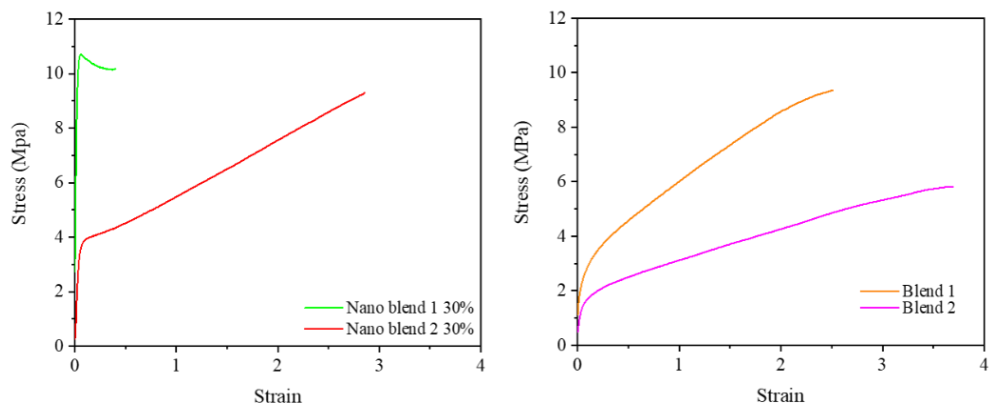
temperature, the storage modulus ( $G'$ ) of all three films decreased. However, the film Blend 2 shows a considerable reduction in  $G'$  when compared to the other films. As discussed above, this result is attributed to the differences in the film structure, where for sample Blend 2, the continuous phase is composed mostly of MMA/BA, while for Nano Blend 2 30% and CS2 the glassy, hydroplasticizable polymer phase tends towards a more continuous structure.



**Figure 3-7** – DMTA Curves of CS 2, Blend 2 and Nano blend 2 30%.

Although film formation at ambient temperature was not possible in the case of CS1, for Blend 1 and Nano Blend 1, which contain identical polymeric components but in different initial colloidal states, cohesive films were obtained. For films formed at higher temperature (60 °C),

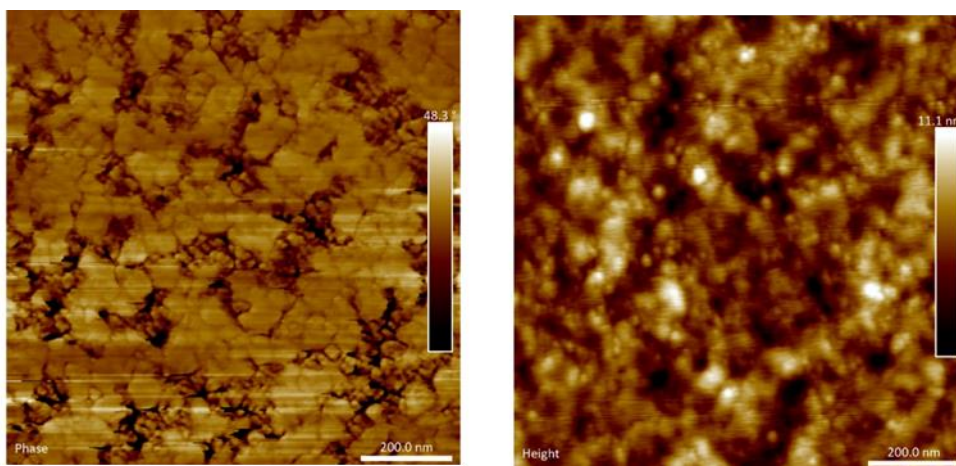
the CS1 system showed exceptionally high modulus in the tensile test (see **Figure S3-3**), which, similar to the discussion above, suggests that the hydroplasticizable polymer forms a continuous matrix. When comparing to the corresponding blends with a lower  $T_g$  hydroplasticizable component (Blend 2 and Nano Blend 2 30%), it can be seen that the higher  $T_g$  results in a significant increase in the Young's modulus (see **Figure 3-8**). In the case of Nano Blend 1 the ultimate strain is low and the sample is brittle. This is likely due to the limited degree of interpenetration of the high  $T_g$  hydroplasticizable polymer that forms a near continuous matrix during film formation as can be seen in the AFM images shown in **Figure 3-9**. Note that similar to the results of the MFFT, the effect of reducing the molecular weight of the hydroplasticizable polymer on the tensile properties was negligible (see **Figure S3-2**).



**Figure 3-8** – Tensile properties of the films cast from Nano Blends (A) and Blends (B).

**Table 3-9** - Tensile properties of the Nano blend and Blend systems

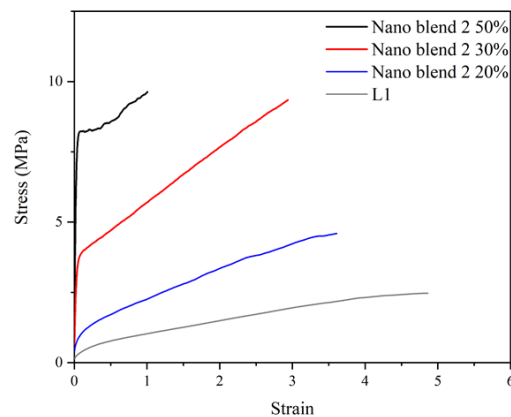
Samples	Young's Modulus (MPa)	Yield Strength (MPa)	Ultimate tensile Strength (MPa)
Blend 1	36 ( $\pm 1.6$ )	2.6	9.2
Blend 2	24 ( $\pm 1.2$ )	1.53	5.8
Nano blend 1 30%	368 ( $\pm 5.4$ )	10.6	10.2
Nano blend 2 30%	98 ( $\pm 2.1$ )	3.9	9.5



**Figure 3-9** - AFM phase (left) and height (right) images of films surface following film formation of Nano Blend 1.

In order to see the influence of the hydroplasticized polymer content on the mechanical properties of the films, blends of NanoH2 and L1 were used to prepare films with varying

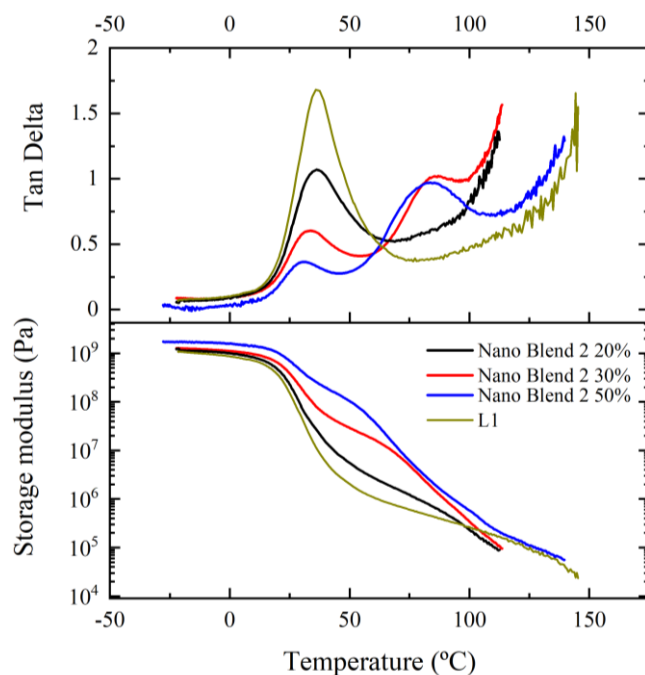
hydroplasticizable polymer content and their tensile properties were measured. The tensile properties of the samples can be found in **Figure 3-10** and **Table 3-10**. It can clearly be observed that the ultimate tensile strength, yield stress and Young's modulus increase with the hydroplasticizable polymer content. The thermomechanical properties of the film containing different amounts of hydroplasticizable polymer content were also investigated by DMTA and the results are presented in **Figure 3-11**. As can be seen, similar to the DMTA results discussed for **Figure 3-7**, a relatively low glass transition temperature corresponding to latex L1 and a high glass transition temperature at around 70 °C corresponding to the dry  $T_g$  of the hydroplasticizable polymer was observed. As the hydroplasticized polymer content increased, the value of the modulus between the two  $T_g$ s also increased in agreement with the tensile data.



**Figure 3-10** – Tensile properties of the Nano Blend 2 with varying hydroplasticizable polymer content.

**Table 3-10** – Tensile properties of Nano Blends.

Samples	Young's Modulus (MPa)	Yield Strength (MPa)	Ultimate tensile Strength (MPa)
L1	-	2.7	2.7
Nano blend 2 20%	11 ( $\pm 0.4$ )	1.05	4.60
Nano Blend 2 30%	98 ( $\pm 2.1$ )	3.94	9.50
Nano blend 2 50%	182 ( $\pm 8.9$ )	8.24	9.60

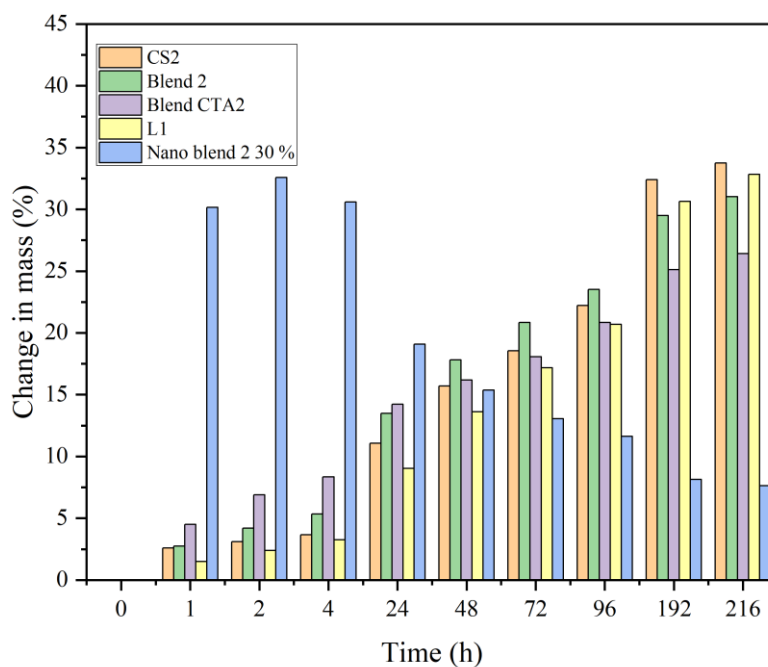
**Figure 3-11** – DMTA Curves of films prepared with Nano Blends 2 containing varying hydroplasticizable polymer content and MMA/BA latex (L1).

### 3.3.3 Water sensitivity of films with hydroplasticizable domains

The discussion above has focused on the positive effects that the hydroplasticizable polymer can have on the MFFT and mechanical properties has so far ignored the potential drawbacks associated with having a high fraction of water sensitive polymer in the system. Considering this, water uptake measurements, in which the change in mass was recorded over time, were performed for L1, CS2, Blend 2, Blend CTA2, and Nano Blend 2 30%. The results can be found in **Figure 3-12**. Most samples showed similar behavior with the exception of Nano blend 2, which showed significant increase in mass during the first day before decreasing on the second day until reaching a plateau. The anomalous behavior of Nano Blend 2 30% can be attributed to the considerable amount of surfactant used to synthesize NanoH2. This excess of surfactant initially absorbs water before being dissolved and released, resulting in a subsequent reduction in the measured weight. In contrast, the other samples all show a slow increase in the mass due to uptake of water, reaching near equilibrium values at approximately 9 days. Remarkably, there was almost no difference in water uptake between the hydroplasticizable systems and the blank latex L1, which contains no hydrophilic co-monomer.

This relatively limited change in water sensitivity compared to conventional systems can be understood by considering the hydroplasticization model of Tsavalas and Sundberg.<sup>1</sup> With a hydroplasticizable polymer with MMA/EA/S/MAA composition of 40/40/5/15, as used in the hydroplasticizable component of the samples shown in **Figure 3-12**, the estimated amount of water absorbed by the hydroplasticizable polymer is 7 wt%. Considering that the hydroplasticizable polymer only makes up 30 wt% of the total formulation, the amount of water absorbed that can be attributed to the hydroplasticizable polymer in the final sample is around 2

wt%. Based on the values in **Figure 3-12**, it is apparent that the amount of water absorbed due to the hydroplasticization effect is negligible when compared to other effects. Thus, by utilizing structured latexes in which the total amount of hydroplasticizable polymer is low, it is possible to utilize the hydroplasticization effect to improve film formation and mechanical properties, whilst avoiding drawbacks associated with water sensitivity.



**Figure 3-12** – Water uptake measurement of CS2, Blend 2, Blend CTA2, L1, Nano Blend 2 30%.



### 3.4. Conclusions

In conclusion, in this chapter it has been highlighted that the hydroplasticization effect can be utilized advantageously to result in low MFFT, high modulus films. When the hydroplasticizable component is placed in the shell of a core/shell latex, the film formation properties are highly dependent on the wet  $T_g$  of the shell polymer ( $MFFT \approx T_{g, wet}$ ). Following film formation, a continuous phase of the shell polymer is formed which leads to a very high modulus. In the case of latex blends, the MFFT was substantially lower and was determined largely by the other non-hydroplasticized component of the latex blend. The hydroplasticization effect was only noticed at high hydroplasticized polymer content where the MFFT became dependent on the wet  $T_g$  of the hydroplasticized polymer. In the blend systems, the particle size of the hydroplasticizable polymer played an important role in the mechanical properties, with small particle sizes leading to improved mechanical properties. Although the absorption of small amounts of water is sufficient to substantially alter the  $T_g$  in the wet state, it is negligible in comparison to the water uptake measured in films. This indicates the design of structured latexes containing a hydroplasticizable component can lead to low MFFT, high modulus films, whilst avoiding drawbacks associated with water sensitivity.

### 3.5. References

- (1) Tsavalas, J. G.; Sundberg, D. C. Hydroplasticization of Polymers: Model Predictions and Application to Emulsion Polymers. *Langmuir* **2010**, *26* (10), 6960–6966. <https://doi.org/10.1021/la904211e>.
- (2) Lei, Y.; Child, J. R.; Tsavalas, J. G. Design and Analysis of the Homogeneous and Heterogeneous Distribution of Water Confined within Colloidal Polymer Particles. *Colloid Polym. Sci.* **2013**, *291* (1), 143–156. <https://doi.org/10.1007/s00396-012-2693-z>.
- (3) Voogt, B.; Huinink, H.; van de Kamp-Peeters, L.; Erich, B.; Scheerder, J.; Venema, P.; Adan, O. Hydroplasticization of Latex Films with Varying Methacrylic Acid Content. *Polymer (Guildf)*. **2019**, *166*, 206–214. <https://doi.org/10.1016/j.polymer.2019.01.074>.
- (4) Dron, S. M.; Paulis, M. Tracking Hydroplasticization by DSC: Movement of Water Domains Bound to Poly(Meth)Acrylates during Latex Film Formation. *Polymers (Basel)*. **2020**, *12* (11). <https://doi.org/10.3390/polym12112500>.
- (5) Nunes, J. D. S.; Asua, J. M. Synthesis of High Solid Content Low Surfactant/Polymer Ratio Nanolatexes. *Langmuir* **2013**, *29*, 3895–3902.
- (6) Nunes, J. D. S.; Asua, J. M. Theory-Guided Strategy for Nanolatex Synthesis. *Langmuir* **2012**, *28* (19), 7333–7342. <https://doi.org/10.1021/la3006647>.
- (7) Tzitzinou, A.; Keddie, J. L.; Geurts, J. M.; Peters, A. C. I. A.; Satguru, R. Film Formation of Latex Blends with Bimodal Particle Size Distributions: Consideration of Particle Deformability and Continuity of the Dispersed Phase. *Macromolecules* **2000**, *33* (7), 2695–2708. <https://doi.org/10.1021/ma991372z>.

## **Chapter 4. Film formation of hard-core/soft-shell latex particles**

### **4.1. Introduction**

In Chapters 2 and 3, systems that contained a component that is plasticized by water were used in order to reduce the MFFT, whilst targeting films with good mechanical performance. In the rest of the thesis, the effect of colloidal structure is explored using two phase systems that combine a low  $T_g$  and a high  $T_g$  polymer. In this chapter hard-core/soft-shell latexes are targeted to evaluate the impact of having a soft-deformable shell to promote film formation. To do so, a series of polystyrene-core/soft-shell latexes with varying amounts of hard polystyrene phase and varying soft phase composition are synthesized and the film formation behaviour is studied. The hard-core/soft-shell latexes are compared with latex blends of similar composition. The film formation process is explored using a combination of MFFT measurements and tensile tests to gain an understanding of the physical processes occurring as the dispersion of multiphase latex particles is dried to give a structured film.

## 4.2. Experimental

### 4.2.1 Materials

Methyl methacrylate (MMA, technical grade, Quimidroga), styrene (S, technical grade, Quimidroga) and butyl acrylate (BA, technical grade, Quimidroga) were used without any further purification. Potassium persulfate (KPS, >98%, Sigma Aldrich) and sodium dodecyl sulfate (SDS, >98%, Sigma Aldrich) were used as supplied. Deionised water was used throughout the work.

### 4.2.2 Latex synthesis

#### 4.2.2.1. Preparation of polystyrene core

Two different methods were used to prepare polystyrene latexes. First, semi-batch emulsion polymerization was used to synthesize an initial polystyrene seed (PS1). Polymerizations were carried out in a 1 L glass reactor equipped with a reflux condenser, a stainless steel anchor stirrer, sampling device, a feeding inlet, a Pt-100 probe and nitrogen inlet. The reactor was loaded with the initial charge and the temperature was raised to 80°C under nitrogen flux with constant stirring at 250 rpm. The feeding of the pre-emulsion started when the temperature was equilibrated and was completed in 180 min. The reaction was kept at the reaction temperature for an additional 1 hr for post-polymerization. Seeded emulsion polymerization was used to prepare a polystyrene latex with larger particle size distribution (PS2), using the same reaction procedure as PS1. The amount of each component used in the synthesis can be seen in **Table 4-1**.

**Table 4-1.** Recipe for polystyrene latexes.

Stages	Initial Charge		Pre-emulsion				
Component	Water (g)	SDS (g)	PS1 (g)	Water (g)	SDS (g)	KPS (g)	St (g)
PS1	473	22	-	472	5.4	7.2	955
PS2	120	-	15	375	14	3.9	487

#### 4.2.2.2. Preparation of core/shell latex particles

Seeded semi-batch emulsion polymerization was used to prepare the core/shell particles. The polystyrene latexes were used as seed and a second polymer phase composed of MMA/BA was synthesized. Two different shell compositions were used in this work, the samples named M1 have an MMA/BA composition of 30/70 wt/wt while N1 samples have an MMA/BA composition of 50/50 wt/wt.

The reaction was carried out under similar conditions to the polystyrene synthesis. Briefly, the reactor was loaded with the initial charge and the temperature was raised to 80°C under nitrogen flux. After the temperature was equilibrated, the feeding of the pre-emulsion was started and completed in 180 min. The reaction was kept at the reaction temperature for an additional 1 hr for post-polymerization for both procedures. **Table 4-2** shows the composition of the core/shell latexes. The codes for the latex follow the pattern X1(Y/Z); where X corresponds to the composition of the shell, either M for MMA/BA 30/70 wt/wt or N for MMA/BA 50/50 wt/wt, and Y and Z correspond to the relative wt% of core and shell respectively. For example M1(40/60) corresponds to a latex with 40 wt% polystyrene core and 60 wt% shell with MMA/BA composition 30/70 wt/wt.

**Table 4-2.** Composition of M1 and N1 core/shell latexes

Stages		Initial Charge		Pre-emulsion			
Component	C/S Ratio	PS1 (g)	Water (g)	SDS (g)	KPS (g)	MMA (g)	BA (g)
<b>M1</b>	(35/65)	70	66.5	1.2	0.3	19.5	45.5
<b>M1</b>	(40/60)	87	66.5	1.2	0.3	19.5	45.5
<b>M1</b>	(50/50)	130	66.5	1.2	0.3	19.5	45.5
<b>M1</b>	(60/40)	195	66.5	1.2	0.3	19.5	45.5
<b>M1</b>	(65/35)	241	66.5	1.2	0.3	19.5	45.5
<b>M1</b>	(70/30)	303	66.5	1.2	0.3	19.5	45.5
<b>N1</b>	(35/65)	70	66.5	1.2	0.3	32.5	32.5
<b>N1</b>	(40/60)	87	66.5	1.2	0.3	32.5	32.5
<b>N1</b>	(50/50)	130	66.5	1.2	0.3	32.5	32.5
<b>N1</b>	(60/40)	195	66.5	1.2	0.3	32.5	32.5
<b>N1</b>	(65/35)	241	66.5	1.2	0.3	32.5	32.5
<b>N1</b>	(70/30)	303	66.5	1.2	0.3	32.5	32.5

Lastly, a group of core/shell latexes with a larger particle size was synthesized. In this case, PS2 was used as a seed. **Table 4-3** shows the recipes used to obtain the core/shell latexes with a larger particle size. The samples were named M2 and they were prepared only for two core/shell compositions, 65/35 wt/wt and 70/30 wt/wt. The M2 (70/30) and M2 (65/35) latexes were used to explore the effect of the packing fraction of the hard phase. The strategy to increase the packing was blending latexes with different particle sizes. i.e, M1(70/30 wt/wt) and M2 (70/30 wt/wt). The samples were blended with 10, 25, 50, 75 and 90 wt% of M1.

**Table 4-3.** Composition of M2 Core/shell latexes

Stages Component	Initial charge		Pre-emulsion			
	PS2 (g)	Water (g)	SDS (g)	KPS (g)	MMA (g)	BA (g)
<b>M2(65/35)</b>	303	66.5	1.2	0.3	19.5	45.5
<b>M2(70/30)</b>	241	66.5	1.2	0.3	19.5	45.5

#### 4.2.2.3. Preparation of hard/soft latex blends

To compare the film formation process of core/shell latex and the blended system, conventional latexes composed of MAA/BA 50/50 wt/wt and 30/70 wt/wt were prepared via semi-batch emulsion polymerization. The reaction was performed at 80°C under nitrogen flux. The pre-emulsion was fed for 2 h and the sample was kept reacting for an additional hour to finish the polymerization. The composition of the conventional latexes can be found in **Table 4-4**. The blends were prepared by mixing the respective latexes with PS1. The composition of the hard/soft latexes blends were 35/65, 40/60, 50/50, 60/40, 65/35 and 70/30 wt/wt, as the core/shell system.

**Table 4-4.** Composition of conventional latexes

Stages Component	Initial charge		Initiator solution		Pre-emulsion			
	Water (g)	SDS (g)	Water (g)	KPS (g)	Water (g)	SDS (g)	MMA (g)	BA (g)
<b>Latex 50/50</b>	170	1.2	20	1.5	111	4.6	153	153
<b>Latex 30/70</b>	170	1.2	20	1.5	111	4.6	92	214

### 4.2.3 Characterizations

The detailed characterization techniques used to measure the properties of the latexes and films cast from the latexes are provided in Appendix I.

## 4.3. Results and discussion

### 4.3.1 Synthesis of core/shell and conventional latexes.

All the latexes were obtained as stable dispersions with high conversion (> 98%). The samples were characterized in terms of particle size distribution, molecular weight, and gel content. These results are shown in **Table 4-5**. As can be seen, the particle size increased with the increasing amount of the soft-shell used. This is to be expected as the soft shell grows from the seed latex and therefore particle size is directly related to the relative amount of second stage polymer. Based on the particle size of the core/shell latexes relative to the initial PS seed latex, the thickness of the shells varies from 8 nm (M1(70/30) and N1(70/30)) to 19 nm (M1(35/65) and N1(35/65)). These values are in approximate agreement with theoretical calculations based on the relative volume of PS to acrylic polymer, for which estimates of shell thickness range from 5 nm for M1(70/30) and N1(70/30) to 15 nm for M1(35/65) and N1(35/65). The results from the GPC show that the core-shell latexes had a slightly increased molecular weight as well as an increased polydispersity. This result arises due to the presence of a second population of higher molecular weight acrylic chains that is generated in addition to the polystyrene core. In the case



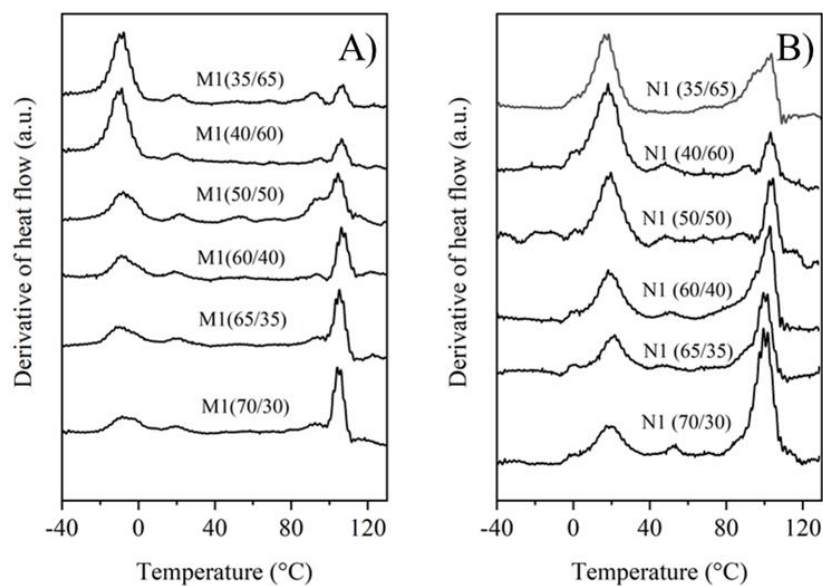
of the M1 latexes this population is of higher molar mass relative to the N1 latexes as the fraction of BA is higher. There was negligible gel content in all cases.

**Table 4-5.** Particle size, molecular weight and gel content of core/shell and conventional latexes.

	Core/shell Ratio	Particle size (nm)	PDI	Mw (kg/mol)	Đ	Gel content (%)
<b>PS1</b>	-	75	0.06	171	3.2	<5
<b>PS2</b>	-	385	0.07	379	5.1	<5
<b>M1</b>	(35/65)	113	0.03	521	4.1	<5
<b>M1</b>	(40/60)	104	0.04	509	4.0	<5
<b>M1</b>	(50/50)	98	0.01	449	3.0	<5
<b>M1</b>	(60/40)	93	0.03	457	3.2	<5
<b>M1</b>	(65/35)	99	0.08	510	3.3	<5
<b>M1</b>	(70/30)	91	0.04	497	3.6	<5
<b>N1</b>	(35/65)	113	0.05	158	2.5	<5
<b>N1</b>	(40/60)	102	0.05	184	3.0	<5
<b>N1</b>	(50/50)	99	0.08	188	3.0	<5
<b>N1</b>	(60/40)	97	0.08	193	3.1	<5
<b>N1</b>	(65/35)	95	0.10	183	2.7	<5
<b>N1</b>	(70/30)	91	0.08	204	3.2	<5
<b>Latex 50/50</b>	-	89	0.03	103	2.4	<5
<b>Latex 30/70</b>	-	81	0.05	142	2.8	<5

The experimental  $T_g$  of samples M1 and N1 were determined via DSC measurements as shown in **Figure 4-1**. In all cases the thermograms showed two distinct  $T_g$ s. The  $T_g$  at around 110 °C can be ascribed to the polystyrene core. A second  $T_g$  was observed at -15 °C for the M1

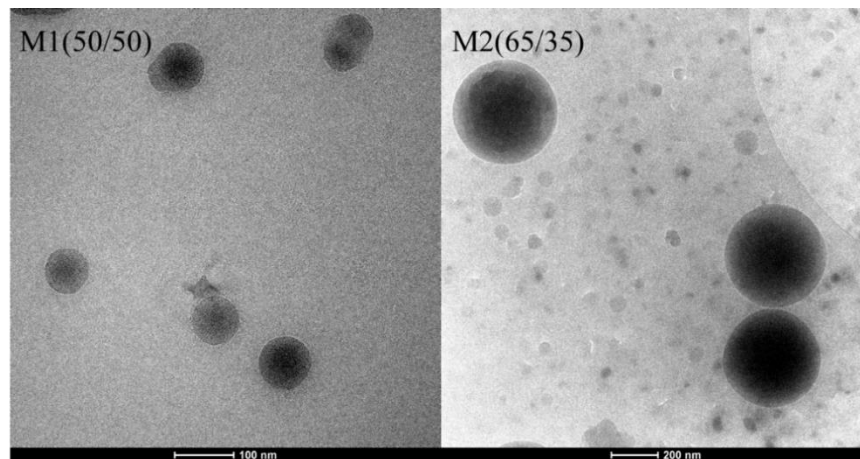
samples and at 15°C for the N1 samples. This shift is in accordance with the increased amount of MMA in the N1 samples which would increase the  $T_g$ . The change in the hard/soft phase can be seen by the area of the peaks, where the area of the low  $T_g$  peak increases with the amount of the soft phase relative to that at 110 °C.



**Figure 4-1** - Plots of first derivative of heat flow obtained from DSC for (A) M1 samples consisting of a soft phase of MMA/BA 30/70 wt/wt and various soft/hard compositions and (B) N1 samples consisting of a soft phase of MMA/BA 50/50 wt/wt and various soft/hard compositions.

Particle morphology in multiphase latex systems can be determined by both thermodynamic and kinetic factors.<sup>22</sup> In this work the hard polystyrene phase is more

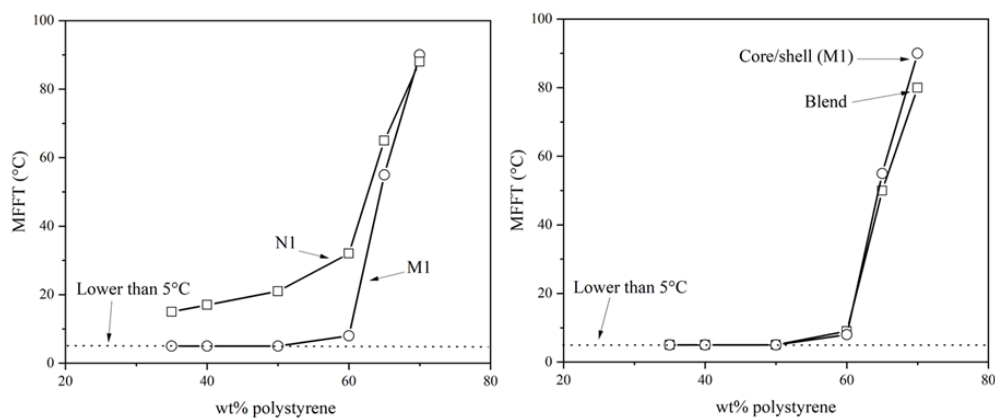
hydrophobic than the soft acrylic phase and therefore the most favorable thermodynamic morphology is a polystyrene core/acrylic shell structure. To confirm this core shell structure, transmission electron microscopy (TEM) was used. The TEM images of M1 (50/50) and M2 (65/35) as representative samples can be found in **Figure 4-2**. As can be seen, the difference in the contrasts shows that the particles are composed of two phases, the center of the particle with higher electronic density and a second phase on the surface, indicating that the phases are arranged in a core-shell like structure where the polystyrene is the core and the acrylic phase compose the shell.



**Figure 4-2** - Transmission electron microscopy image of M1 (50/50) and M2 (65/35).

### 4.3.2. Film formation behaviour of hard-core/soft-shell particles

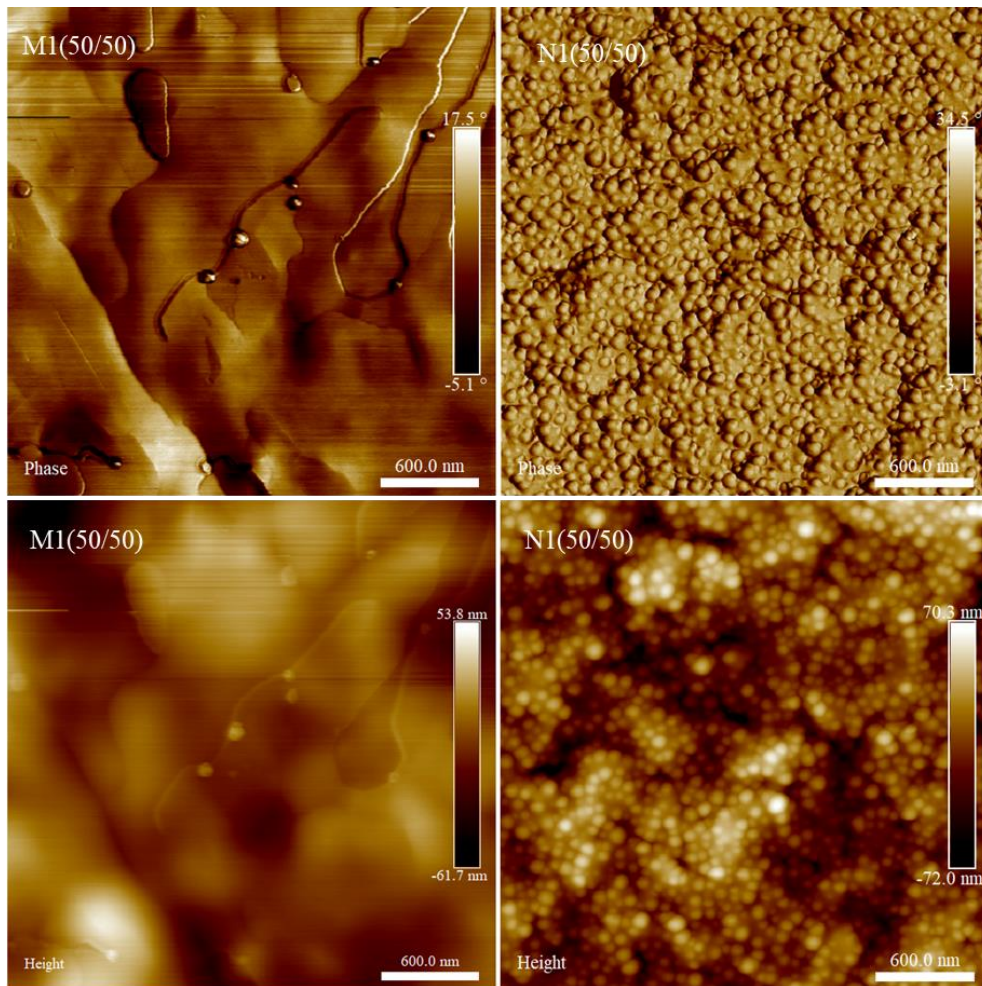
In order to compare the influence of particle structure on the film formation process, the MFFT of the various core/shell latexes was measured. In the case of the M1 latexes, which used a 30/70 wt/wt MMA/BA composition in the shell, the results were compared with blends of homogeneous latex particles with the same hard/soft phase composition using varying weight percentage of PS1 and Latex 30/70. **Figure 4-3** shows the MFFT as a function of polystyrene wt% for the two families of core-shell particles using different shell composition, as well as the comparative latex blends.



**Figure 4-3** (Left) MFFT as a function of wt% polystyrene for the core/shell latexes with soft phase consisting of MMA/BA 30/70 wt/wt (M1, circles) and MMA/BA 50/50 wt/wt (N1, squares). (Right) Comparison of the MFFT as a function of wt% polystyrene for the core/shell latexes with soft phase consisting of MMA/BA 30/70 wt/wt (M1, circles) and blends of single phase latexes of identical composition (PS1 and Latex 30/70).

Looking first at the film formation of the M1 and N1 core-shell latexes, it can be seen that at low amount of the hard phase, the MFFT is basically unaffected. In the case of M1 the MFFT is below the measurable limit in this area, but it can be seen for the N1 system that the MFFT is very close to the  $T_g$  of the soft phase determined by DSC ( $\approx 15$  °C). While at low polystyrene content the MFFT is largely unaffected, for both families of core-shell latexes a critical point is observed around 60 wt%, where the MFFT shows a sharp increase with small increases in polystyrene content. As can be seen from the right panel of **Figure 4-3**, this transition is seen in both core-shell latexes and in latex blends. Taking the density of polystyrene as  $1050 \text{ kg/m}^3$  and the density of the acrylic phase as  $1200 \text{ kg/m}^3$ , a 60 wt% PS latex corresponds to 63 vol% PS. This transition thus corresponds to the approximate limit of random hard sphere packing ( $\phi=64$  vol%) which is understandable given that above this limit deformation of the polystyrene phase would be necessary to prevent large stresses developing in the drying film.

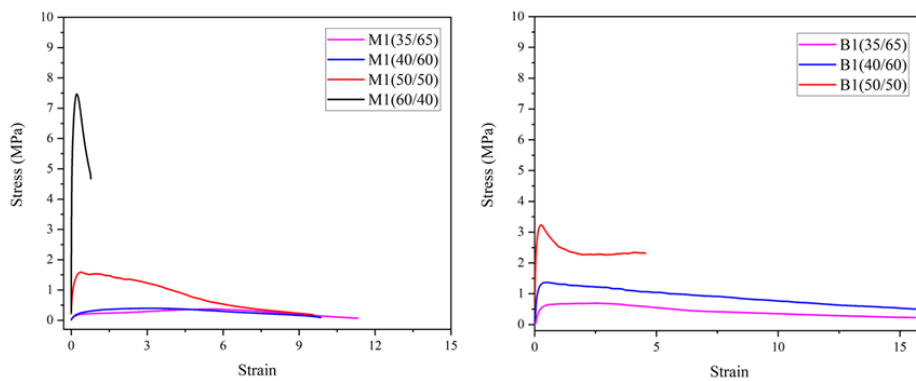
The film structure was examined via atomic force microscopy of the top surface of the film for samples cast from M1(50/50) and N1(50/50) (see **Figure 4-4**). In the case of the latex with the lower  $T_g$  soft phase (M1(50/50)) the surface is more continuous and the polystyrene phase seems to be covered with the soft phase layer. On the other hand, the N1(50/50) sample has a film surface in which the non-deformable polystyrene particles are dispersed in a continuous soft phase matrix. These images indicates that the  $T_g$  of the soft phase polymer affects its phase migration towards the film surface; The lower the  $T_g$  of the soft polymer, the higher the extent of migration.



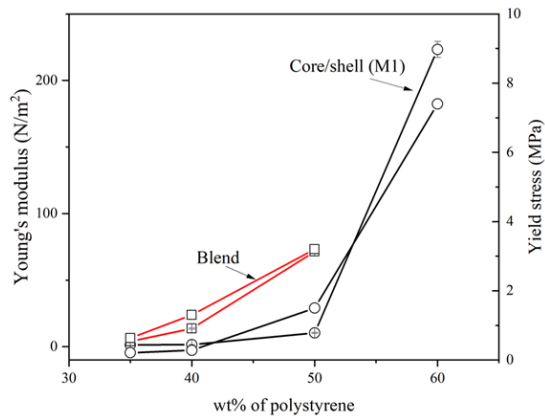
**Figure 4-4** - AFM phase and height images of surfaces of M1(50/50) and N1(50/50) films.

### 4.3.3. Mechanical properties of hard-core/soft-shell systems

The mechanical properties of the blends and core/shell latexes able to form films at room temperature and with approximately the same thickness were analysed using the tensile test. **Figure 4-5** shows the tensile tests for the films cast from the M1 system (MMA/BA 30/70 wt/wt) and the comparative blends of hard and soft latexes. In both cases, at high amounts of the soft phase, the materials show liquid like behaviour with relatively low modulus and a very high elongation at break. For samples containing higher amounts of hard phase the materials show an initial elastic deformation followed by a yield point beyond which significant strain softening occurred. For these samples the yield stress clearly increases with the amount of the hard phase. The Young's modulus was determined for all these samples and the results can be seen in **Figure 4-6**. As expected, the Young's modulus also increases with the amount of the hard phase. In comparison to the latex blends with the same composition, the increase in Young's modulus and yield stress occurs at higher wt% hard phase. However, for the blends, samples with a hard phase content higher than 50 wt% led to crack formation in the case of the thicker films used in tensile measurements. The differences in both the mechanical properties and the film formation behaviour of core/shell and blends latexes is likely due to the increased probability of interconnected hard domains in the case of the latex blends, which hinders film formation but results in a higher modulus.



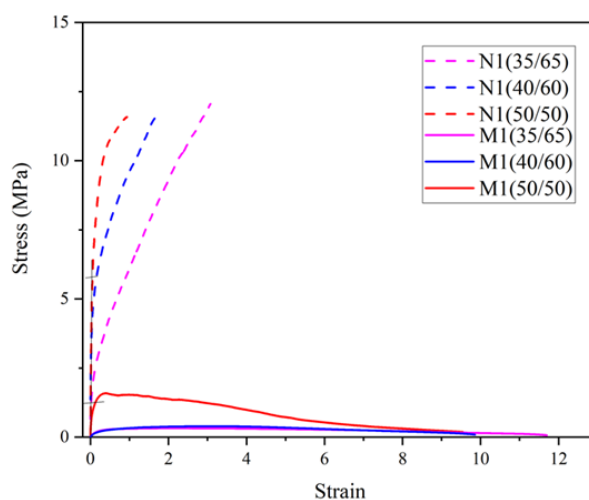
**Figure 4-5** (Left) Tensile properties of the films prepared using core/shell latexes with a soft phase composition MMA/BA 30/70 wt/wt (M1) and (right) with blends (PS1 and Latex 30/70) with different wt% hard phase.



**Figure 4-6** - Young' modulus and yield stress of the films prepared using core/shell latexes with a soft phase composition MMA/BA 30/70 wt/wt (M1) and blends (PS1 and Latex 30/70) with different wt% hard phase.



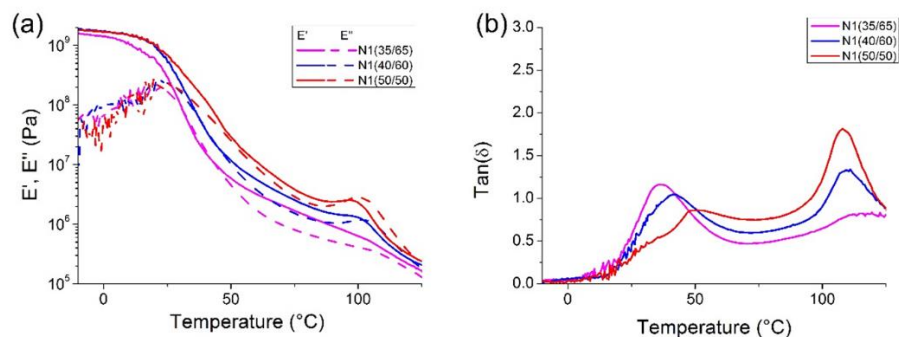
**Figure 4-7** shows the tensile properties for the N1 samples which have a shell composition of MMA/BA 50/50 wt/wt. It can be seen that similar to the M1 samples with the soft shell, the Young's modulus and yield stress increased with the amount of the hard phase. However, the use of a higher  $T_g$  shell in the N1 samples led to a considerable increase in the tensile strength of the films. It is particularly noticeable that above the yield point, M1 samples show a continual decrease in the measured stress, while for the N1 samples the stress continues to increase after the yield point. This suggests that beyond the yield point the mechanical properties are strongly dependent on the soft phase polymer which make the continuous matrix in these samples.



**Figure 4-7** - Tensile properties of the films prepared core/shell latexes with a soft phase composition MMA/BA 50/50 wt/wt (N1) with different wt% shell. For comparative purposes films with a soft phase composition MMA/BA 30/70 wt/wt (M1) are also shown.

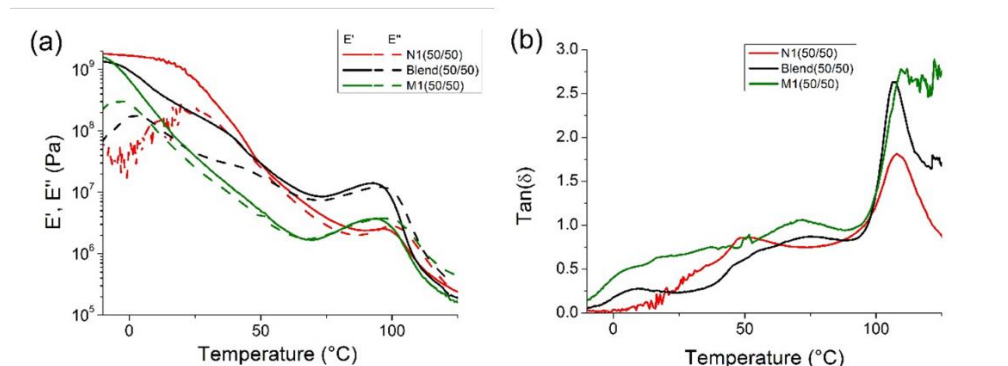
Dynamic mechanical thermal analysis (DMTA) was performed to investigate how the different hard/soft phase ratio would affect thermomechanical behaviour of core/shell latexes films. The analysis was limited to samples able to form a film at room temperature. For this reason, latexes of N1 with amounts of hard phase higher than 60 wt% could not be performed. The storage modulus ( $E'$ ), the loss modulus ( $E''$ ) and  $\tan(\delta)$  as a function of temperature for N1 samples are plotted in **Figure 4-8**. As can be seen, there are two notable transitions at around 30 °C and 110 °C. These events are associated with the glass transition temperature of the soft phase (shell) and hard phase (core), respectively. Comparing the trend in the storage modulus for the three samples, it can be observed that as the wt% of polystyrene increases, the storage modulus in the region between the  $T_g$ 's of the hard and soft phases increases, in agreement with the tensile data above.

Note that in accordance with the Kerner equation <sup>6</sup> for a hard phase dispersed in a soft matrix the modulus in this intermediate region is closer to the modulus of the soft phase ( $E' \approx 10^6$  Pa) than the hard phase ( $E' \approx 10^9$  Pa). This is in contrast to results presented in the previous chapter (see **Figure 3-7**) where due to morphological differences in the film, even though the hard phase (the hydroplasticizable polymer) was present in much lower relative concentrations, the modulus was roughly an order of magnitude higher. This highlights the limitation of the soft-shell strategy for improving the mechanical properties of latex-based films.



**Figure 4-8** DMTA results of films cast from core-shell latexes with different amounts of soft phase consisting of MMA/BA 50/50 wt/wt (N1) (a) Storage and loss modulus and (b) tan delta.

The thermomechanical properties of the core/shell latexes films were also explored in terms of shell composition and the results were compared with the blended system equivalent to the composition of sample M1(50/50). **Figure 4-9** shows  $E'$ ,  $E''$  and  $\tan(\delta)$  as a function of temperature for M1(50/50), N1(50/50) and blend (50/50). As can be seen, for the samples M1(50/50) and blend (50/50) the storage and loss modulus start to decrease at around -5 °C in agreement with the lower  $T_g$  of the soft phase in these systems. Since the hard phase is identical in all cases there is no change in the transition at around 100 °C. In agreement with the tensile results shown above, in the region between the two  $T_g$ s the modulus of the blend system is higher than that of the core-shell latex with identical composition (M1(50/50)). As commented above, this is believed to occur due to the increased possibility of hard phase interconnectivity when simple latex blends are used as compared to the use of hard-core/soft-shell systems in which the soft shell limits direct contact between hard domains.



**Figure 4-9** DMTA results of films cast from core-shell latexes with MMA/BA 50/50 wt/wt (N1) and MMA/BA 30/70 wt/wt (M1) with 50 wt% hard phase. Comparative blends made from PS1 and Latex 30/70 are also shown. (a) Storage and loss modulus and (b) tan delta.

#### 4.3.4. Effect of hard phase packing on the minimum film formation temperature

It was shown above that while increasing the amount of the hard phase leads to an improvement in the stiffness of the resulting film, above 60 wt% hard phase content there is steep increase in the MFFT. This increase was related to the maximum packing fraction of the polystyrene cores within the soft MMA/BA matrix. Above this value there is insufficient soft phase to fill the void between the non-deformable hard phase domains. With this in mind, the MFFT can potentially be manipulated by controlling the size distribution of the hard phase domains. It was thought that using bimodal distributions of particles, the packing fraction of the hard phase domains should be increased such that the MFFT could be lowered for high hard phase contents.

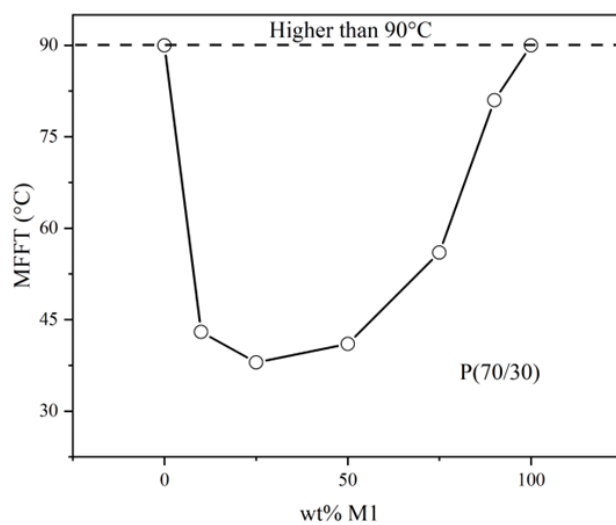
To achieve this goal, an additional latex was synthesized with identical monomer compositions to sample M1(70/30) but with larger particle size. **Table 4-6** shows the samples used to prepare the blend and their respective particle sizes.

**Table 4-6** Particle sizes of core/shell latex particles used to prepare blends with higher packing.

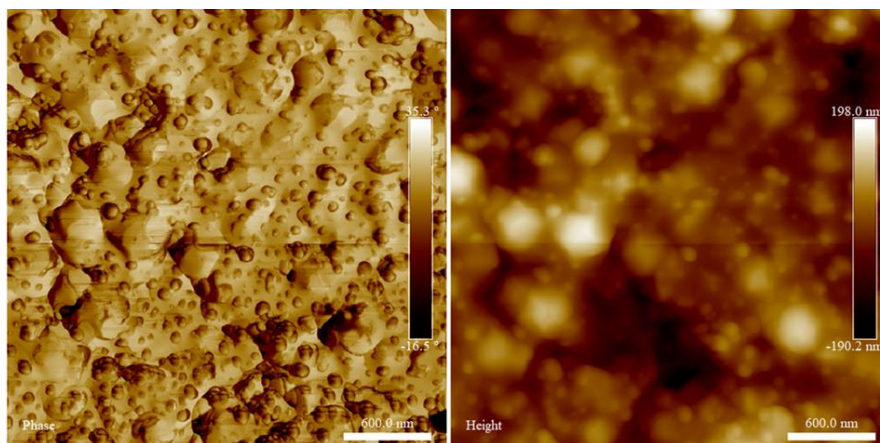
Sample	M1 (70/30)	M2 (70/30)
Size (nm)	91	400
PDI	0.04	0.08

Latex blends were prepared with different amounts of the small and large core-shell latexes. **Figure 4-10** shows the MFFT as a function of small/large ratio for both blends. When the monodisperse samples were used, the MFFT was greater than 90°C (the upper limit of the equipment) in both cases. This is unsurprising as, as commented above, in these systems the amount of polystyrene is above the random packing limit and therefore the  $MFFT \approx T_{g,hard}$ . Remarkably, when the two systems were blended, the MFFT decreased significantly. Thus while both latexes have  $MFFT > 90^\circ C$  the blend with 25 wt% of the smaller particle (M1) showed a reduction of the MFFT by at least 50 °C. This minimum in the MFFT corresponds to the expected maximum in the packing fraction of hard spheres in a bimodal systems.<sup>29</sup> Therefore, the results suggest that when the system is arranged so that higher packing of the hard phase can be achieved, a higher amount of the hard phase can be used before the MFFT is compromised. **Figure 4-11** shows the AFM phase and height images of a film surface for the blend between

M1(70/30) and M2 (70/30) with 25 wt% of small particles. The images shows both large and small hard phase domains dispersed in a continuous soft phase, indicating the formation of a continuous film.



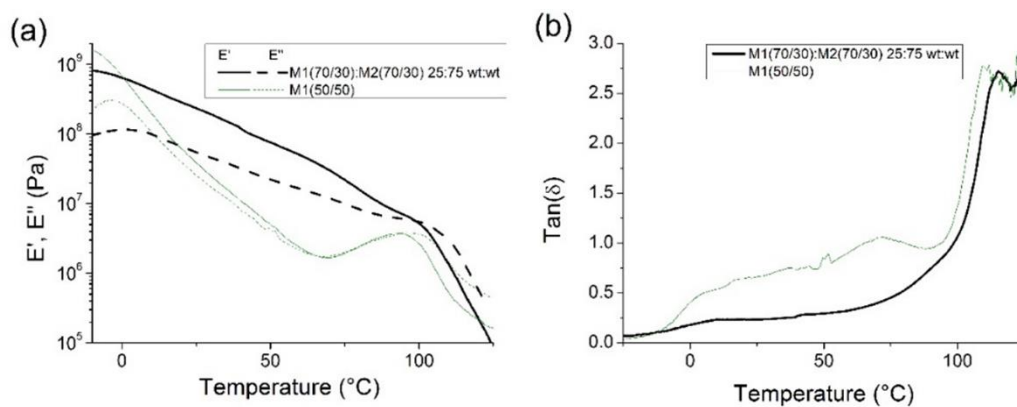
**Figure 4-10** - MFFT as a function of weight % of M1 for the core/shell blend 70/30 wt/wt.



**Figure 4-11** – AFM phase and height images of a film surface dried from a blend between M1(70/30) and M2 (70/30) with the 25wt% of the small particles.

To get an idea of the mechanical properties, films of the blend with 25 wt% M1 (corresponding to the sample with minimum MFFT in **Figure 4-10**) were cast at 50 °C and 60% relative humidity. Similar to the monodisperse sample with high polystyrene content (M1 (60/40)), the film cast from the blend was stiff but also fairly brittle. To get a quantitative measure of the mechanical properties of these systems DMTA was performed. The comparison of the DMTA for this blend, which contains 70wt% hard polystyrene phase, with M1(50/50), which has identical polymer composition but only 50 wt% hard polystyrene phase, is shown in **Figure 4-12**. It can be seen that at higher hard phase content the characteristic drop in the modulus after the soft phase  $T_g$  is reduced and  $E'$  remains higher than  $10^8$  Pa even 50 degrees above than the soft phase  $T_g$ . Furthermore, in the  $\tan(\delta)$  plot it can be seen that there is no major increase in dissipation until the hard phase  $T_g$  is approached. This suggests mechanical behavior that is

more closely related to the polystyrene phase than the soft acrylic component, which may be related to the interconnected structure of the hard phase at very high hard phase content.



**Figure 4-12** – DMTA results of films cast from a core-shell latex blend with hard/soft of 70/30 wt/wt with 25 wt% of M1 and 75 wt% M2. (a) Storage and loss modulus and (b) tan delta. For comparative purposes the DMTA of sample M1(50/50) is also shown.

#### 4.4. Conclusions

The work presented here demonstrates that the film formation of hard-core/soft-shell latex particles can be understood based on the volume fraction of the soft phase, where the shell must fill the void space between the non-deformable core during film formation. In the present work, it



was found that at low amounts of the hard phase, the MFFT values were near the  $T_g$  of the soft phase and were independent of the amount of hard phase. When the amount of the hard phase exceeded 60 wt% the MFFT increased sharply, which was attributed to the volume of soft phase being insufficient to fill the void space between the non-deformable hard phase domains. Importantly, it was shown that the maximum packing fraction of the hard phase can be increased by using bimodal particle size distributions, which leads to systems with a high fraction of the hard phase but low MFFT. However, although the soft-shell structure allows for film formation at relatively high concentration of hard phase, the improvement in mechanical performance is relatively limited due to the dispersed nature of the hard phase in the final film.

#### 4.5. References

- (1) Tsavalas, J. G.; Sundberg, D. C. Hydroplasticization of Polymers: Model Predictions and Application to Emulsion Polymers. *Langmuir* **2010**, *26* (10), 6960–6966. <https://doi.org/10.1021/la904211e>.
- (2) Lei, Y.; Child, J. R.; Tsavalas, J. G. Design and Analysis of the Homogeneous and Heterogeneous Distribution of Water Confined within Colloidal Polymer Particles. *Colloid Polym. Sci.* **2013**, *291* (1), 143–156. <https://doi.org/10.1007/s00396-012-2693-z>.
- (3) Nunes, J. D. S.; Asua, J. M. Synthesis of High Solid Content Low Surfactant/Polymer Ratio Nanolatexes. *Langmuir* **2013**, *29*, 3895–3902. <https://doi.org/10.1021/la400686e>.
- (4) Nunes, J. D. S.; Asua, J. M. Theory-Guided Strategy for Nanolatex Synthesis. *Langmuir* **2012**, *28* (19), 7333–7342. <https://doi.org/10.1021/la3006647>.
- (5) Tzitzinou, A.; Keddie, J. L.; Geurts, J. M.; Peters, A. C. I. A.; Satguru, R. Film Formation of Latex Blends with Bimodal Particle Size Distributions: Consideration of Particle Deformability and Continuity of the Dispersed Phase. *Macromolecules* **2000**, *33* (7), 2695–2708. <https://doi.org/10.1021/ma991372z>.

- (6) Kerner, E. H. The Elastic and Thermo-Elastic Properties of Composite Media. *Proc. Phys. Soc. Sect. B* **1956**, 69 (8), 808. <https://doi.org/10.1088/0370-1301/69/8/305>.

# Chapter 5. Film formation of high poly(vinyl chloride) content latex particles

## 5.1. Introduction

In **Chapter 4**, it was shown that for systems with a low  $T_g$  film forming polymer in the shell, relatively high fractions of hard phase polymer can be incorporated before the MFFT is significantly increased. Although, the improvement in the mechanical properties is limited these systems, it provides an opportunity to incorporate significant amounts of non-film forming polymers into latex systems for use in a number of applications. In this chapter, the potential of incorporating high fractions of poly(vinyl chloride) (PVC) into film forming systems through the synthesis of poly(vinyl chloride) core/acrylic shell latex particles is explored. This could be attractive because although PVC is widely produced as an aqueous dispersion and has relatively low cost compared to many other waterborne polymers, it is not commonly used in film forming applications due to the high  $T_g$ .

With the aim of synthesizing film forming latex particles with high PVC content, this work starts from a series of PVC latexes with particle size ranging from 75 to 800 nm that are used as

a seed in the semi-batch emulsion polymerization of an acrylic polymer to generate a PVC-core/acrylic-shell latex. The film formation properties of these latexes and blends of latexes of different size distributions is explored and the mechanical properties of the final materials are reported.

## 5.2. Experimental

### 5.2.1. Materials

Methyl methacrylate (MMA, technical grade, Quimidroga) and butyl acrylate (BA, technical grade, Quimidroga) were used without any further purification. Ammonium persulfate (APS, >98%, Sigma Aldrich) and sodium dodecyl sulfate (SDS, >98%, Sigma Aldrich) were used as supplied. Poly(vinyl chloride) (PVC) latexes were provided by INOVYN Manufacturing Belgium S.A. and all the latexes were used as received. The properties of the as-received latexes are given in **Table 5-1**. Deionized water was used throughout the work.

**Table 5-1** – Characteristics of the PVC latexes

Samples	Solid content (wt%)	Particles size (nm)	PDI	M <sub>w</sub> (g/mol)	Đ	Gel content (%)
PVC-1	34	76	0.05	1.95 × 10 <sup>5</sup>	2.8	<5
PVC-2	36	385	0.08	1.95 × 10 <sup>5</sup>	3.5	<5
PVC-3	41	820	0.10	-	-	-

## 5.2.2. Latex synthesis

### 5.2.2.1. Preparation of poly(butyl acrylate) (PBA) and poly(methyl methacrylate -co- butyl acrylate) latexes.

The latexes were synthesized via semi-batch emulsion polymerization. The polymerizations were carried out in a jacketed 1 L glass reactor equipped with a reflux condenser, a stainless steel anchor stirrer, sampling device, a feeding inlet, a Pt-100 probe and nitrogen inlet following the recipe shown in **Table 5-2**. The reactor was loaded with the initial charge and the temperature was raised to 80 °C under nitrogen flux with constant stirring at 250 rpm. Following the addition of the initiator solution as a single shot, the pre-emulsion was fed over the course of 120 min. The reaction was kept at the reaction temperature for an additional 1 hr for post-polymerization.

**Table 5-2** – Composition of the poly(butyl acrylate) (PBA) and poly(methyl methacrylate -co- butyl acrylate) latexes.

Latex	-	PBA	P(MMA/BA)
Stages	Component	Amount (g)	Amount (g)
<b>Initial Charge</b>	Water	320	320
	SDS	1.2	1.2
<b>Initiator solution</b>	Water	20	20
	APS	1.5	1.5
<b>Pre-Emulsion</b>	Water	111	111
	SDS	4.6	4.6
	MMA	-	153
	BA	306	153

Seeded semi-batch emulsion polymerization was used to synthesize the PVC/acrylic particles. The size of the PVC used as seed and the composition of the acrylic phase were varied following the recipes given in **Table 5-3**. Note that the mass of PVC reported in **Table 5-3** corresponds to the mass of the latex used in each case, from which the mass of PVC used can be calculated from the solid content (see **Table 5-1**). Different PVC/acrylic ratios were used depending on the composition of the acrylic phase. When PBA was used as the acrylic phase, the PVC/acrylic ratio was 80/20 wt/wt. When an MMA/BA 50/50 wt/wt copolymer was used as the acrylic phase, the PVC/acrylic ratio was 70/30 wt/wt. Polymerizations were carried out in a jacketed 1 L glass reactor equipped with a reflux condenser, a stainless steel anchor stirrer, sampling device, a feeding inlet, a Pt-100 probe and nitrogen inlet. First, the PVC latex was added to the reactor as the initial charge. The temperature was raised to 80 °C under nitrogen flux and mechanical stirring at 250 rpm. The pre-emulsion was fed over the course of 120 min. The reaction was kept at the reaction temperature for an additional 1 hr for post-polymerization.

**Table 5-3** – Composition of the core/shell latexes

Stages	Component	PVC-1 /PBA	PVC-1 /P(MMA/BA)	PVC-2 /PBA	PVC-2 /P(MMA/BA)	PVC-3/PBA
<b>Initial Charge</b>	PVC-1 (g)	772	475	-	-	-
	PVC-2 (g)	-	-	764	444	-
	PVC-3 (g)	-	-	-	-	648
	Water (g)	-	-	-	-	100
<b>Pre- emulsion</b>	Water (g)	35	35	35	35	35
	SDS (g)	1.2	1.2	1.2	1.2	1.2
	APS (g)	0.25	0.25	0.25	0.25	0.25
	MMA (g)	-	32.5	-	32.5	-
	BA (g)	65	32.5	65	32.5	65

### 5.2.3. Characterization

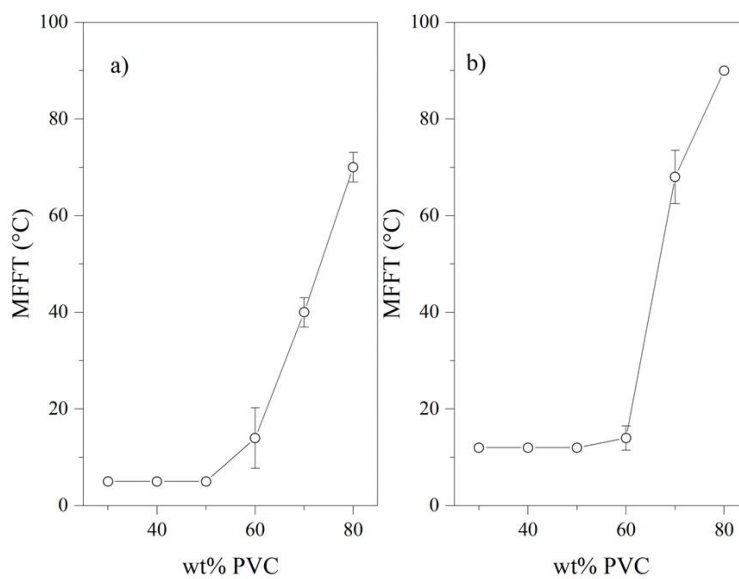
The detailed characterization techniques used to measure the properties of the latexes and films cast from the latexes are provided in Appendix I.

## 5.3. Results and discussion

### 5.3.1. Limits on the PVC content in simple latex blends

To gain an initial insight into the upper limits of PVC content that can be used in latex blends before the film formation process is hindered, blends of low  $T_g$  acrylic latexes and PVC-1 were made. The acrylic latexes were made up of a homopolymer of poly(butyl acrylate) and a copolymer of poly(methyl methacrylate-co-butyl acrylate) with properties shown in **Table S5-1 in Appendix 5**. The blends were prepared varying the weight percentage of PVC-1 relative to the acrylic phase on a dry weight basis and for each blend the MFFT was measured (see **Figure 5-1**). As can be seen, at low fractions of PVC, the MFFT was around 10 °C for the MMA/BA copolymer, which approximately corresponds to its  $T_g$ , and around 5°C for the BA homopolymer (the lower limit of the measurement). Above 60% (wt/wt) PVC the MFFT increased substantially in both cases and at 80% PVC the MFFT approached the  $T_g$  of the PVC homopolymer. Thus, for simple latex blends film formation at ambient temperature is not possible for PVC content greater than 60 wt%. This is in agreement with the results of the previous chapter and previous work on simple latex blends of high  $T_g$ /low  $T_g$  acrylic latexes where a limit for film formation was

established around 55 wt%.<sup>1</sup> Note that when thicker films were targeted to perform mechanical testing some noticeable stratification occurred with an acrylic enriched top surface.



**Figure 5-1** - MFFT as a function of the weight percentage of PVC for the blends of PVC-1 and PBA (a) and blends of PVC-1 and P(MMA/BA) (b) latex blends.

### 5.3.2. Synthesis of PVC/acrylic hybrid latexes.

To try and improve the film formation behavior of high-PVC content systems, a number of PVC/acrylic hybrid latexes were synthesized that targeted a structure in which the low  $T_g$  acrylic phase is predominantly located at the surface of the particles. The different sized PVC



latexes were used as a seed from which to grow the second stage acrylic polymer. The weight fraction between core and shell was different depending on the shell composition. For the PBA shell, 80 wt% of PVC was used, while for the P(MMA/BA) shell 70 wt% of PVC was used. The lower quantity of PVC used in latter system is due to the high MFFT observed for PVC-P(MMA/BA) blends at a ratio of 80/20 wt/wt (see **Figure 5-1**).

In all cases the latexes were obtained as stable dispersions with a solids content around 40 wt%. The molecular weight distribution, the particle size distribution and the  $T_g$ s of the final hybrid latexes are given in **Table 5-4**. The signal in the GPC was dominated by the PVC used as seed and therefore the molecular weight distributions of the final latexes are similar to the initial PVC. The major difference was the presence of some high molecular weight acrylic polymer which led to higher dispersity values. Note that in no case was any significant amount of gel formed.

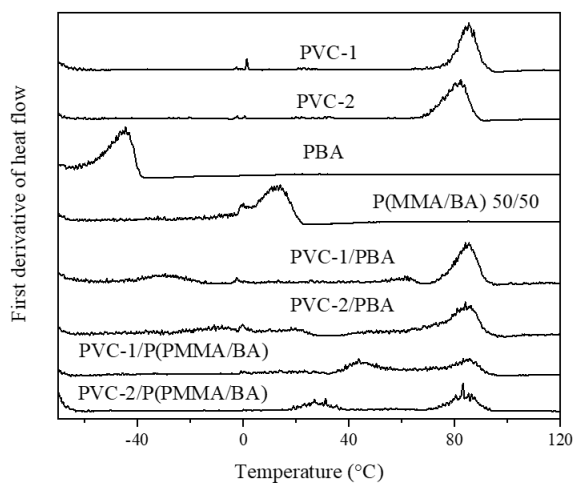
The presence of the acrylic polymer was visible in the DSC, which showed a transition at around 80 °C corresponding to the  $T_g$  of PVC and a second transition at lower values (see **Figure 5-2**). It is important to note that the transition at lower temperatures was substantially higher in the hybrids than the  $T_g$  of the homogeneous acrylic latexes. Thus, while the PBA latex had a  $T_g$  around - 45 °C, in the hybrid the  $T_g$  was broad with an onset at least 20 °C higher. This suggests that the acrylic phase exists as a blend between acrylic and PVC chains, leading to a  $T_g$  of intermediate values. It is important to note that previous work has demonstrated that PVC is in fact compatible with both PBA and PMMA and forms homogeneous blends with a single  $T_g$  when cast from solution.<sup>2</sup> However, for PVC/PBA blends prepared by in-situ polymerization, as performed in this work, Walsh and Sham have reported that for PBA content in excess of 10%

heterogeneous blends with two distinct  $T_g$ s can be observed.<sup>3</sup> This has been attributed to the system passing through a two-phase region during the synthesis.

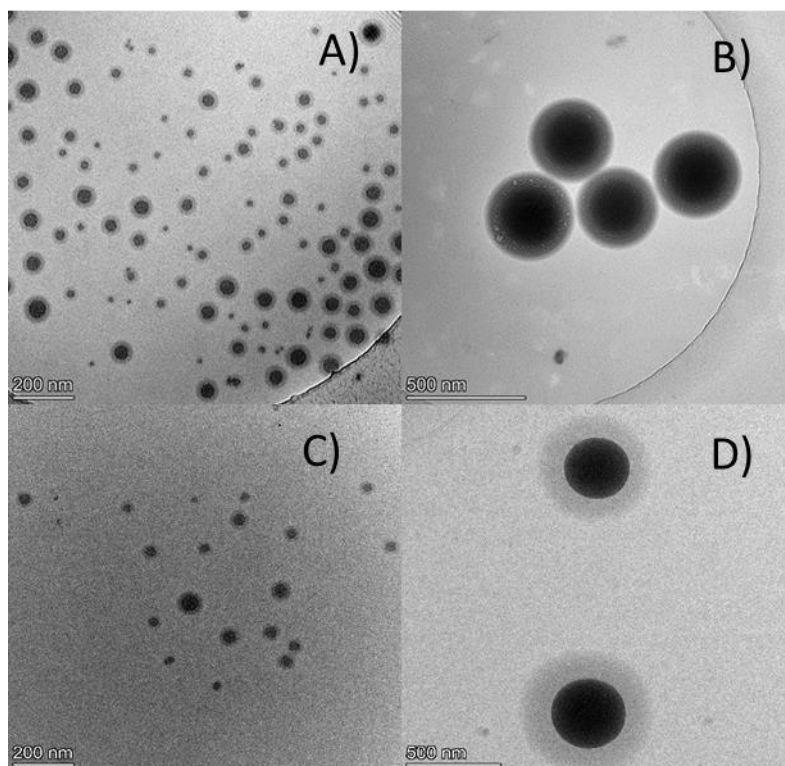
Following polymerization of the acrylic monomers a slight increase in the average particle size of the latexes compared with the PVC seed was observed, which is expected if the acrylic polymer is polymerized within the PVC particle. Analysis of the particle morphology by cryo-TEM demonstrated that the particles have a core-shell structure with a core of PVC and a shell of P(MMA/BA) or PBA (see **Figure 5-3**). As discussed above this shell polymer may also contain some PVC. While monomodal particle size distributions were observed in the case of reactions with PVC-1 and PVC-2 (the PVC latexes with lower particle size), in the case of PVC-3/PBA a bimodal particle size distribution was observed following the polymerization of the acrylic monomer (see **Figure 5-4**). The presence of a small population of particles indicated that secondary nucleation occurred in this system, likely as a result of the low number of particles, which results in an increase in the probability of homogeneous nucleation. In addition, as the total surface area of PVC is decreased for PVC-3, the surfactant added during feeding can exist as micelles, which may promote heterogeneous nucleation.

**Table 5-4** – Characteristics of the core/shell latexes

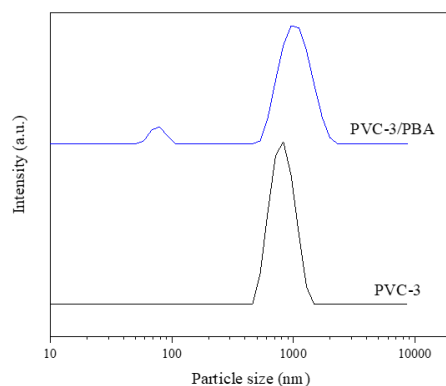
Sample	PVC/acrylic fractions (wt/wt)	Particle size (nm)	PDI	M <sub>w</sub> (g/mol)	Đ	Gel content (%)
PVC-1/PBA	80/20	80	0.06	2.06 × 10 <sup>5</sup>	4.0	<5
PVC-2/PBA	80/20	402	0.06	2.48 × 10 <sup>5</sup>	4.4	<5
PVC-3/PBA	80/20	815	0.38	-	-	-
PVC-1 /P(MMA/BA)	70/30	84	0.05	2.04 × 10 <sup>5</sup>	6.2	<5
PVC-2 /P(MMA/BA)	70/30	410	0.049	2.28 × 10 <sup>5</sup>	3.58	<5



**Figure 5-2** - First derivative of reversible heat flow as a function of temperature measured by DSC for PBA, P(MMA/BA) and PVC/Acrylic samples.



**Figure 5-3** - TEM image of PVC-1/P(MMA/BA) on A), PVC-2/ P(MMA/BA) on B), PVC-1/PBA on C) and PVC-2/PBA core/shell particles on D).



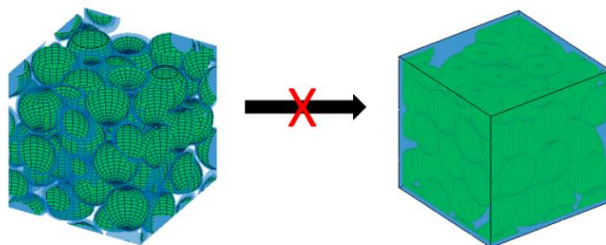
**Figure 5-4** – Particle size distribution of PVC-3 and PVC-3-PBA.

### 5.3.3. Film formation of PVC/acrylic hybrid latexes.

The minimum film formation temperature of the PVC/acrylic latexes was recorded as shown in **Table 5-5**. In all cases the MFFT was above 80 °C which indicates that film formation is dependent on being above the  $T_g$  of PVC. This result is in agreement with the results for simple latex blends shown above for which above 60 wt% PVC there was a steep increase in the MFFT. This observation can be attributed to the relatively low fraction of the film forming acrylic component in the system. As shown in the schematic in **Figure 5-5**, as water is removed the latex will be expected to form a randomly packed structure. In order to form a cohesive film below the  $T_g$  of PVC, the acrylic phase must deform to occupy the void space between PVC domains. However, assuming a randomly packed structure of the PVC domains, 20 wt% acrylic phase is clearly insufficient to occupy the void space and therefore the  $T_g$  of the PVC must be exceeded in order to promote film formation.

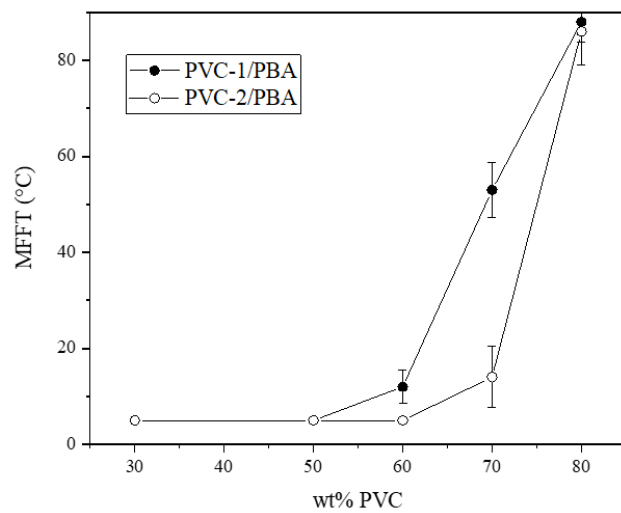
**Table 5-5** – Minimum film formation temperature of PVC/acrylic latexes.

Sample	MFFT (°C)
PVC-1/PBA	88
PVC-2/PBA	86
PVC-3/PBA	87
PVC-1/P(MMA/BA)	90
PVC-2/P(MMA/BA)	86



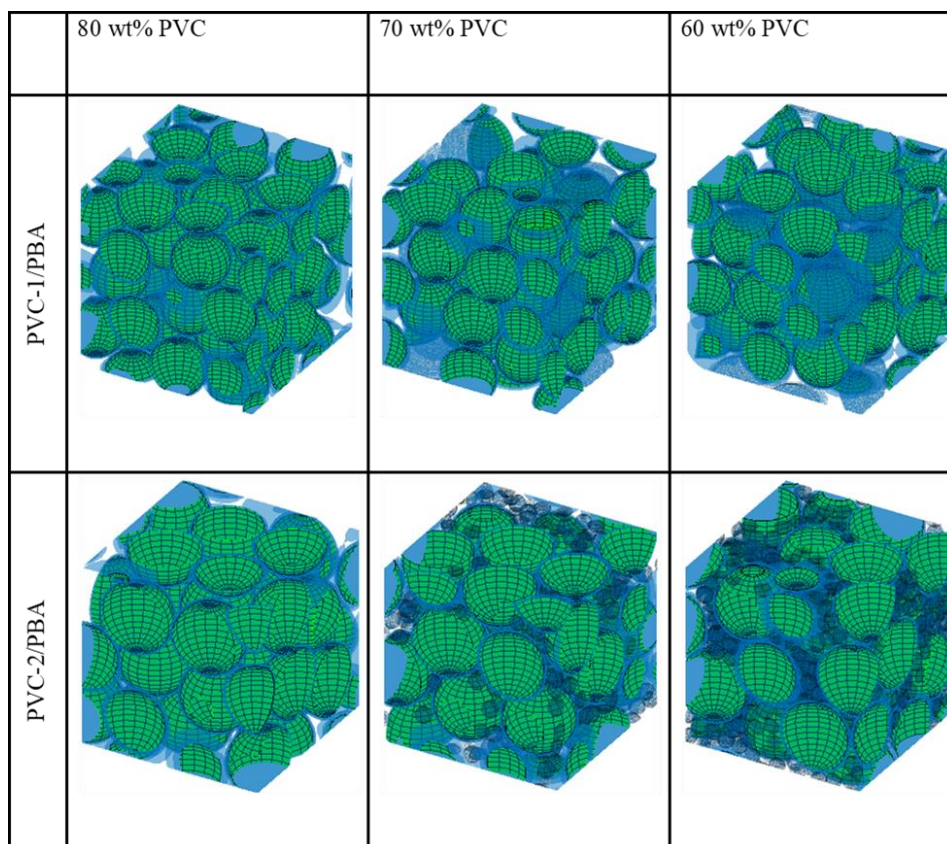
**Figure 5-5** – Schematic showing a 250 nm × 250 nm × 250 nm volume of the packed structures of PVC-1/acrylic core/shell latex at 80 wt% PVC content and the necessary structure for a cohesive film after film formation with the acrylic filling all the void space. The initial structure shows the idealized image of the core/shell structure with the green PVC core and the blue acrylic shell.

In order to promote film formation at lower temperatures the PVC/acrylic latexes made using PBA were blended with the PBA homopolymer latex and the MFFT was recorded. This has the effect of reducing the total PVC content and, as can be seen in **Figure 5-6**, led to a reduction in the MFFT. The reduction of the MFFT by addition of the acrylic latex occurred at lower amounts of added acrylic in the case of the larger PVC-2/PBA core/shell latex. The reason for this likely lies in the relative particle size of the PVC/acrylic hybrids and the PBA latex. In the case of PVC-2/PBA the core/shell latex is significantly larger than the added acrylic latex. As a result, when the latex blend is dried the acrylic latex is predominantly located in the interstitial spaces between the larger core/shell latex and therefore aids film formation. In contrast, in the case of PVC-1 the core/shell latex is approximately the same size as the added acrylic latex. As a result, in this case the poly(butyl acrylate) is not evenly dispersed and has to undergo substantial movement to fill the gaps between the PVC domains. This is shown schematically in **Figure 5-7** which compares the packed structures of PVC-1/PBA, PVC-2/PBA and blends of these latexes with PBA at different total PVC content. The packed structures were generated for latex blends using the collision-driven packing generation algorithm reported by Skoge et al.<sup>4</sup> It may be noted that although there are differences between the MFFTs, these improvements are negligible when compared to the case of the simple latex blends shown in **Figure 5-1**.



**Figure 5-6** - MFFT as a function of the total wt% of PVC for the PVC/acrylic + PBA latex blends.





**Figure 5-7** – Schematic showing packed structures of blends of PVC/acrylic latexes with PBA. Top) 250 nm × 250 nm × 250 nm volume of the packed structures of PVC-1/acrylic core/shell latex with increasing amounts of added PBA (blue). Bottom) 1000 nm × 1000 nm × 1000 nm volume of the packed structures of PVC-2/acrylic core/shell latex with increasing amounts of added PBA (blue).

#### 5.3.4. Film formation of blends of PVC/acrylic hybrid latexes.

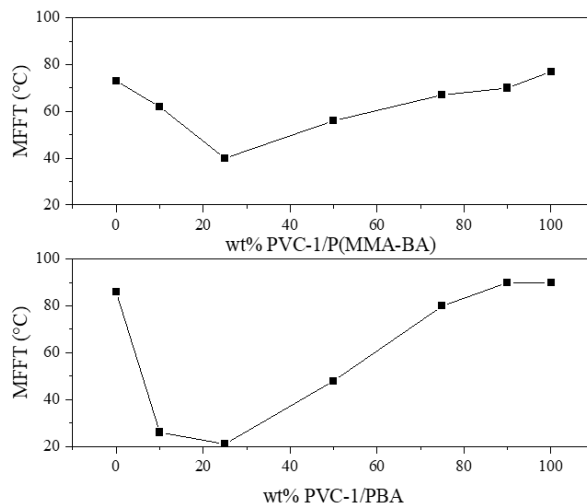
The results above suggest that at high PVC content it is necessary for the system to be above the  $T_g$  of the PVC phase, which can be understood by considering the packing of the spherical PVC latex particles within the low  $T_g$  acrylic matrix. The maximum random packing fraction of monodisperse spherical particles is around 64 vol% and therefore for PVC content above this value there is insufficient acrylic phase to fill in the void space between particles. There are two factors that can increase this limiting value of 64 vol%. The first is a deviation from the spherical PVC domains. This is very difficult to achieve practically, although is the natural effect of increasing the temperature as the PVC domains can be deformed from their initial spherical shape during film formation if the temperature exceeds the  $T_g$ . The second, as discussed in the previous chapter, is a change in the particle size distribution of the PVC domains. While monodisperse spheres have a maximum randomly packed volume fraction of 64 vol%, spherical particles with broad or multimodal size distributions can substantially increase this value.

The effect of the particle size distribution on the MFFT was explored by making blends of the hybrid latexes. In these systems it is known that the maximum obtainable packing fraction of the spherical PVC domains depends on the particle size ratio between large and small PVC particles (L/S); the higher is the ratio, the better is the packing. Considering this, the first system to be investigated was the blends between PVC-1/PBA and PVC-3/PBA. The latexes were blended considering a final system containing 25 wt% of PVC-1/PBA. Unfortunately in this system, phase separation was clearly visible in the final dried film, which had a hard, white phase in the lower portion of the film and a tacky, transparent phase at the surface (see **Figure S5-1** in

**Appendix 4).** Based on the peaks related to the carbonyl stretching of the acrylic phase ( $1729\text{ cm}^{-1}$ ) and the C-Cl stretching of the PVC ( $612\text{ cm}^{-1}$ ) Fourier transform infrared spectroscopy confirmed an enrichment of the acrylic phase at the air-film interface and an enrichment of PVC at the substrate-film interface (see **Figure S5-2 in Appendix 4**). The most likely cause of this was the population of small acrylic particles formed in the PVC-3 system (see **Figure 5-4**). During film formation the larger, denser PVC-rich particles sediment while the smaller acrylic particles will be enriched at the film surface.<sup>5</sup>

Considering the phase separation observed when using PVC-3/PBA, a second set of experiments were performed using blends of hybrids from the PVC-1 and PVC-2 systems. The two core/shell latexes were blended with varying fractions of the smaller core/shell latex particles and the MFFT was recorded for each blend. **Figure 5-8** shows the MFFT as a function of the weight percentage of smaller particles. In both cases it can clearly be observed that while both small and large hybrid particles had an MFFT that was around the  $T_g$  of PVC, by making blends of these high MFFT latexes, a significantly lower MFFT was obtained. In both cases there is a minimum in the MFFT for 25 wt% of the smaller latex particles. Where the shell was composed of PBA, the minimum in the MFFT was around  $20\text{ }^\circ\text{C}$ . where the shell was composed of an MMA/BA 50/50 wt/wt copolymer, the minimum in the MFFT was around  $40\text{ }^\circ\text{C}$ , which is in reasonable agreement with the  $T_g$  of the acrylic phase observed in the DSC (see **Figure 5-2**). The critical film thickness was also evaluated (see **Figure S5-3 (Appendix 4)**), giving a continuous film up to  $350\mu\text{m}$  when PBA shell was used and  $216\text{ }\mu\text{m}$  for the MMA/BA 50/50 wt/wt copolymer shell. Note that the lower MFFT for the P(MMA/BA) system at 0 and 100 wt% is likely

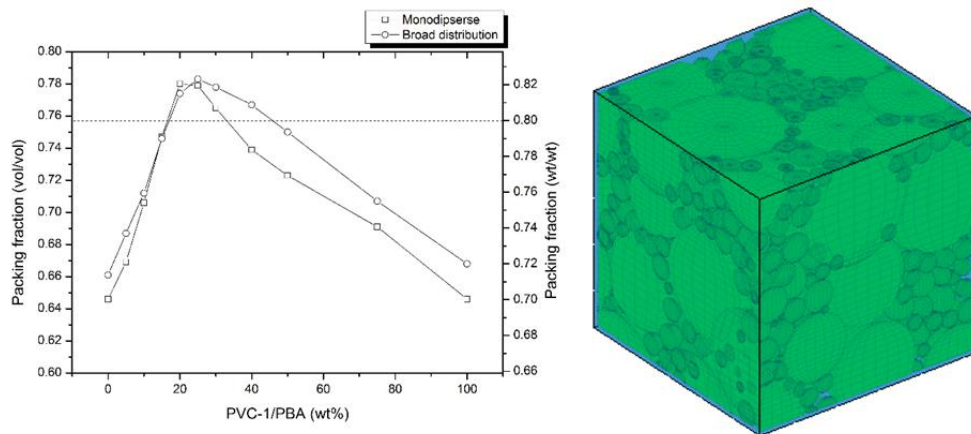
related to the lower initial amounts of PVC for this system (30 wt% as compared to 20 wt% for the PBA system).



**Figure 5-8** – MFFT of core/shell latex blends as a function of weight percent of smaller particles.

These trends in the MFFT are in agreement with theoretical considerations of the packing of bimodal distributions of hard spherical particles. In order to demonstrate this, packing simulations of the PVC phase were performed for a series of blends with the particle sizes of the initial PVC dispersions. Two sets of simulations were performed. In the first case it was assumed that both latexes in the blend consisted of a single particle size, i.e. a blend of two monodisperse latexes was assumed. In the second case, the true particle size distribution of PVC-1 and PVC-2 was considered. In the simulation the particle size distribution was represented as a Gaussian distribution from which particles were randomly selected.

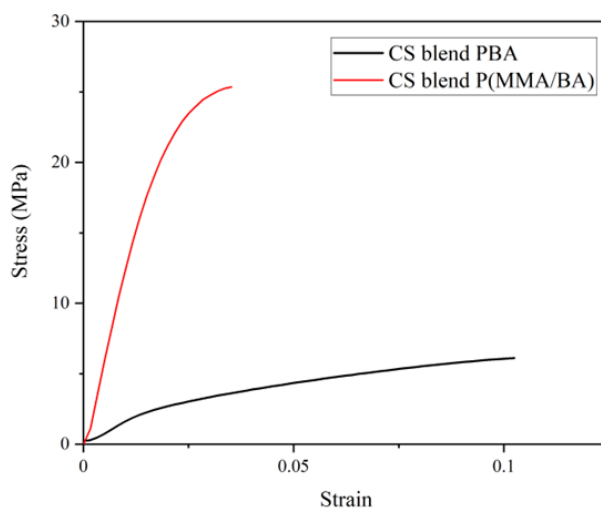
The results from the packing simulations are shown in **Figure 5-9**. It can be seen that the packing fraction has a maximum at ca. 25 wt% of the smaller particles which corresponds to the minimum observed in the MFFT experiments. This is true considering both blends of monodisperse latexes and also when considering the true particle size distributions for both latexes. A maximum volume fraction of PVC of around 0.78 was determined from the simulations which corresponds to a weight fraction of approximately 0.82 assuming a density of  $1.38 \text{ g/cm}^3$  for PVC and  $1.08 \text{ g/cm}^3$  for PBA. Thus, in this case the bimodal nature of the blends means that a lower amount of film-forming acrylic polymer is needed in order to fill the void space between the PVC domains.



**Figure 5-9** – Maximum packing fraction of spherical PVC domains in a poly(butyl acrylate matrix) for different relative amounts of PVC-1 (wt%). The figure shows a packed structure of 78 vol% PVC (green spheres) as a mixture of PVC-1 and PVC-2 at 25 wt% PVC-1/PBA.

### 5.3.5. Mechanical properties of films cast from PVC/acrylic hybrid latexes.

The results above indicate that the shell composition and the packing fraction of the PVC phase can be designed to significantly reduce the MFFT. For both PVC/PBA and PVC/P(MMA/BA) systems the mechanical properties of the blends with lowest MFFT were measured by tensile stress-strain measurements to understand their potential use in real applications. Blends of PVC-1/PBA and PVC-2/PBA at 25:75 wt:wt and blends of PVC-1/P(MMA/BA) and PVC-2/P(MMA/BA) at 25:75 wt:wt were made and the samples were dried in a humidity chamber at 55°C and 55% humidity. **Figure 5-10** and **Table 5-6** shows the tensile properties of the resulting dried films. As can be seen, the blend with P(MMA/BA) in the shell has a Young's modulus of 1302 MPa, while the blend with PBA has a Young's modulus of 178 MPa. The high modulus observed for the core-shell (CS) blend P(MMA/BA) system is a reflection of two different factors. First, the large fraction of PVC leads to a composite with high "hard" phase content and therefore a relatively high modulus would be expected. Second, as shown in the DSC of the polymers in **Figure 5-2**, the  $T_g$  of the acrylic phase is substantially higher than expected on the basis of the polymer composition. As commented above, this is thought to be the result of partial miscibility of the PVC with the acrylic phase and leads to a  $T_g$  above ambient temperature and a high modulus in the tensile test. In the case of the CS blend PBA system the fraction of PVC is higher but the  $T_g$  of the acrylic phase is lower and therefore the Young's modulus and tensile strength is reduced. In both cases the high fraction of hard phase leads to relatively brittle samples with low elongation at break.



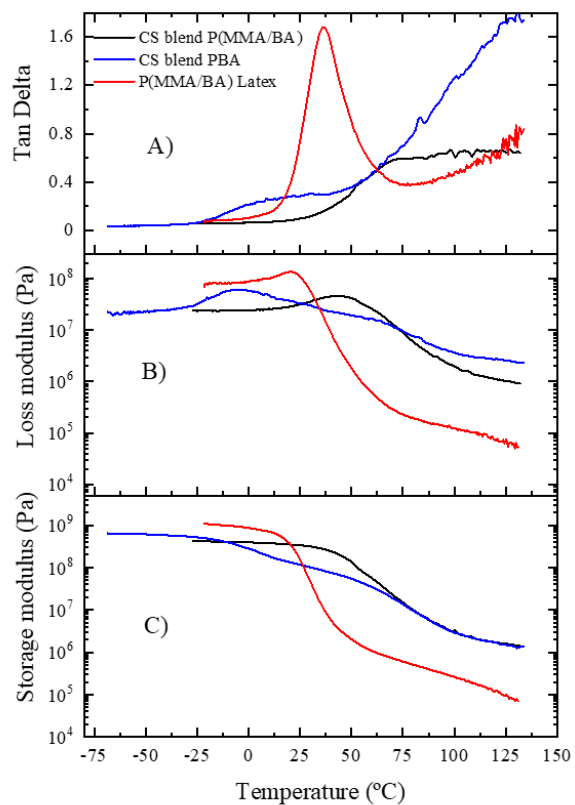
**Figure 5-10** - Tensile properties of the films prepared core/shell latexes blends containing 25% (w/w) of smaller particles. Comparison between shell composed of PBA (CS blend PBA) and P(MMA/BA) (CS blend P(MMA/BA)).

**Table 5-6** – Tensile properties of core/shell latex blends.

Sample	CS blend PBA	CS blend P(MMA/BA)
Young's modulus (MPa)	178.8±1	1302 ± 23
Elongation at break (%)	10	3.5
Ultimate strength (MPa)	6	25

The thermomechanical properties of the core/shell blended films were also explored by dynamic mechanical thermal analysis (DMTA) and the results can be seen in **Figure 5-11**. For comparison, a film cast from the homogeneous P(MMA/BA) latex is also shown. For the homogeneous latex a single relaxation can be observed corresponding to the  $T_g$  of the acrylic copolymer, with an onset of the decrease in storage modulus around 15 °C. Above this temperature there is a significant decrease in the modulus with a plateau modulus of around  $1 \times 10^6$  Pa. In the films cast from the hybrid CS blend PBA system two transitions were observed. At low temperatures the film has a high storage modulus of  $\approx 1 \times 10^9$  Pa as both PVC and acrylic phases are in the glassy state. In agreement  $T_g$  of the acrylic phase in the DSC shown in **Figure 5-2**, starting from -25 °C there is a broad transition above which the value of the storage modulus is reduced to  $\approx 1 \times 10^8$  Pa. As already stated, this transition occurs at significantly higher temperatures than what may be expected for a butyl acrylate homopolymer as the result of some partial miscibility with PVC. Above 70 °C there is the onset of a second transition which corresponds to the  $T_g$  of the PVC phase. This results in a continual decrease in the storage modulus and a continuous increase in  $\tan(\delta)$  with increasing temperatures. In the case of the CS blend P(MMA/BA) system similar behavior is observed although likely due to the overlap of the transitions corresponding to the  $T_g$  of the acrylic and PVC phases a single broad transition is observed with onset around 40 °C.





**Figure 5-11** - DMTA results of films cast from core-shell latexes blends where A) is  $\tan(\delta)$ , B) loss modulus and C) the storage modulus.

## 5.4. Conclusions

In conclusion, in this work it has been demonstrated that film formation of PVC rich latexes can be promoted by targeting particle morphologies and size distributions that maximize the packing of the high  $T_g$  PVC domains in an acrylic matrix. In simple blends of PVC latexes with film forming acrylic latexes, systems with MFFT's below 20 °C were only possible where the  $T_g$  of the acrylic phase was low and where the PVC content was below 60 wt%. In order to obtain film forming systems with higher amounts of PVC in the blend it was shown that increasing the packing density of the PVC in the acrylic matrix is required. This was achieved by blending two PVC core/acrylic shell latexes of different sizes. Using this strategy, it was possible to reach up to 80 wt% PVC content with low MFFT. As a result of the high PVC content, films cast from these latexes had relatively high Young's modulus but were also fairly brittle.

## 5.5. References

- (1) Lepizzera, S.; Lhommeau, C.; Dilger, G.; Pith, T.; Lambla, M. Film-Forming Ability and Mechanical Properties of Coalesced Latex Blends. *J. Polym. Sci. Part B Polym. Phys.* **1997**, *35* (13), 2093–2101. [https://doi.org/10.1002/\(SICI\)1099-0488\(19970930\)35:13<2093::AID-POLB10>3.0.CO;2-](https://doi.org/10.1002/(SICI)1099-0488(19970930)35:13<2093::AID-POLB10>3.0.CO;2-).
- (2) Walsh, D. J.; McKeown, J. G. Compatibility of Polyacrylates and Polymethacrylates with Poly(Vinyl Chloride): 1. Compatibility and Temperature Variation. *Polymer (Guildf)*. **1980**, *21* (11), 1330–1334. [https://doi.org/https://doi.org/10.1016/0032-3861\(80\)90203-7](https://doi.org/https://doi.org/10.1016/0032-3861(80)90203-7).
- (3) Walsh, D. J.; Sham, C. K. In-Situ Polymerization of n-Butyl Acrylate in Poly(Vinyl Chloride). *Polymer (Guildf)*. **1984**, *25* (7), 1023–1027. [https://doi.org/https://doi.org/10.1016/0032-3861\(84\)90091-0](https://doi.org/https://doi.org/10.1016/0032-3861(84)90091-0).
- (4) Skoge, M.; Donev, A.; Stillinger, F. H.; Torquato, S. Packing Hyperspheres in High-Dimensional Euclidean Spaces. *Phys. Rev. E* **2006**, *74* (4), 41127. <https://doi.org/10.1103/PhysRevE.74.041127>.

- (5) Schulz, M.; Keddie, J. L. A Critical and Quantitative Review of the Stratification of Particles during the Drying of Colloidal Films. *Soft Matter* **2018**, *14* (30), 6181–6197. <https://doi.org/10.1039/C8SM01025K>.



## **Chapter 6. Film formation of two-stage acrylic latexes: towards soft-core/hard-shell systems**

### **6.1. Introduction**

In Chapters 4 and 5, the film formation of latex particles composed of hard-core/soft-shell latexes was extensively explored. The results demonstrated that while large fractions of high  $T_g$  non-film forming polymer could be added to these systems without significant increases in the MFFT, the improvement in mechanical properties was limited. In this chapter, two-stage latex particles in which the second stage polymer has a high  $T_g$  are considered. These systems lead to an enrichment of the hard phase at the particle surface, resulting in a soft-core/hard-shell type morphology that should improve the reinforcing effect of the hard phase. However, as discussed in Section 1.4.1.3, previous work targeting a hard shell structure has led to conflicting results, even for relatively similar formulations, with some authors demonstrating evidence for a true

core/shell type structure and others demonstrating a “patchy” structure with small domains of hard phase at the surface (see **Figure 1-9**).

In order to gain a better understanding of the nature of two stage systems in which the second stage polymer has a high  $T_g$ , in this chapter the effect of subtle changes to the particle structure is explored with respect to both the mechanical properties of the final film as well as the film formation behavior. To do so, a series of latexes are synthesized in which the core is composed of a butyl acrylate rich copolymer of varying  $T_g$  and particle size, and the second stage polymer is made up of a methyl methacrylate rich copolymer of varying  $T_g$  with varying volume fractions relative to the core. Firstly, the synthesis of these systems by two-stage semi-batch emulsion polymerization is reported. Subsequently, the film formation behavior and the mechanical properties of the dried films are compared.

## **6.2. Experimental**

### **6.2.1. Materials**

The monomers used in this work, methyl methacrylate (MMA, technical grade, Quimidroga), styrene (S, technical grade, Quimidroga) and butyl acrylate (BA, technical grade, Quimidroga) were used without any further purification. Potassium persulfate (KPS, >98%, Sigma Aldrich) sodium dodecyl sulfate (SDS, >98%, Sigma Aldrich), 1,4-Butanediol diacrylate (BDA,>98%, Sigma Aldrich), tert-dodecylmercaptan (TDM,>98%, Sigma Aldrich) were used as supplied. Deionized water was used throughout the work.

### 6.2.2. Synthesis of seed latexes

Semi-batch emulsion polymerization was used to synthesize the BA, MMA/BA 30/70 wt/wt and MMA/BA 50/50 wt/wt latexes in a 1 L jacketed glass reactor equipped with a nitrogen inlet, a thermocouple, a condenser and a stainless steel anchor-type stirrer. The composition of the latex can be found in **Table 6-1**. For the synthesis of the small-seed latexes, the reactor was loaded with the initial charge and the temperature was raised to 80 °C under nitrogen flux and continuous stirring (250 rpm). After the temperature was equilibrated, the initiator solution was added as a shot. The resultant solution was stirred for 5 min, and then the feeding of the pre-emulsion was started and completed in 180 min. The system was held at the reaction temperature for an additional 60 min. The large-seed latexes were prepared by seeded semi-batch emulsion polymerization, using the previously synthesized small-seed latex particles as a seed. As shown in **Table 6-1** the latexes are coded based on the particle size (small, S, or large, L) and the monomer feed composition (a-e). Composition a is exclusively butyl acrylate. Composition b contains a 0.1 wt% of TDM as chain transfer agent. Composition c contains 0.6 wt% of BDA as crosslinker. Compositions d and e are copolymers of MMA and BA with composition MMA/BA 30/70 and 50/50 wt/wt respectively.

**Table 6-1** – Composition of the core latexes

		<i>Small-seed Latexes</i>					<i>Large-seed Latexes</i>		
<b>Code</b>		S <sub>a</sub>	S <sub>b</sub>	S <sub>c</sub>	S <sub>d</sub>	S <sub>e</sub>	L <sub>a</sub>	L <sub>b</sub>	L <sub>c</sub>
	Reagent	Amount (g)					Amount (g)		
<b>Initial Charge</b>	Seed	0					7 (S <sub>a</sub> )	7 (S <sub>b</sub> )	7 (S <sub>c</sub> )
	Water	220					120		
	SDS	1.5					-		
<b>Initiator Solution</b>	Water	20					-		
	KPS	0.95					-		
	Reagent	Amount (g)					Amount (g)		
<b>Monomer Feed</b>	Water	420	420	420	420	420	575	575	575
	SDS	4	4	4	4	4	4.38	4.38	4.38
	MMA	-	-	-	142	237	-	-	-
	BA	475	475	475	333	237	487	487	487
	BDA	0	0	2.9	0	0	-	2.97	
	TDM	0	0.475	0	0	0	-	-	0.535
	KPS	0	0	0	0	0	0.97	0.97	0.97

### 6.2.3. Synthesis of two-stage latex particles

A series of two-stage latex particles composed of a low  $T_g$  seed and a high  $T_g$  second stage polymer was synthesized via seeded semi-batch emulsion polymerization (**Table 6-2**). The small and large latexes reported in **Table 6-1** were used as seeds. Parameters such as the composition of the hard phase and the ratio of soft/hard polymer were explored. The composition of the hard phase polymer was varied by changing the MMA/EA content with a constant fraction



of 15 % (w/w) of styrene in all the samples. The synthesis was carried out by adding the required amount of seed to the reactor and heating to 80 °C under nitrogen flux with stirring at 250 rpm. After the temperature stabilized, the initiator solution was added as a shot. The amount of water in the initiator solution was adjusted to give final latexes with comparable solid contents. The monomer solution was fed for 30 min. Following monomer addition, the reaction temperature was held for an additional hour in order to ensure complete polymerization. The reaction codes in **Table 6-2** correspond to the type of seed used (small, S, or large, L with composition a-e) and composition (1-4) and weight percentage of second stage polymer (20-40). For example, sample S<sub>a</sub>4-30 corresponds to a latex that is synthesized using seed S<sub>a</sub> (small seed with composition 'a' (100% butyl acrylate)) with 30 wt% of a second stage polymer with composition 4 (MMA/EA/S 42.5/42.5/15 wt/wt/wt).

**Table 6-2** – Composition of two-stage latex particles

	Samples	Ratio	Seed	Initiator solution		Monomer feed			
	Code	Core/shell	type	Amount (g)	KPS (g)	Water (g)	MMA (g)	S (g)	EA (g)
Small particles	S <sub>a</sub> 1-20	80/20	S <sub>a</sub>	100	0.05	15	8.7	1.6	-
	S <sub>a</sub> 1-30	70/30	S <sub>a</sub>		0.08	20	14.5	2.5	-
	S <sub>a</sub> 1-35	65/35	S <sub>a</sub>		0.10	25	18.3	3.2	-
	S <sub>a</sub> 2-30	70/30	S <sub>a</sub>		0.08	20	12	2.5	2.5
	S <sub>a</sub> 3-30	70/30	S <sub>a</sub>		0.08	20	9.4	2.5	5.1
	S <sub>a</sub> 4-30	70/30	S <sub>a</sub>		0.08	20	7.25	2.5	7.25
	S <sub>b</sub> 1-20	80/20	S <sub>b</sub>		0.05	15	8.7	1.6	-
	S <sub>b</sub> 1-30	70/30	S <sub>b</sub>		0.08	20	14.5	2.5	-
	S <sub>c</sub> 1-20	80/20	S <sub>c</sub>		0.05	15	8.7	1.6	-
	S <sub>d</sub> 1-20	80/20	S <sub>d</sub>		0.05	15	8.7	1.6	-
S <sub>e</sub> 1-20	80/20	S <sub>e</sub>	0.05	15	8.7	1.6	-		
Large particles	L <sub>a</sub> 1-20	80/20	L <sub>a</sub>	0.05	15	8.7	1.6	-	
	L <sub>a</sub> 1-30	70/30	L <sub>a</sub>	0.08	20	14.5	2.5	-	
	L <sub>a</sub> 1-35	65/35	L <sub>a</sub>	0.10	25	18.3	3.2	-	
	L <sub>a</sub> 4-30	70/30	L <sub>a</sub>	0.08	20	7.25	2.5	7.25	
	L <sub>b</sub> 1-20	80/20	L <sub>b</sub>	0.05	15	8.7	1.6	-	
	L <sub>b</sub> 1-30	70/30	L <sub>b</sub>	0.08	20	14.5	2.5	-	
	L <sub>c</sub> 1-20	80/20	L <sub>c</sub>	0.05	15	8.7	1.6	-	

### 6.2.4. Characterization

The detailed characterization techniques used to measure the properties of the latexes and films cast from the latexes are provided in Appendix I.

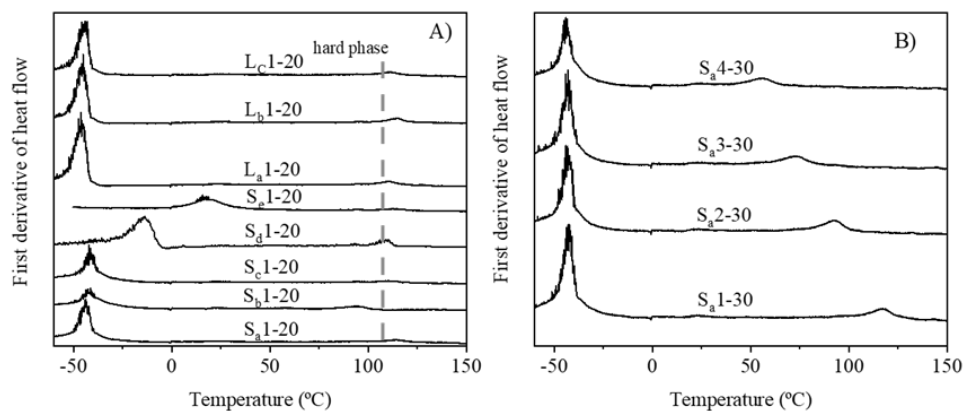
## 6.3. Results and discussion

### 6.3.1. Latex synthesis

All the samples synthesized gave a stable latex dispersion with high conversion (>99%). The main characteristics such as average particle size, molecular weight and gel content can be found in **Table 6-3**. In the latex seeds, two different methods were used for the synthesis, either non-seeded (S series) or seeded (L series) semi-batch emulsion polymerization. As expected, the seeded reactions led to growth of the seeds and therefore the L series of particles has larger size. The other major difference in the seeds was the composition of the polymer. Samples L<sub>a</sub> and S<sub>a</sub> consisted of only butyl acrylate and therefore had significant gel content due to intermolecular chain transfer reactions followed by termination by combination as has been reported previously.<sup>1</sup> In Samples L<sub>b</sub> and S<sub>b</sub> additional chain transfer agent was added which led to a reduction in the gel content. For reactions with small amounts of a crosslinking agent to the system (L<sub>c</sub> and S<sub>c</sub>), slightly higher gel contents were observed when compared to L<sub>a</sub> and S<sub>a</sub>. Lastly, a set of small latex seeds containing MMA/BA 30/70 wt/wt (S<sub>d</sub>) and MMA/BA 50/50 wt/wt (S<sub>e</sub>) in their formulation was synthesized. The gel content of these samples was substantially reduced which may be attributed to a reduction in the extent of intermolecular transfer. Since the butyl acrylate rich seeds make up the majority fraction of the final latexes, these trends are also observed in the final two-stage latexes with a slight reduction in gel content values.

The glass transition temperature ( $T_g$ ) of the seeds and two-stage latexes was determined via DSC and the results can be found in **Table 6-3** and **Figure 6-1**. As can be seen in **Figure 6-1**, the initial poly(butyl acrylate) seeds have  $T_{gS}$  of approximately -45 °C. No significant

differences in the thermal properties were observed comparing the  $S_a$ ,  $S_b$  and  $S_c$  latexes, which are all essentially homopolymers of poly(butyl acrylate). However, for the seeds containing MMA ( $S_a$  and  $S_e$ ), the low  $T_g$  peaks are shifted to higher temperatures as expected. For the two-stage latexes, the presence of the hard phase could be detected at high temperatures, although due to the relatively low amounts the signal was weak compared to that of the BA-rich soft phase. For the case of latexes with a second stage polymer of composition 1, the hard polymeric phase was composed of MMA/S 85/15, giving  $T_g$  values of approximately 115°C (see **Figure 6-1 (A)**). In samples with second stage polymer composition 1-4, the composition of the hard phase was changed by varying the content of ethyl acrylate (EA). As expected, the  $T_g$  decreased with the increase in fraction of EA and the sample  $S_{a4-30}$  with the highest EA content has a  $T_g$  of 52 °C (See **Figure 6-1(B)**).



**Figure 6-1.** DSC thermograms of two-stage latexes with small and large latex particles (A) and with different compositions of hard phase (B)

**Table 6-3** – Characteristics of seeds and two-stage latexes

Sample	Particle size (nm)	PDI	M <sub>w</sub> (g/mol)	Đ	Gel content (%)	Seed polymer T <sub>g</sub> (°C)	Second stage polymer T <sub>g</sub> (°C)
<b>S<sub>a</sub></b>	68	0.04	5.6×10 <sup>4</sup>	2.0	72	-42	-
<b>S<sub>b</sub></b>	67	0.06	7.5×10 <sup>4</sup>	2.1	<5	-42	-
<b>S<sub>c</sub></b>	69	0.04	5.6×10 <sup>4</sup>	1.9	78	-42	-
<b>S<sub>d</sub></b>	79	0.04	6.6×10 <sup>5</sup>	7.4	8	-13	-
<b>S<sub>e</sub></b>	78	0.07	1.1×10 <sup>5</sup>	9.5	9	20	-
<b>L<sub>a</sub></b>	363	0.01	2.5×10 <sup>5</sup>	3.7	66	-47	-
<b>L<sub>b</sub></b>	366	0.02	4.7×10 <sup>5</sup>	6.3	<5	-47	-
<b>L<sub>c</sub></b>	369	0.04	4.8×10 <sup>5</sup>	6.4	88	-47	-
<b>S<sub>a</sub>1-20</b>	73	0.06	7.4×10 <sup>4</sup>	2.1	60	-42	115
<b>S<sub>a</sub>1-30</b>	75	0.04	2.2×10 <sup>5</sup>	4.1	54	-42	117
<b>S<sub>a</sub>1-35</b>	86	0.08	2.3×10 <sup>5</sup>	3.0	58	-42	116
<b>S<sub>a</sub>2-30</b>	76	0.04	2.2×10 <sup>5</sup>	4.6	65	-42	93
<b>S<sub>a</sub>3-30</b>	76	0.07	2.2×10 <sup>5</sup>	4.9	63	-42	72
<b>S<sub>a</sub>4-30</b>	75	0.08	1.7×10 <sup>5</sup>	3.4	57	-42	55
<b>S<sub>b</sub>1-20</b>	73	0.06	1.4×10 <sup>5</sup>	3.0	<5	-42	113
<b>S<sub>b</sub>1-30</b>	75	0.04	2.5×10 <sup>5</sup>	4.0	<5	-42	115
<b>S<sub>c</sub>1-20</b>	72	0.06	1.0×10 <sup>5</sup>	2.8	72	-42	109
<b>S<sub>d</sub>1-20</b>	84	0.05	5.9×10 <sup>5</sup>	7.0	<5	-13	108
<b>S<sub>e</sub>1-20</b>	83	0.08	2.3×10 <sup>5</sup>	8.6	<5	20	112
<b>L<sub>a</sub>1-20</b>	375	0.04	2.0×10 <sup>5</sup>	3.8	55	-47	109
<b>L<sub>a</sub>1-30</b>	393	0.03	2.4×10 <sup>5</sup>	3.1	60	-47	110
<b>L<sub>a</sub>1-35</b>	401	0.02	3.5×10 <sup>5</sup>	3.9	58	-47	112
<b>L<sub>a</sub>4-30</b>	396	0.03	2.0×10 <sup>5</sup>	4.2	61	-47	52
<b>L<sub>b</sub>1-20</b>	376	0.03	3.6×10 <sup>5</sup>	5.7	<5	-47	112
<b>L<sub>b</sub>1-30</b>	390	0.04	4.7×10 <sup>5</sup>	6.1	<5	-47	113
<b>L<sub>c</sub>1-20</b>	375	0.04	1.5×10 <sup>5</sup>	3.5	74	-47	112

The morphology of the two-stage latexes containing different relative fractions of the seed and the second stage polymer were investigated via transmission electron microscopy (TEM) (see **Figure 6-2**). It can be noted that in all cases, there was no significant amount of secondary nucleation observed. This is in agreement with the measured particle sizes shown in Table 3, which are in line with the theoretical values assuming no secondary nucleation. The two-stage latexes show distinct morphologies depending on the content of the hard polymer and the particle size of the seed. On the one hand, the two-stage latexes obtained using the large seed had apparently different morphologies depending on the fraction of hard phase. While a core/shell-like structure was apparent for L<sub>a</sub>1-35, when the amount of second stage polymer was reduced, sample (L<sub>a</sub>1-20), a more “patchy” surface structure was observed, which implies incomplete shell formation at the particle surface as has previously been observed.<sup>2,3</sup>

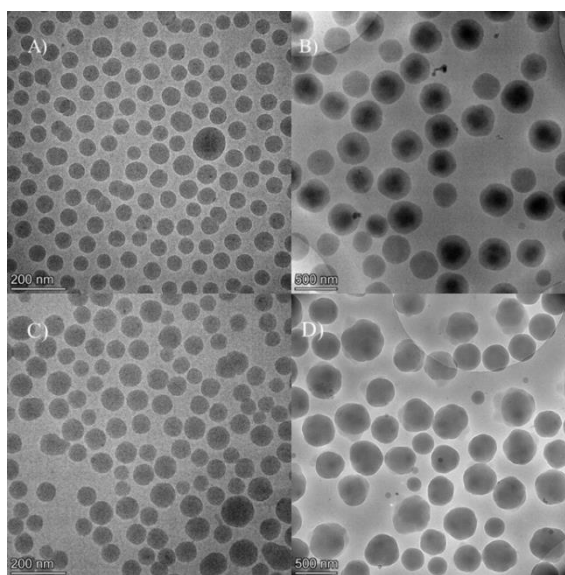
On the other hand, in the case of the small two-stage latexes, no contrast was observed between the two phases in the TEM, even for the higher content of the hard phase in S<sub>a</sub>1-35 (See **Figure 6-2 (A) and (B)**). Note that the morphology of a small two-stage latex using a non-crosslinked PBA (S<sub>b</sub>1-20) and a crosslinked PBA (S<sub>c</sub>1-20) was also investigated and similar results were observed (see **Figure S6-1** in Appendix V). One reason for the lack of contrast in these samples may be some partial phase mixing at the interface of the two polymers. As previously commented by Dos Santos et al,<sup>4</sup> at the interface between two immiscible polymers there is an interphase region in which partial mixing occurs. The interphase profile,  $\varphi_i(x)$ , as function of distance,  $x$ , from the interface,  $x_0$ , can be approximated by

$$\varphi_i(x) = \frac{1}{2} \left( 1 + \tanh \frac{x - x_0}{\lambda} \right)$$

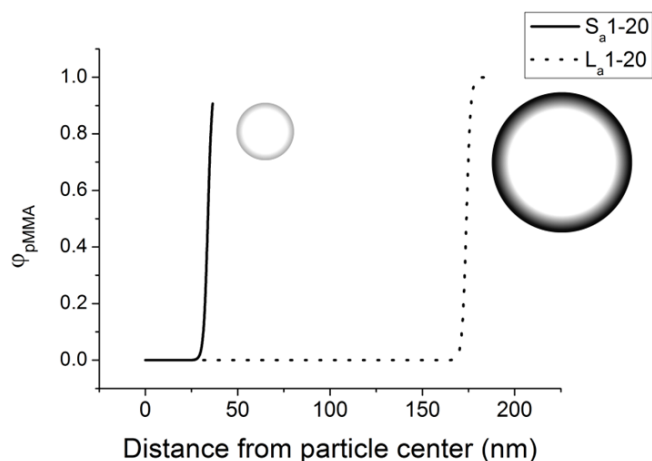
where  $\lambda$  is the interphase width given by

$$\lambda = \frac{2a}{\sqrt{6\chi}}$$

where  $\chi$  is the Flory interaction parameter, estimated to be 0.047 for poly(methyl methacrylate) and poly(butyl acrylate) at room temperature,<sup>5</sup> and  $a$  is the monomer length, taken to be 0.6 nm. Taking these values into account and by adjusting the value of  $x_0$  such that the correct relative volume fraction of the two phases is reached, the approximate composition profiles for the L<sub>a</sub>1-20 and S<sub>a</sub>1-20 are shown in **Figure 6-3**.



**Figure 6-2.** TEM image of two-stage latex particles S<sub>a</sub>1-35 (A), L<sub>a</sub>1-35 (B), S<sub>a</sub>1-20 (C) and L<sub>a</sub>1-20 (D)

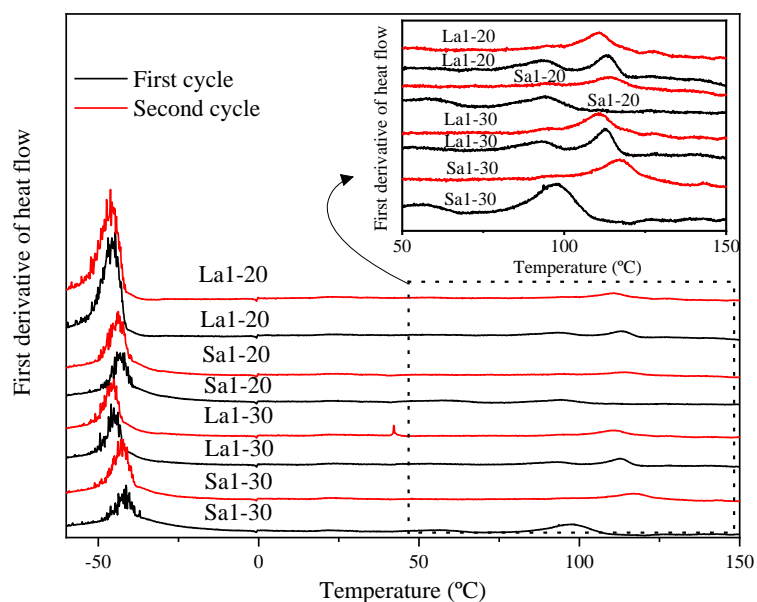


**Figure 6-3.** Estimated interphase profile for  $S_a1-20$  and  $L_a1-20$  which differ only in the particle size of the initial seed. The spheres show approximate morphologies of the particles with the black phase representing the second stage polymer assuming a true core/shell structure.

It can be seen from **Figure 6-3** that for the small particles, the phase mixing model predicts that all the second stage polymer is contained in the interphase region and therefore the second-stage polymer would be expected to exist in a mixed phase where the  $T_g$  is substantially reduced. In contrast, in the case of the larger particles, the interphase region contains only a small fraction of the second stage polymer. These differences result because the interphase region has a fixed width that accounts for a larger relative volume of polymer in the small particles. These effects of phase mixing cannot be observed in the second cycle DSC thermograms shown in **Figure 6-1**, likely due to substantial thermal annealing that can occur in the film. However, phase mixing is clearly visible in the first cycle measurements shown in **Figure 6-4**, in which the  $T_g$  of the second stage polymer is significantly reduced. As suggested by the



calculated interphase profiles shown in **Figure 6-3**, the effects of phase mixing appear to be more important in the case of the smaller two-stage latexes where the interphase region occupies relatively larger volume.



**Figure 6-4** Comparison of first and second cycle DSC thermograms for latexes  $S_{a1-20}$ ,  $S_{a1-30}$ ,  $L_{a1-20}$  and  $L_{a1-30}$  showing the shift in the  $T_g$  of the higher  $T_g$  phase in the second cycle for latexes with lower particle size

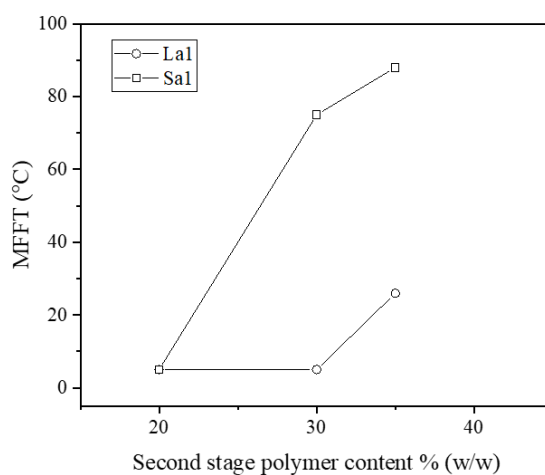
## 6.4. Film formation

### 6.4.1. Effect of particle size of the seed

Given the apparent difference in particle morphologies and phase mixing as a function of particle size, the film formation of two-stage systems with different particles sizes was then explored. **Figure 6-5** shows the MFFT as a function of the second-stage polymer content for large and small two-stage latexes. As can be seen, dramatic differences in the trends of MFFT were observed for these two systems. Both small and large two-stage latexes had a low MFFT when the fraction of the second-stage polymer was 20%. In the case of small two-stage latexes there was a sharp increase in the MFFT above this value such that above 20 wt% second-stage polymer, film formation at room temperature was not possible. On the other hand, large latexes showed low MFFT values, and the MFFT only increased when the second-stage polymer content reached 35 wt%.

These results can be explained by considering the differences in their particle morphology. For latex  $L_a1-20$ , the TEM images shown in **Figure 6-2 (D)** suggests a lobed structure where the second stage polymer exists in isolated patches as has previously been reported for similar systems.<sup>2,3</sup> This means that this system does not have a shell fully covering the surface of the seed and therefore deformation of the high  $T_g$  phase is not required for film formation and interdiffusion of the soft phase would be possible. As the fraction of the hard phase was increased to 35% in  $L_a1-35$ , a more uniform shell formed on the surface of the particles (see **Figure 6-2 (B)**), which would block the deformation and interdiffusion of the soft phase and therefore increase the MFFT. In the case of the small latexes  $S_a1-20$  and  $S_a1-35$ , the spherical

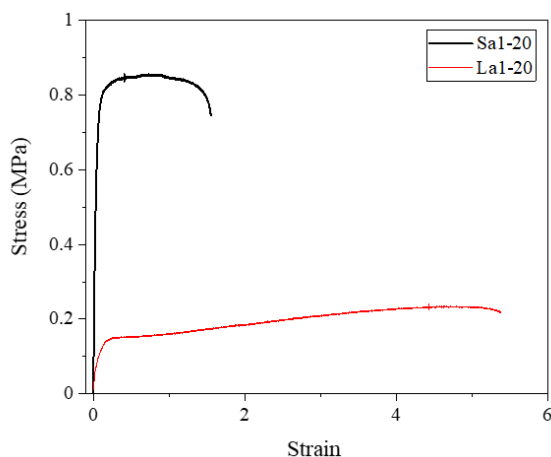
structure observed in the TEM suggests a morphology that is closer to a true core-shell particle which hinders particle deformation and interdiffusion of the soft phase. These latexes are therefore more similar structurally to latexes that are used as redispersable powders, for which film formation is undesirable. However, due to the apparent phase mixing, when the shell is relatively thin, such as in S<sub>a</sub>1-20, the low  $T_g$  of the interphase region results in reasonably low MFFT.



**Figure 6-5** – Minimum film formation temperature as a function of the amount of shell phase. The large samples correspond to L<sub>a</sub>1-20, L<sub>a</sub>1-30 and L<sub>a</sub>1-35 and the small samples to S<sub>a</sub>1-20, S<sub>a</sub>1-30 and S<sub>a</sub>1-35

Based on the explanation above, the mechanical properties would also be expected to be significantly different depending on the particle size. To probe this, the mechanical properties of the samples able to form a film at temperatures lower than 22 °C (S<sub>a</sub>1-20 and L<sub>a</sub>1-20) were

initially investigated in terms of their tensile properties. **Figure 6-6** shows the stress-strain curves for films prepared using small ( $S_a1-20$ ) and large ( $L_a1-20$ ) two-stage latexes and the tensile properties of these films are summarized in **Table 6-4**. Despite having identical overall polymer composition, it can be seen that these systems have significantly different mechanical behaviour; the film prepared with the small two-stage latex ( $S_a1-20$ ) shows higher Young's modulus and ultimate tensile strength compared to the system prepared using large two-stage latex ( $L_a1-20$ ). However, the opposite was observed for the flexibility of the films and  $S_a1-20$  exhibits lower elongation at break than  $L_a1-20$ . These trends are in agreement with the arguments outlined above where the more uniform shell assumed for  $S_a1-20$  would lead to a continuous phase of the high  $T_g$  second stage polymer whereas the patchy structure assumed for  $L_a1-20$  would lead to a more discontinuous network with reduced modulus.

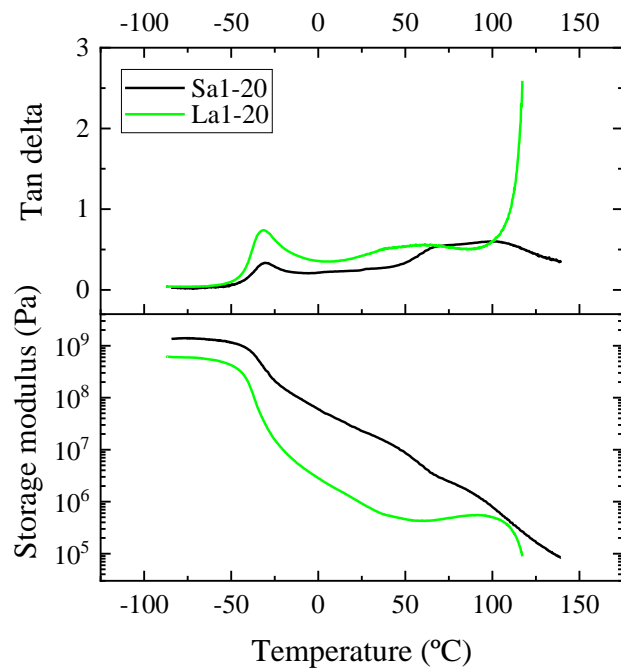


**Figure 6-6** – Stress-Strain curves of films cast from small ( $S_a1-20$ ) and large ( $L_a1-20$ ) two-stage latexes

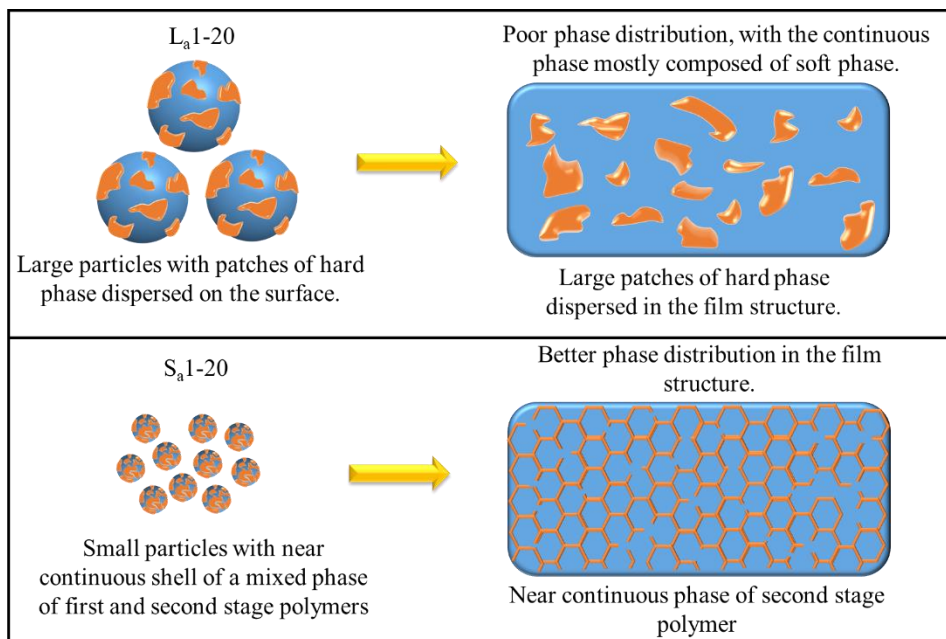
**Table 6-4** – Tensile properties of films cast from small (S<sub>a</sub>1-20) and large (L<sub>a</sub>1-20) two-stage latexes

Sample	Young's Modulus (MPa)	Elongation at break (%)	Ultimate tensile Strength (MPa)
<b>S<sub>a</sub>1-20</b>	11.5 (±0.18)	150	0.85
<b>L<sub>a</sub>1-20</b>	2.6 (±0.03)	538	0.23

The differences in mechanical properties can also be observed in the thermomechanical properties of S<sub>a</sub>1-20 and L<sub>a</sub>1-20, which were investigated via DMTA as shown in **Figure 6-7**. The tan ( $\delta$ ) curves show a peak at  $-40$  °C, which corresponds to the  $T_g$  of the soft (PBA) phase. A second  $T_g$  corresponding to the second stage polymer is apparent at high temperatures ( $\approx 100$  °C), although in the case of S<sub>a</sub>1-20 it is less obvious, which again may be attributed to the higher degree of phase mixing. The main difference in the two samples occurs above the  $T_g$  of the soft phase; in the case of L<sub>a</sub>1-20 the storage modulus ( $G'$ ) shows a dramatic decrease at temperatures higher than the  $T_g$  of the soft (PBA) phase while this decrease is more gradual for the films of S<sub>a</sub>1-20. These results are again in agreement with the proposed film structure shown in **Scheme 6-1** in which L<sub>a</sub>1-20 appears as a poly(butyl acrylate) continuous phase with the second-stage polymer dispersed, while S<sub>a</sub>1-20 results in a structure closer to a continuous network of second-stage polymer.



**Figure 6-7** – DMTA Curves of S<sub>a</sub>1-20 and L<sub>a</sub>1-20.

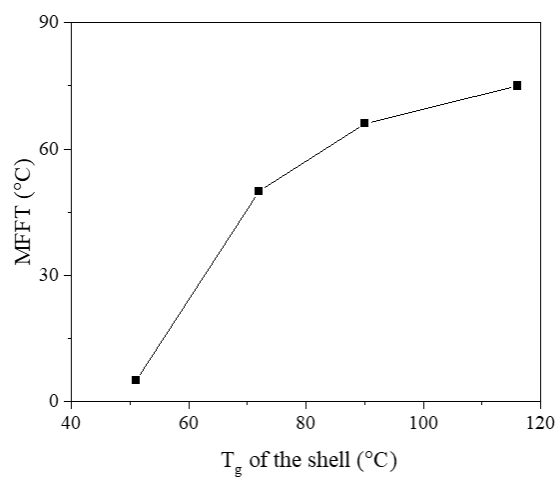


**Scheme 6-1** – Schematic representation of latex S<sub>a</sub>1-20 and L<sub>a</sub>1-20 and their different phase distribution throughout the film structure

#### 6.4.2. Effect of second stage monomer composition

The S<sub>a</sub>1-20 system described above is particularly interesting as it appears to demonstrate that as the morphology is closer to a true core/shell type structure the mechanical properties are substantially improved. Based on this, the use of varied monomer compositions of the two phases was investigated to try to reach systems with low MFFT but improved mechanical performance. Thus, seed S<sub>a</sub> (soft PBA phase) was used to synthesize a series of two-stage latexes where the hard phase fraction was kept at 30 % (w/w) but different T<sub>g</sub> values

of the second-stage polymer were targeted (samples S<sub>a</sub>1-30, S<sub>a</sub>2-30, S<sub>a</sub>3-30 and S<sub>a</sub>4-30). The MFFT plotted as a function of T<sub>g</sub> of the second-stage polymer is shown in **Figure 6-8**. It can be seen that the MFFT decreases with the T<sub>g</sub> of the hard phase, with a significant drop in the MFFT for S<sub>a</sub>4-30 (MFFT < 5 °C). In this case, the T<sub>g</sub> is sufficiently reduced such that the particle is capable of deformation at ambient temperature. Note that as expected based on results shown previously, an analogous two-stage latex with identical polymer composition but higher particle size, L<sub>a</sub>4-30, also had an MFFT that was at the lower limit of measurement (MFFT < 5 °C).

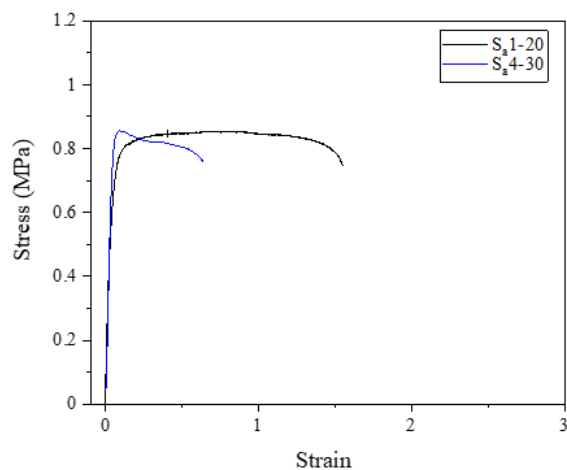


**Figure 6-8** – MFFT as a function of hard phase T<sub>g</sub>. The samples correspond to S<sub>a</sub>1-30, S<sub>a</sub>2-30, S<sub>a</sub>3-30 and S<sub>a</sub>4-30

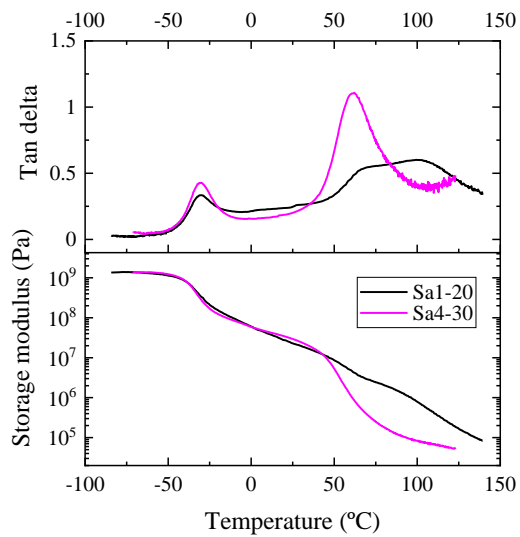
Although by lowering the T<sub>g</sub> of the second-stage polymer it was possible to achieve MFFTs below room temperature with higher amounts of the second stage polymer, the



improvements in mechanical properties when compared to a system with lower amount of higher  $T_g$  second stage polymer were negligible. For example, **Figure 6-9** and **Figure 6-10** show the tensile properties and thermomechanical properties of  $S_{a1-20}$  and  $S_{a4-30}$ . Although latex  $S_{a4-30}$  has a higher amount of the second stage polymer, the lower  $T_g$  of the second stage polymer led to a film with similar mechanical properties to  $S_{a1-20}$  at ambient temperature. Moreover, the incorporation of a higher fraction of second stage polymer in the case of  $S_{a4-30}$  led to a decrease in elongation at break. In the DMTA, the only major difference was that due to the lower  $T_g$  of second stage polymer in the case of  $S_{a4-30}$  where there was a substantial drop in the mechanical properties above 50 °C. Thus, these results suggest that the absolute amount of hard phase is less important than the distribution of the phase within the film in terms of reinforcing mechanical properties. It may be noted that similar to the results with lower amount of second stage polymer (i.e. comparing  $S_{a1-20}$  and  $L_{a1-20}$  in **Figure 6-7**), a significantly higher modulus was observed in the region between the soft and hard phase  $T_g$ s when comparing a small to a large two stage latex ( $S_{a4-30}$  vs  $L_{a4-30}$ ) (see **Figure S6-2**).



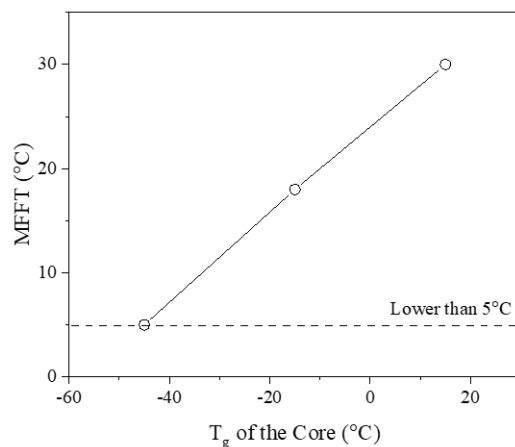
**Figure 6-9** – Stress-Strain curves of two-stage latex films of Sa1-20 and Sa4-30.



**Figure 6-10** – DMTA curves of Sa4-30 and Sa1-20.

### 6.4.3. Effect of first stage monomer composition

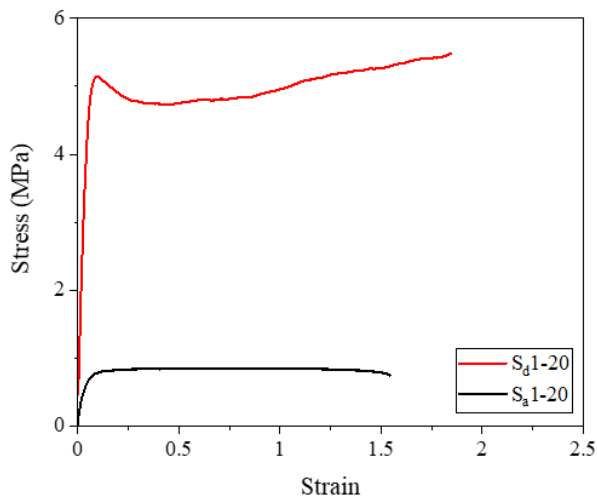
In addition to varying the second stage polymer composition, the influence of the composition of the polymer seed was also explored. This is particularly important as the use of poly(butyl acrylate) homopolymers leads to low MFFT but also leads to relatively soft, adhesive-like films. Seed latexes composed of MMA/BA 30/70 wt/wt ( $S_d$ ) and MMA/BA 50/50 wt/wt ( $S_e$ ) were used to synthesize two-stage latexes containing 20 wt% of the second stage polymer. The MFFT of the two stage latexes containing a different composition of the soft phase were measured and the results are shown as a function of the glass transition temperature of the seeds in **Figure 6-11**. It can be seen that the MFFT gradually increased with the  $T_g$  of the soft phase and the MFFT was significantly higher than the  $T_g$  of the seed latex. This indicates that the second stage polymer has a strong influence on the film formation behaviour, which may be expected due the core-shell like structure. Furthermore, as phase mixing would lead to an increase in the  $T_g$  of any seed polymer in the interphase region it would be expected that the MFFT would be substantially higher than the  $T_g$  of the seed polymer as is observed.



**Figure 6-11** – MFFT as a function of soft phase  $T_g$ . The samples correspond to latexes S<sub>a</sub>1-20, S<sub>d</sub>1-20 and S<sub>e</sub>1-20

The tensile properties of films cast from S<sub>a</sub>1-20 and S<sub>d</sub>1-20, which have MFFT lower than 22 °C were measured. The results can be seen in **Figure 6-12** and **Table 6-5**. The stress-strain curves show that the tensile properties of the film varied significantly with the  $T_g$  of the soft phase. The film cast from S<sub>d</sub>1-20 has a higher Young's modulus and ultimate tensile strength than S<sub>a</sub>1-20. However, the elongation at break was very similar in both systems. The thermomechanical properties of both systems can be found in **Figure S6-3** in Appendix V. It can be seen that S<sub>d</sub>1-20 shows a significantly higher modulus than S<sub>a</sub>1-20 up until the  $T_g$  of the second stage polymer. These results show that the mechanical properties of the film can be considerably improved by increasing the  $T_g$  of the core, whilst still ensuring a relatively low MFFT. It may also be noted that sample S<sub>d</sub>1-20 has a Young's modulus and tensile strength more than an order of magnitude

higher than that of films cast from latexes of similar composition but with the inverse hard core/soft shell morphology.



**Figure 6-12** – Tensile curves of Sa1-20 and Sd1-20.

**Table 6-5** – Tensile properties of films cast from two-stage latexes with different compositions of the soft phase.

Samples	Young's Modulus (MPa)	Elongation at break (%)	Ultimate tensile Strength (MPa)
<b>S<sub>a</sub>1-20</b>	11.5 (±0.18)	150	0.85
<b>S<sub>d</sub>1-20</b>	80.6 (±1.32)	180	5.47

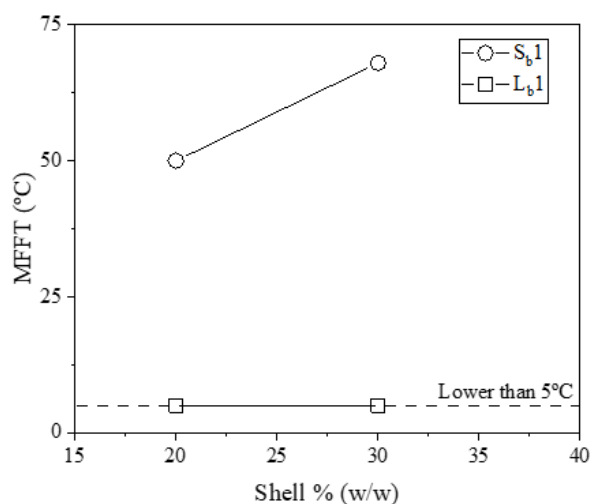
As the composition of the core polymer plays a significant role, both in film formation and in mechanical properties, the effect of crosslinking the initial seed latex was also explored.

Crosslinking of the seed would be expected to lead to only limited interpenetration of the soft, seed polymer but would also result in a higher modulus and more elastomeric character of the film. In order to explore this effect, a series of small and large two stage latexes were synthesized in which the core was either non-crosslinked (seed  $S_b$  by addition of chain transfer agent) or crosslinked (seed  $S_c$  by addition of difunctional monomer).

For samples  $L_c1-20$  and  $S_c1-20$ , where the core was crosslinked, no difference in the MFFT was observed and in both cases the MFFT was at the lower limit of the measurement. In terms of mechanical properties, a slight increase in the modulus was observed in both samples when compared with  $L_a1-20$  and  $S_a1-20$  (see **Figure S6-4** in Appendix V). In the case of  $L_c1-20$  there was a significant reduction in the elongation at break which suggests only a limited degree of interpenetration of the soft seed polymer due to crosslinking. In the case of  $S_c1-20$  the elongation at break was virtually unaffected which, as commented above, may be related to the mechanical properties being largely dictated by the second stage polymer.

When chain transfer agent was added in order to eliminate the formation of gel, surprising results were obtained. It was initially thought that by reducing the extent of network formation in the seed polymer, film formation would be easier, resulting in lower MFFTs. However, as shown in **Figure 6-13**, whilst the large samples ( $L_b1-20$  and  $L_b1-30$ ) formed a film relatively easily in agreement with the other examples in this work, the smaller two stage latexes ( $S_b1-20$  and  $S_b1-30$ ) resulted in  $MFFT > 50$  °C, even when the second stage polymer content was low. For these latexes, a seemingly continuous film was formed at temperatures lower than the MFFT, but very small cracks were observed throughout the structure. Given that the low  $T_g$  linear poly(butyl acrylate) that forms 80 wt% of the sample should readily form a film, the only clear explanation

for this result is that the seed is fully encapsulated by the second stage polymer. Crack formation during film formation may therefore be related to the inability of the non-cross-linked, low  $T_g$  core to withstand the build-up of stress during film formation. Further evidence for this argument is given by the TEM images of the film cross-section in **Figure S6-5 in Appendix V**, which show that the poly(butyl acrylate) (light phase) is apparently dispersed in a network of the second stage polymer.






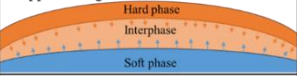



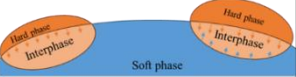
**Figure 6-13** - Minimum film formation temperature as a function of the amount of hard phase in two stage latexes in which the core is synthesized in the presence of chain transfer agent.

## 6.5. Conclusions

In conclusion, in this work the film formation behaviour of two stage latex particles synthesized with a high  $T_g$  second stage polymer has been studied. Aiming to obtain film-forming two-stage latexes with low MFFT, the influence of the seed polymer and the amount and composition of second stage polymer was explored. The most significant effect was related to the initial particle size of the seed, which led to apparent differences in the particle morphology as shown in **Scheme 6-2**. When small seed particles were used, a structure approaching that of a true core/shell system was observed, leading to a more continuous phase of high  $T_g$  polymer in the final film and, therefore, to superior mechanical properties. However, as a result of this structure, the smaller two-stage latexes also resulted in a significant increase in the MFFT, even when the second stage polymer content was low. At higher second stage polymer content, the MFFT could be reduced to values lower than 22 °C by reducing the  $T_g$  of the hard phase (shell) but without any significant improvement in the mechanical properties of the film. It was also shown that the mechanical properties of these two stage latexes could be improved by increasing the  $T_g$  of the polymer in the initial seed latex, although the MFFT also increases in this case. In summary, the synthesis of two-stage latexes with small particle size offers a route to a film structure that leads to significantly improved mechanical properties whilst maintaining sufficiently low MFFT, even when the amount of high  $T_g$  polymer in the system is relatively limited.



**Scheme 6-2** – Schematic representation of the variations in the particle morphology of soft-core/hard-shell latexes and the consequences to the film formation properties.

<i>Hard phase fraction (w/w)</i>	20%	30%	35%	Phase Mixing
<i>Small two-stage latex particles</i>	 Low MFFT	 High MFFT	 High MFFT	Majority of second stage polymer exists in phase mixed region and structure approaching true core/shell is reached 
<i>Large two-stage latex particles</i>	 Low MFFT	 Low MFFT	 Low MFFT	Relatively small fraction of second stage polymer in interphase region. Patchy surface structure 

## 6.6. References

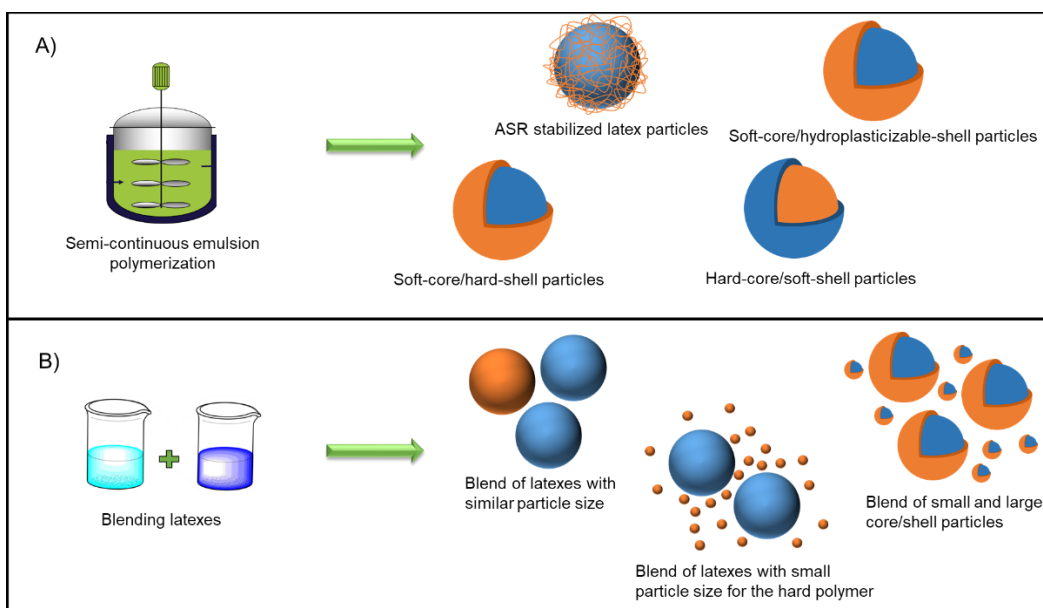
- (1) Ballard, N.; de la Cal, J. C.; Asua, J. M. The Role of Chain Transfer Agent in Reducing Branching Content in Radical Polymerization of Acrylates. *Macromolecules* **2015**, *48* (4), 987–993. <https://doi.org/10.1021/ma502575j>.
- (2) Abdeldaim, H.; Reck, B.; Roschmann, K. J.; Asua, J. M. Cracking in Films Cast from Soft Core/Hard Shell Waterborne Polymer Dispersions. *Macromolecules* **2023**, *56* (9), 3304–3315. <https://doi.org/10.1021/acs.macromol.3c00321>.
- (3) Sommer, F.; Duc, T. M.; Pirri, R.; Meunier, G.; Quet, C. Surface Morphology of Poly(Butyl Acrylate)/Poly(Methyl Methacrylate) Core Shell Latex by Atomic Force Microscopy. *Langmuir* **2002**, *11* (2), 440–448. <https://doi.org/10.1021/LA00002A013>.
- (4) Domingues Dos Santos, F.; Fabre, P.; Drujon, X.; Meunier, G.; Leibler, L. Films from Soft-Core/Hard-Shell Hydrophobic Latexes: Structure and Thermomechanical Properties. *J. Polym. Sci. Part B Polym. Phys.* **2000**. [https://doi.org/10.1002/1099-0488\(20001201\)38:23<2989::AID-POLB10>3.0.CO;2-D](https://doi.org/10.1002/1099-0488(20001201)38:23<2989::AID-POLB10>3.0.CO;2-D).
- (5) Ruzette, A.-V.; Tencé-Girault, S.; Leibler, L.; Chauvin, F.; Bertin, D.; Guerret, O.; Gérard, P. Molecular Disorder and Mesoscopic Order in Polydisperse Acrylic Block Copolymers Prepared by Controlled Radical Polymerization. *Macromolecules* **2006**, *39* (17), 5804–5814. <https://doi.org/10.1021/ma060541u>.

## Chapter 7. Conclusions

The main goal of this PhD thesis was to explore the influence of the morphology of multiphase latex particles on the film formation process and the mechanical properties of the final film. It is widely known that film morphology has a considerable influence on the properties of the films. Therefore, understanding how to target specific film structures should allow for the direct control of the film properties. This is an important issue when it comes to the development of VOC-free latex systems designed to achieve good mechanical properties whilst having a low minimum film formation temperature (MFFT). As highlighted in the introduction (Chapter 1), balancing the mechanical properties and MFFT can be achieved by mixing hard, high  $T_g$  and soft, low  $T_g$  polymers, where the hard phase enhances the mechanical properties, while the soft polymer allows for relatively low MFFT values. Such systems can be produced either by blending latexes or synthesising heterogeneous polymers that combine both phases in the same particle.

To better understand the effect of particle morphology on film formation behavior, in this thesis, a series of multiphase latex particles with distinct morphologies were synthesized. For each target morphology, a range of latexes with different characteristics (molecular weight, particle size, gel content and  $T_g$ ) was made (see **Figure 7-1A**). Chapters 2 and 3 focussed on particles containing alkali soluble resin stabilized or hydroplasticized phases where water is used to plasticize one phase, leading to lower MFFTs. Chapters 4, 5 and 6 focussed on the synthesis of hard-core/soft-shell and soft-core/hard-shell latexes, where a low  $T_g$  phase was used to reduce the MFFT and a high  $T_g$  phase was used to improve mechanical properties. These structured

particles were also compared with equivalent blended systems (see **Figure 7-1B**). In this final chapter some general conclusions about the influence of particle morphology on film formation and film properties will be drawn from the collective results of individual chapters.



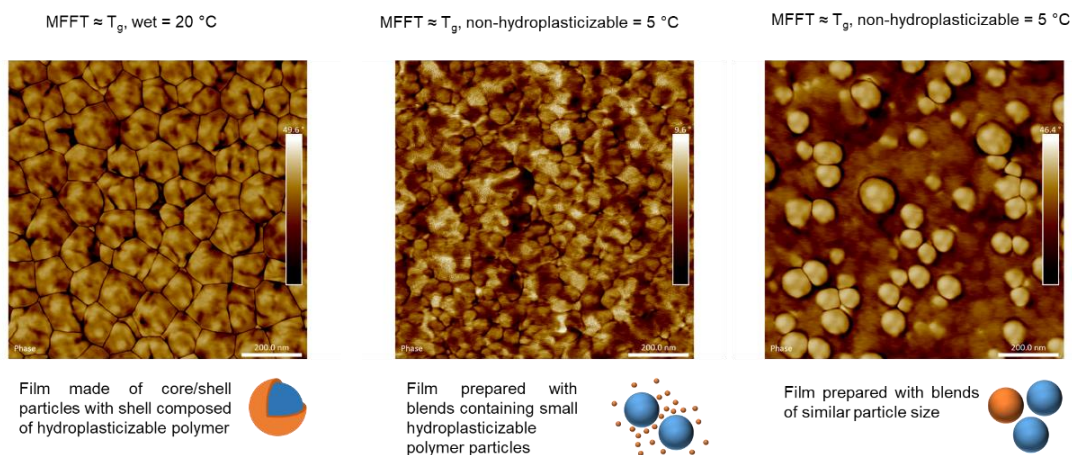
**Figure 7-1** – Scheme of the different latex composites prepared in this work. With hybrid latexes in (A) and blends in (B).

The first strategy described in Chapters 2 and 3 was focused on exploring the film formation of latex particles in the presence of hydroplasticizable polymers. It was shown that film formation could be largely understood based on the hydroplasticization capacity of the polymer. The wet conditions during the drying process of the latexes mean these systems have lower

glass transition temperatures in the dispersed state, but the hydroplasticized phase dries to form a high  $T_g$  phase, leading to enhanced mechanical properties of the final film.

However, it was seen that the contribution of hydroplasticization strongly depends on the structural features of the latex system as summarized in **Figure 7-2**. When the hydroplasticizable component was placed in the shell of a core/shell latex, the film formation properties were highly dependent on the wet  $T_g$  of the shell polymer ( $MFFT \approx T_{g,wet}$ ) and the final film structure appeared to consist of an interconnected layer of the hydroplasticizable polymer. In contrast, in the case of latex blends and for ASR stabilized resins, the MFFT was generally lower and was determined largely by the other, non-hydroplasticized component of the latex blend which formed the majority phase.

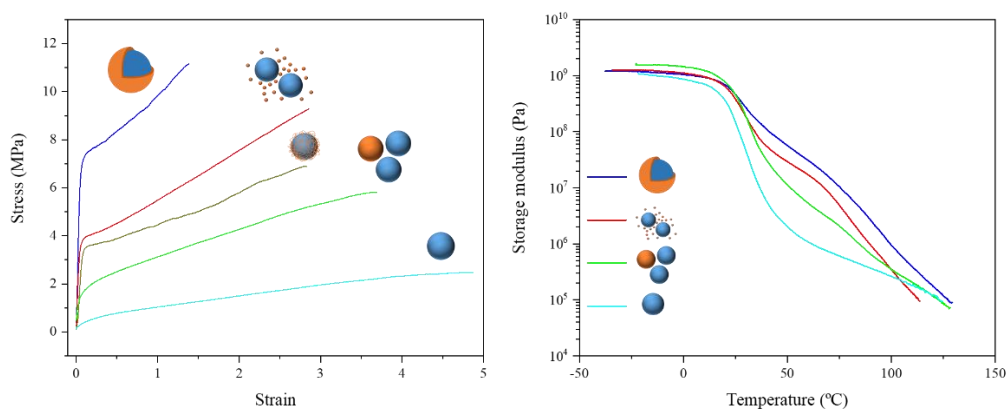
The film structure of blends and the ASR stabilized systems depended on the relative particle size of the two components. In blends where the particle size of the hydroplasticizable component was large relative to the main non-hydroplasticizable polymer, the hydroplasticizable component was dispersed in a matrix of soft polymer in the final film. In contrast, where the particle size of the hydroplasticizable component was small relative to the main non-hydroplasticizable polymer, it tended towards a more continuous network structure. In the case of alkali soluble resin stabilized latexes, the ASR exists as small, micelle-like structures and therefore it behaves similar to blends with small hydroplasticized latexes, such that the ASR forms a near continuous phase in the final film.



**Figure 7-2** – Difference in MFFT and film structure for hydroplasticizable latex systems with different initial particle morphologies as discussed in Chapter 3 (samples correspond to CS2, Nano Blend 2 30% and Blend 2 from Chapter 3 from left to right). All three systems contain identical polymeric components with 70 wt% of an MMA/BA 50/50 copolymer as the non-hydroplasticizable component (blue in the cartoon) and 30 wt% of an MMA/S/EA/MAA 40/5/40/15 copolymer as the hydroplasticizable component (orange in the cartoon).

As discussed above, the hydroplasticization effect can influence film formation, but can also strongly affect the mechanical properties as the water is removed from the hydroplasticized polymer to leave a high  $T_g$ , glassy polymer. As can be seen in **Figure 7-3**, which shows tensile and DMTA data for a number of hydroplasticizable latex systems with identical polymeric components but different morphologies, in all cases there was a substantial increase in the Young's modulus and tensile strength compared to a control sample consisting of a simple homogeneous latex of MMA/BA 50/50. This is due to the high  $T_g$  of the dried hydroplasticizable

polymer which constitutes a “hard” phase in the film. The biggest improvement in mechanical properties was seen in the core/shell system which, as discussed above tends to lead to a network of the high  $T_g$ , hydroplasticizable polymer. As the degree of connectivity of the network decreases and the low  $T_g$  MMA/BA phase becomes more continuous, the improvement in mechanical properties was less obvious.



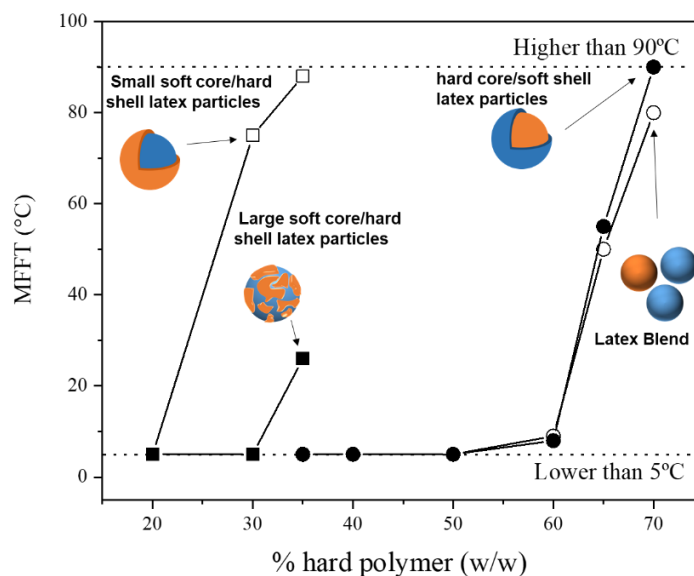
**Figure 7-3** – Tensile stress-strain and DMTA curves of films cast from hydroplasticizable latexes with different initial particle morphology. Samples correspond to L1 (Cyan), CS2 (blue line), Nano Blend 2 30% (Red line), Blend 2 (Green) from Chapter 3 and ASR/Latex 2 (dark yellow) from Chapter 2. With the exception of the control sample which is a standard MMA/BA 50/50 latex, all systems contain identical polymeric components with 70 wt% of an MMA/BA 50/50 copolymer as the non-hydroplasticizable component (blue in the cartoon) and 30 wt% of an MMA/S/EA/MAA 40/5/40/15 copolymer as the hydroplasticizable component (orange in the cartoon).

In the second part of the thesis (Chapters 4-6), the film formation of a series of hard-core/soft-shell and inverted core/shell latexes was investigated. With the objective of understanding the effect of the high  $T_g$  polymer (hard phase) on the minimum film formation temperature and the mechanical properties of the films, the relative fraction of hard and soft phase was varied for both systems. The MFFT as a function of hard phase content for comparative latexes is shown in **Figure 7-4**. It can be seen that the critical point at which the MFFT increases is greatly affected by the structure of the polymer particle. Particles containing a low  $T_g$ , soft shell and soft/hard latex blends had relatively low MFFT until a hard polymer content of 60% (w/w), at which point the MFFT increased dramatically. However, when the shell was composed of a high  $T_g$ , hard polymer the MFFT increased at a hard polymer content of around only 20% (w/w).

This behaviour can be explained based on the contribution of the soft polymer to the formation of continuous phase of the film. For hard-core/soft-shell particles and for latex blends, as long as the temperature is higher than the soft phase  $T_g$  the shell is free to undergo deformation and form a continuous phase. The MFFT only rises at the point at which there is insufficient soft phase to fill the void space of the hard phase which, assuming a monodisperse spherical hard phase, corresponds to approximately 64 vol%. As shown in Chapters 4 and 5, by changes in the particle size distribution of the hard phase this limit could be increased to reach hard phase content as high as 80 wt% whilst maintaining low MFFT. In contrast, deformation of the soft polymer in a soft-core/hard-shell polymer is hindered by the presence of the hard polymer shell at very low hard phase fractions. In that case film formation is possible only where shell

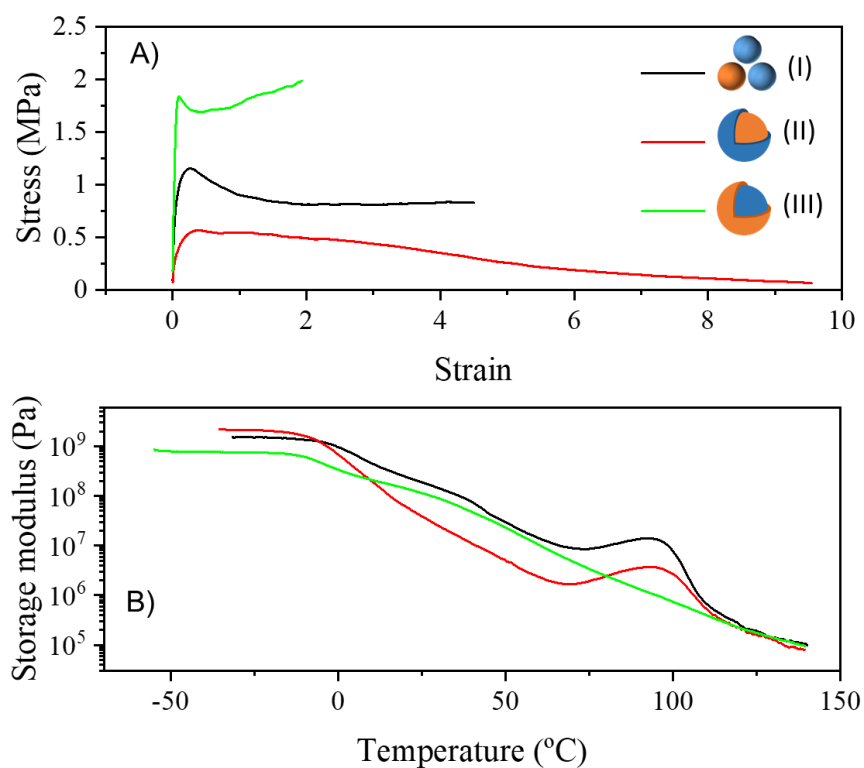


formation is incomplete, which was the case for larger particles studied in this work, or where phase mixing led to a lower effective  $T_g$  of the hard phase, as was the case for smaller particles.



**Figure 7-4** – MFFT as a function of hard polymer content for core/shell and inverted core/shell latexes. The soft-core/hard shell samples corresponds to the series  $S_{a1-X}$  and  $L_{a1-X}$  in chapter 6 with a soft polymer composed of poly(butyl acrylate) and a hard polymer composed of MMA/S 85/15. The hard-core/soft-shell and latex blends samples correspond to the M1 series chapter 4 with a soft polymer composed of BA/MMA 70/30 and a hard polymer composed of polystyrene.

Although the presence of a high  $T_g$  polymer at the surface of the particle limits the amount of hard phase that can be incorporated before the MFFT becomes unacceptably high, it still leads to films with remarkable mechanical properties. In **Figure 7-5** DMTA and tensile stress-strain curves are shown for comparative hard-core/soft-shell latexes (Chapter 4), hard/soft latex blends (Chapter 4) and soft-core/hard-shell latexes (Chapter 6). Although the soft phase is of identical composition (MMA/BA 30/70) in all cases and the amount of hard phase is significantly higher in the case of the hard-core/soft-shell and blend systems (50 wt%), the modulus for the soft-core/hard-shell system is significantly higher. In agreement with the work in Chapters 2 and 3, this was attributed to the formation of a highly connected network structure of hard phase polymer and highlights that the absolute amount of hard phase is less important than the way it is implemented. In fact, as shown in Chapter 5, only by increasing the hard phase significantly above 50 wt% was the hard-core/soft-shell system able to reach similarly high Young's modulus. However in those cases, the low fraction of soft phase material led to brittle materials with low elongation at break.



**Figure 7-5** – Tensile stress-strain (A) and DMTA (B) curves of films cast from core/shell latexes and latex blends. Samples (I, II and III) correspond to B1(50/50) (Chapter 4), M1(50/50) (Chapter 4) and S<sub>d</sub>1-20 (Chapter 6), respectively. The blend and hard-core/soft-shell samples contain 50 wt% of an MMA/BA 30/70 copolymer as the soft phase (blue in the cartoon) and 50 wt% of polystyrene as the hard phase (orange in the cartoon). The soft-core/hard-shell sample contains 80 wt% of an MMA/BA 30/70 copolymer as the soft phase (blue in the cartoon) and 20 wt% of a MMA/S 85/15 copolymer as the hard phase (orange in the cartoon).

To conclude, the film formation of latex particles is strongly affected by the initial particle morphology. In the optimum cases, even with relatively small amounts of added hard phase, the MFFT is only minimally affected but orders of magnitude improvement in the mechanical properties can be obtained. Going forward, it would be of interest to explore more complex morphologies. For example, in the final chapter of this work it was proposed that latexes with a phase gradient may allow for an optimum balance between film formation behaviour and improvement in mechanical properties. In principle gradient morphologies can be directed by controlled feeding strategies and would therefore offer a route to specific design of such structures that could be further explored. In addition, much of the work at this thesis has targeted equilibrium morphologies and therefore non-equilibrium structures may open up new routes for the design of low MFFT latexes with excellent mechanical properties. It is hoped that these developments would contribute to the continued reduction of VOC content in latexes used for coatings applications.

## List of publications and conference presentations

Parts of this thesis have previously been published with additional work currently under review. The list of papers resulting from this work is as follows:

Brito, E.L.; Ballard, N. Film Formation of Alkali Soluble Resin (ASR) Stabilized Latexes. *Prog. Org. Coatings* **2021**, *159*, 106444.

Brito, E. L.; Ballard, N. Film Formation of Hard-Core/Soft-Shell Latex Particles. *J. Polym. Sci.* **2022**, *5*, 410–421.

Brito, E. L.; Willocq, B.; Boschet, F.; Ballard, N. Film Formation of High Poly(Vinyl Chloride) Content Latex Particles. *Prog. Org. Coatings* **2023**, *183*, 107783.

Brito, E.L.; Ballard, N. Film formation of latexes with hydroplasticizable domains. *Reactive & Functional Polymers* **2023**, *191*, 105684.

Brito, E.L.; Ballard, N. Film formation of two-stage acrylic latexes: towards soft-core/hard-shell systems (accepted for *Macromolecular Materials and Engineering*)

Parts of this work have been presented in international conferences, as well in industrial Liaison Program (ILP) meetings.

### **Oral presentations**

#### **“Film formation of polymer dispersions with structured particle morphologies”**

Lopes Brito, E.; Ballard, N. POLYMAT, 19<sup>th</sup> Industrial Liaison Program (ILP) Meetings, UPV/EHU, Polymat, Donostia-San Sebastian, Spain, 2019.

#### **“Film formation of alkali soluble resin stabilized latexes”**

Lopes Brito, E.; Ballard, N. POLYMAT, 20<sup>th</sup> Industrial Liaison Program (ILP) Meetings, UPV/EHU, Polymat, Donostia-San Sebastian, Spain, 2020.

#### **“Film Formation of core/shell latex particles”**

Lopes Brito, E.; Ballard, N. POLYMAT, 21<sup>th</sup> Industrial Liaison Program (ILP) Meetings, UPV/EHU, Polymat, Donostia-San Sebastian, Spain, 2021.

#### **“Film formation of core/shell latex particles”**

Lopes Brito, E.; Ballard, N. POLYMAT, 9<sup>th</sup> PhD-Workshop on Polymer Reaction Engineering. Online due to the Corona pandemic, 2021.

#### **“Film formation of PVC/Acrylic particles”**

Lopes Brito, E.; Ballard, N. POLYMAT, 22<sup>th</sup> Industrial Liaison Program (ILP) Meetings, UPV/EHU, Polymat, Donostia-San Sebastian, Spain, 2022.

## Resumen y Conclusiones

La presencia de compuestos orgánicos volátiles (VOCs por sus siglas en inglés) en los recubrimientos de polímeros a base de solventes convencionales y su impacto ambiental negativo, han resultado en un mayor esfuerzo para el desarrollo de alternativas de base acuosa. Sin embargo, en muchos casos, igualar las propiedades de aplicación de este tipo de polímeros es un desafío. Para sistemas a base de agua, su mecanismo único de formación de película requiere el uso de polímeros con temperaturas de transición vítrea (T<sub>g</sub>) relativamente bajas, lo que puede comprometer las propiedades mecánicas de los recubrimientos. Este problema puede ser potencialmente superado mediante la producción de látex que contengan múltiples fases. En este caso, la presencia de una “fase rígida” de alta T<sub>g</sub> refuerza la estructura y las propiedades mecánicas, mientras que la presencia de una “fase blanda” de baja T<sub>g</sub> ayuda a la formación de la película. Dichos sistemas pueden ser producidos mezclando látex con diferentes composiciones (mezclas) o utilizando partículas poliméricas heterogéneas que combinan ambas fases en la misma partícula.

El enfoque utilizado para comprender la formación de película de partículas de látex multifase se centró en la morfología de las partículas y las características específicas de las fases poliméricas que pueden influir en el comportamiento de formación de películas. Para cada proyecto estudiado, se sintetizaron híbridos polímero-polímero con morfología diseñada y diferentes composiciones (peso molecular, tamaño de partícula, contenido de gel y T<sub>g</sub>). Se prepararon por polimerización en emulsión, sistemas híbridos compuestos por resinas solubles

(ASRs) actuando como estabilizante para las partículas de látex, y partículas de tipo núcleo y coraza, combinando cada fase en núcleo duro con coraza blanda y núcleo blando con coraza dura. . Con el fin de encontrar alternativas y mejorar el desempeño de estos sistemas híbridos, se comparó el potencial de estas partículas estructuradas con una mezcla física de partículas de composiciones equivalentes.

La primera estrategia se centró en explorar la formación de películas de partículas de látex en presencia de polímeros hidroplastificables. La formación de película podría entenderse en base a la capacidad de hidroplastificación del polímero que contiene un grupo carboxílico en su estructura principal. La condición húmeda durante el proceso de secado de los látex hace que estos sistemas sufran temperaturas de transición vítrea más bajas como resultado de la hidroplastificación. Este efecto permitió el uso de polímeros relativamente duros para producir látex híbridos y mezclas con baja temperatura mínima de formación de película (MFFT por sus siglas en inglés). Durante el proceso de formación de película, el polímero hidroplastificable tiende a deformarse y contribuye a la formación de la fase continua. Tal contribución dependerá de las características estructurales del sistema de látex y esta influencia podría verificarse por una serie de películas de látex obtenidas a partir de híbridos núcleo y coraza y mezclas de látex con diferentes tamaños de partículas.

Cuando el componente hidroplastificable se coloca en la coraza de las partículas, las propiedades de formación de película dependen en gran parte de la Tg efectiva (en condiciones húmedas) del mismo ( $MFFT \approx T_{g,wet}$ ). Después de la formación de película, se forma una fase continua del polímero que compone la coraza, llevando a un aumento del módulo. En el caso de las mezclas de látex, la MFFT fue sustancialmente más baja y se atribuye en gran medida a



el otro componente polimérico no hidroplastificado de la mezcla de látex. El efecto de hidroplastificación solo se notó con un alto contenido de polímero hidroplastificado donde la MFFT depende de la Tg efectiva del polímero hidroplastificado. En las mezclas, el tamaño de partícula del polímero hidroplastificable desempeñó un papel importante en las propiedades mecánicas, donde tamaños de partícula pequeños condujeron a mejores propiedades mecánicas. Además, se demostró que, tras la adición de álcali, estos sistemas no son realmente un polímero en solución, sino que se ensamblan en pequeñas estructuras similares a micelas hinchadas con agua. En presencia de un área superficial adicional proporcionada por el látex, una parte de las macromoléculas poliméricas hidroplastificables se adsorbe fuertemente en la superficie, pero una proporción sustancial permanece en forma de agregados coloidales dispersos. La presencia de pequeños agregados poliméricos en la fase acuosa hace que el proceso de formación de película de este sistema sea similar al de una mezcla que contiene pequeñas partículas poliméricas hidroplastificables, lo que da como resultado un perfil de propiedades mecánicas similares. En la segunda parte de esta tesis doctoral, se investigó la formación de películas a partir de una serie de partículas de látex tipo núcleo y coraza, así como núcleo y coraza invertida.. Con el objetivo de comprender el efecto del polímero de baja Tg (fase blanda) en la temperatura mínima de formación de película y su influencia en las propiedades mecánicas, se varió la cantidad de fase rígida para ambos sistemas. Se demostró que el punto crítico en el que la MFFT aumenta sustancialmente se ve muy afectado por la estructura de las partículas. Las partículas que contenían una coraza compuesta por polímero blando, tenían una MFFT relativamente baja hasta una fracción de polímero rígido del 60 % (p/p), donde comienza a aumentar drásticamente. Sin embargo, cuando la coraza esta compuesta por un polímero rígido, la MFFT aumentaba considerablemente a una fracción de polímero rígido de

aproximadamente de 20 % (p/p). Tal comportamiento podría ser explicado por la contribución del polímero blando a la formación de fase continua de la película. Para partículas con núcleo duro con coraza blanda, la coraza puede sufrir deformación y formar una fase continua que permite la formación de una película con MFFT baja. Por otro lado, tal deformación puede verse obstaculizada por la presencia de la coraza de polímero duro en el sistema de núcleo blando con coraza dura. La menor contribución del núcleo blando a la formación de la fase continua conduce al consecuente aumento de la MFFT.

Se usaron pruebas de tracción para investigar el impacto de la morfología de las partículas en el comportamiento mecánico de las películas. Se observó que partículas de núcleo duro con coraza blanda, que contenía 60 % (p/p) de polímero rígido produjo una película con propiedades mecánicas relativamente similares al látex de núcleo blando con coraza que contenía solo 20 % de polímero rígido. Estos resultados evidenciaron la relevancia de tener una distribución adecuada del polímero duro a lo largo de la fase continua, contribuyendo a la mejora de la estructura de la película, incluso con una cantidad sustancialmente menor de polímero rígido.

Dada la importancia del contenido de la fase dura en la mejora de las propiedades mecánicas de la película, se mezclaron partículas de látex de núcleo duro con coraza blanda con diferentes tamaños de partícula para aumentar la fracción de empaquetamiento de la fase rígida y, potencialmente, mejorar el comportamiento mecánico de las películas. Usando esta estrategia, se pudieron obtener películas de látex que contenían hasta un 80% de polímero rígido con baja MFFT. Estas películas evidenciaron módulos de Young superiores a cualquier otra película preparada en este trabajo, con una resistencia máxima a tracción de 28 MPa. El

comportamiento también se atribuyó a una mejor distribución de fases en toda la estructura de la película, donde al aumentar la fracción de empaquetamiento de la fase rígida, menor deformación es necesaria para formar una película continua (baja MFFT) y, en consecuencia, conduce a una disposición más uniforme de la fase rígida y mejora las propiedades mecánicas.

En general, la formación de películas de partículas de látex puede ser comprendida en función de la capacidad de deformación del polímero blando y la miscibilidad entre las fases. Al optimizar la morfología de las partículas de látex, se puede alterar la estructura interna de las películas de látex, lo cual lleva a cambios significativos en las propiedades mecánicas.



## Appendix I. Characterization methods

### I.I. Solid content and monomer conversion

The solid contents and monomer conversions were determined by gravimetry. The samples were transferred to aluminium pans into which 1-2 drops of hydroquinone (1 wt%) solution was added. These pans were transferred to the oven at 60 °C overnight for drying. Global conversions were calculated based on solid content (S.C) and non-polymeric fraction, which consists of initiator and emulsifier.

Solid content is given by:

$$SC = \frac{\text{weight of the solid material}}{\text{weight of latex}} \quad (\text{I. 1})$$

The conversion  $X$  was determined by the following equations:

$$X = \frac{\left( \frac{W_{\text{Dried}}}{W_{\text{Sample}}} \right) - \left( \frac{W_{\text{Non-poly.}}}{W_{\text{total}}} \right)}{W_{\text{M}} / W_{\text{total}}} \quad (\text{I. 2})$$

Where  $W_{\text{Dried}}$  represents the final weight of the sample after drying,  $W_{\text{Sample}}$  the initial weight of the sample,  $W_{\text{Non-poly}}$  the weight of non-polymerizable solids,  $W_{\text{total}}$  the total weight fed in the reactor at the end of the reaction and  $W_{\text{M}}$  is the amount of fed monomer.

## **I.II. Particle size and particle size distribution**

Particle sizes were measured by dynamic light scattering (DLS) in a Zetasizer Nano Z (Malvern instruments). Samples were prepared by diluting a fraction of latex with deionized water. The equipment was operated at 25°C and the reported values were the size distribution as a function of intensity and the average particle size for three repeated measurements.

## **I.III. Differential scanning calorimetry**

The experimental  $T_g$ s were determined by differential scanning calorimetry (DSC) Q2000 modulated DSC (TA instruments). For the dry films, the samples were dried in an oven at 65 °C and analyzed from -80 °C to 150 °C with a heating rate of 10 °C/min for samples in Chapters 2, 5 and 6, and 20°C for samples in Chapter 3. In Chapter 4, the samples were analyzed in modulated mode from -80 °C to 150 °C with a heating rate of 5 °C/min, amplitude (°C) and period of 60 s. A single cycle was recorded when modulated DSC was applied and two cycles used for conventional DSC measurements. For the projects containing hydroplasticizable species (chapters 2 and 3) some samples were analyzed in wet conditions. The wet  $T_g$  of the ASR systems in Chapter 2 was determined by first neutralization of the ASR with an aqueous solution of ammonia 25% (w/w) and then drying in an oven at 65 °C until 20% (ASR 36 and ASR 60) and 35% (ASR 14, ASR 90) of water content remained. The DSC pans were then sealed and analysis

was carried out from – 80 °C to 70 °C with a heating rate of 10 °C. In the case of wet samples of Chapter 3, the latexes were centrifuged at 60000 rpm for 24 hours and the solid phase containing the polymer swollen by water was used to prepare the DSC samples, where 8 mg of the polymer was added in the respective pan. The pans were then sealed and the analysis was carried out from – 50 °C to 90 °C with a heating rate of 20 °C/min.

#### **I.IV. Determination of Acid values of Alkali-soluble resins**

The acid values were determined by conventional acid-base titration, using NaOH solution with a concentration of 0.5 mol. L<sup>-1</sup> as titrant and the ASR dispersion with 5% solid content as analyte. The pH was monitored using a sensION™ pH meter (HACH) and the equivalence point was determined in order to calculate the acid values and pKa.

#### **I.V. Gel content**

The gel content consists of the fraction of the polymer which is not soluble in THF. The soluble and insoluble fraction of the polymer was separated via Soxhlet extraction in THF. For that, the latex was spread on a filter glass fibre pad ( $w_1$ ), dried for 24 h and its weight was measured ( $w_2$ ) before the Soxhlet extraction was then carried out for 24 h. The glass fibre pad was once again dried for 24 h at 65 °C and weighted ( $w_3$ ). The gel content was determined using equation I.3.

$$Gel\ content\ (\%) = \frac{w_3 - w_1}{w_2 - w_1} \times 100 \quad (I.3)$$

## **I.VI. Gel permeation chromatography**

The molecular weights of the soluble fraction of the polymers were determined by gel permeation chromatography (GPC). Following the Soxhlet extraction reported in the gel content experiments (see section I.V), the polymer solution containing the soluble polymer fraction was dried at room temperature and redissolved in GPC grade THF at a concentration of approximately 2.5 mg/mL. The solution was filtered (polyamide  $\Phi = 45 \mu\text{m}$ ) before being injected into the GPC via an autosampler (Water 717). A pump (LC-20A, Shimadzu) controlled the THF flow at 1 mL/min. The GPC was composed of a differential refractometer (Waters 2410) and three columns in series (Styragel HR2, HR4 and HR6, with pore sizes ranging from  $10^2$  to  $10^6$  Å). Measurements were performed at 35 °C. Molecular weights were determined using a calibration curve based on polystyrene standards.

## **I.VII. Microscopic techniques**

Particle morphologies were determined by transmission electron microscopy (TEM) using a Jeol TM-1400 Plus series 120kV electron microscope. The latexes were diluted with deionized water (0.05 wt%) placed on copper grids covered with Formvar R and dried at low temperatures. The samples of chapters 5 and 6, the samples were stained with vapor of  $\text{RuO}_4$  for 20 min. In the case of the film, slices of films were prepared in a microtome equipped with a diamond knife at -25 °C and then deposited on the copper grids. Similar to the dispersions, the films were stained with vapor of  $\text{RuO}_4$  for 10 min.



Atomic Force Microscopy (AFM) images were obtained using an atomic force microscope Bruker Nanoscope V Dimension Icon in tapping mode with a silicon nitride cantilever equipped with a rotated super sharp silicon tip. The nominal resonant frequency of the cantilever was 320 kHz and the spring constant was 40 N/m. The films were prepared using a spin coater operating at 16 rpm for 30 seconds (ramp 1), followed by another ramp of 32 rpm for 30 s and then left to complete the drying for 1 day at 22 °C and 55 % humidity. All the samples were cast using mica as substrate.

### **I.VIII. Critical micellar concentration (CMC)**

The measurements of critical micelle concentration (CMC) were performed using a force tensiometer model Sigma 700 from Biolin Scientific, equipped with an autotitrator (Schott Titronic). The measurements were carried out in water, using the Du Noüy ring method and the concentration of ASR was varied by adding an ASR solution with 2 g.L<sup>-1</sup>.

### **I.IX. Determining the amount of ASR adsorbed on the latexes surface**

The amount of ASR adsorbed to the latex surface was calculated by separation of the latex and ASR phases by ultracentrifugation. The centrifugations were carried out in polypropylene copolymer tubes (capacity 30 ml each) in a RLM rotor model P70AT (Hitachi Koki) which holds 8 tubes. A Hitachi CP100NX ultracentrifuge was used for all runs. The latexes were centrifuged at 30,000 rpm and 4 °C for 4 h and subsequently the supernatant was collected and

analyzed via gravimetry and the fraction of polymer in the water phase was correlated to the total amount of ASR present in the sample.

### **I.X. Film casting**

Latex films were produced by casting 1.5 g of latex (solids contents 40%) in rectangular silicone molds (26 mm × 56 mm) and allowing to dry at 23 °C and 55 % of relative humidity for 5 days. In the case of using ASR solutions (solid content around 20 %) 3.0 g of solution were used to cast the film to compensate for the lower solid content.

### **I.XI. Weight loss measurements**

The measurements of mass loss were performed on an analytical balance (Sartorius) coupled to a computer that recorded the mass as a function of time using a specially written 232Key program. The measurements were carried out in duplicate at a relative humidity level of 55±5 %, and temperature of 23±1 °C.

### **I.XII. Adaptive speckle imaging interferometry measurements**

The adaptive speckle imaging interferometry measurements were carried out using the Horus® Film Formation Analyzer from Formulaction. The instrument is in a backscattering configuration: the camera sensor (CMOS) and the laser source are on the same side with respect to the analyzed sample and are gathered in a single measuring head. The measuring head is

rigidly fixed on a vertical mast screwed to the aluminium base plate. The samples were deposited on a glass substrate using an automatic film applicator with 120  $\mu\text{m}$  of thickness and just after the drawdown of the latex, the substrate was placed under the laser beam and the measurement was started.

### **I.XIII. Minimum film Formation Temperature (MFFT).**

The MFFT measurements were performed using an MFFT-Bar (model 90 from Rhopoint) with a range of temperatures from 0°C to 90°C based on the MFFT measurement described in ISO 2115. All the films were cast using a film applicator with 120  $\mu\text{m}$  wet thickness. The MFFT was measured after 2 hr and was defined as the point at which continuous homogeneous films without cracks were observed.

### **I.XIV. Water uptake**

In order to measure the amount of absorbed water by the films, the films were formed by casting the latexes onto round silicon moulds and drying them at 22 °C and 55% relative humidity for several days until a constant weight was achieved. All the resulting films had similar weights (~0.5 g). The obtained films were weighed ( $m_0$ ) and were placed into different flasks containing a large excess of distilled water. Then, the films were removed from the flask at given times, they were dried with paper and weighed ( $m_t$ ). After weighing the films, they were replaced in their respective flask. The change in mass was calculated as follows:

$$\text{Change in mass (\%)} = \frac{m_t - m_0}{m_0} \times 100 \quad (1.4)$$

### **I.XV. Tensile Tests**

Tensile stress-strain measurements were carried out for the latex films with a tensile testing machine (Stable Micro Systems Ltd., Godalming, UK) with a constant velocity of 0.42 mm/s. The results reported were the average of 2-3 repeated measurements.

### **I.XVI. Dynamic Mechanical Thermal Analysis (DMTA)**

The thermomechanical behavior of the latex films was investigated by Dynamic Mechanical Analyzer (DMA), using a Triton 2000 DMA from Triton technology. The tension mode was selected and constant heating rate and frequency were set at 4 °C/min and 1 Hz respectively. The range of temperature for all the films was from -40 to 140 °C.

### **I.XVII. Simulations of packing of binary particles**

Packing simulations were performed using the collision-driven packing generation algorithm reported by Skoge *et al.*<sup>1</sup> In all cases, simulations were conducted with at least 2500 particles. In some systems where there was a large difference in the particle diameter simulations with up

to 50000 particles were performed to ensure that the final packed structure was statistically representative.

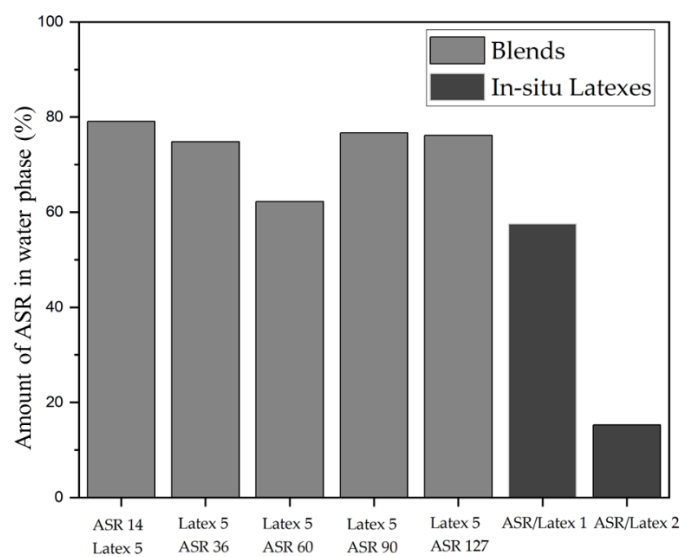
## References

- (1) Skoge, M.; Donev, A.; Stillinger, F. H.; Torquato, S. Packing Hyperspheres in High-Dimensional Euclidean Spaces. *Phys. Rev. E* **2006**, *74* (4), 41127. <https://doi.org/10.1103/PhysRevE.74.041127>.



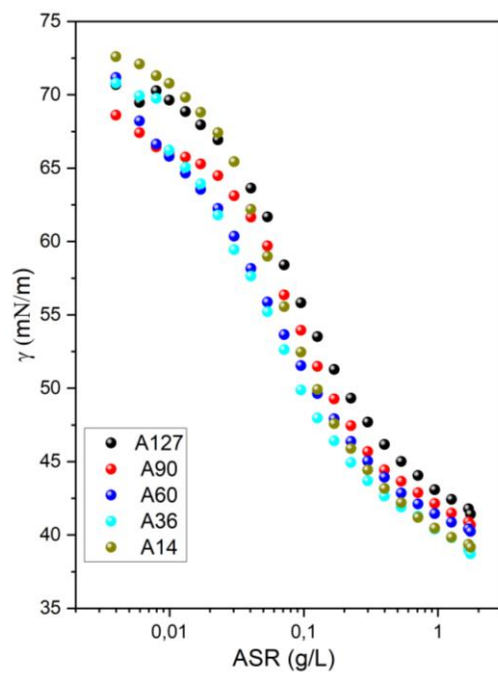
## Appendix II. Supporting Information for Chapter 2

### II.I. Amount of ASR in the water phase



**Figure S2-1.** Weight fraction of ASR in water phase for blends and ASR/Latex systems.

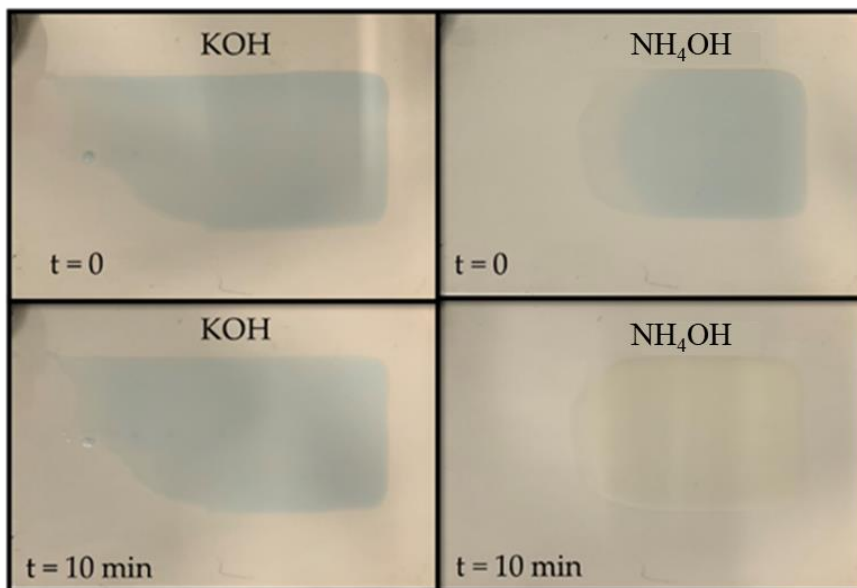
## II.II. Surface tension of ASRs



**Figure S2-2.** Surfaces tension measurements for different ASRs.

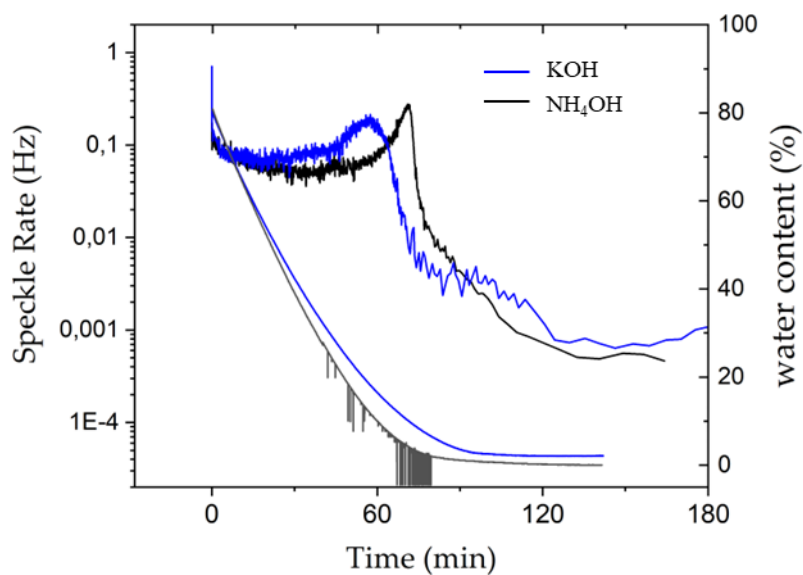


**II.III. Images of the drying process of ASR films using different bases.**



**Figure S2-3.** Drying process of ASR 60 films neutralized with KOH and NH<sub>4</sub>OH in presence of bromothymol blue.

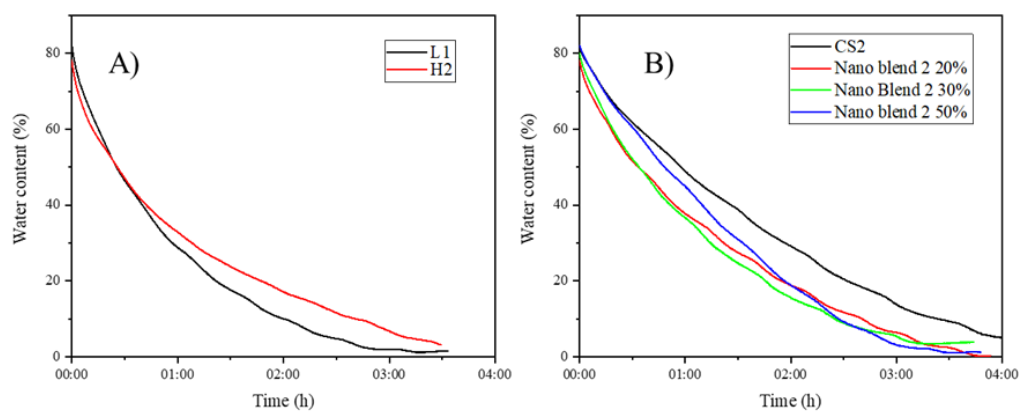
#### II.IV. Drying process of ASR with different bases



**Figure S2-4.** Different phases of the drying process and weight loss observed on the neutralized ASR 60. Continuous lines represent the speckle rate while the water content is given by the dashed lines. It can be observed that in the KOH neutralized ASR the residual water content is significantly higher than for the ammonium hydroxide neutralized ASR.

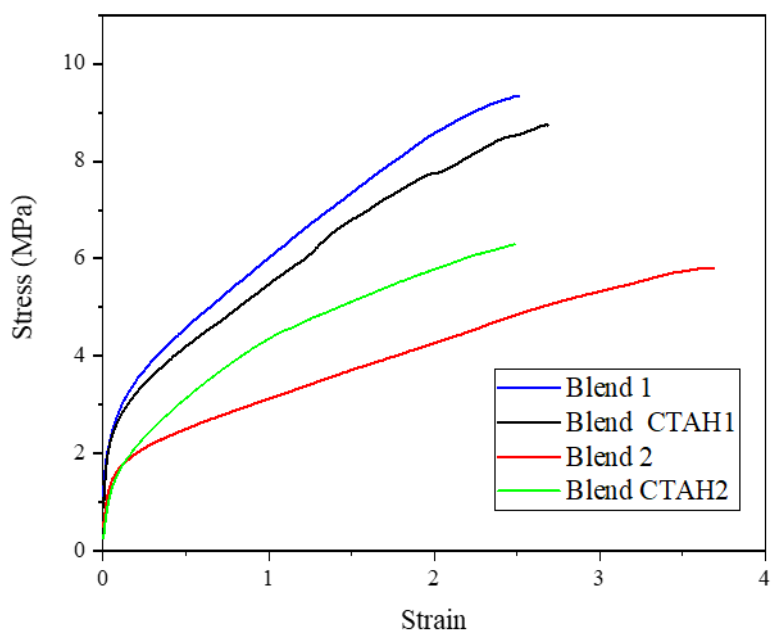
## Appendix III. Supporting Information for Chapter 3

### III.I. Weight loss measurements



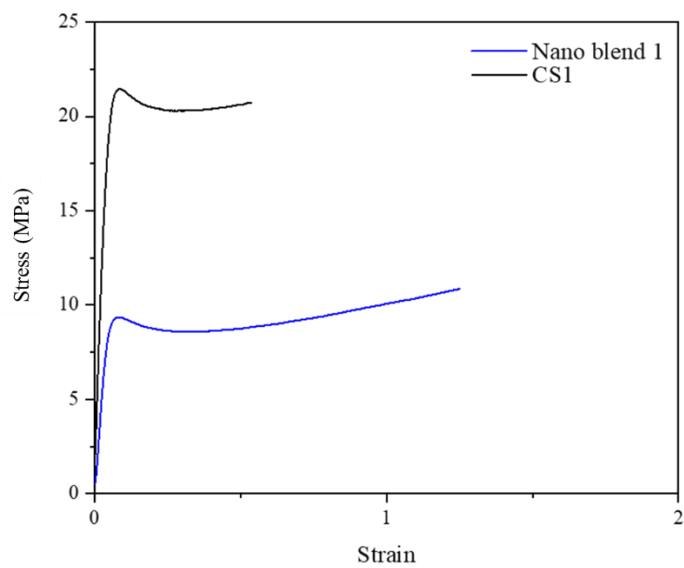
**Figure S3-1.** Weight loss measurements of A) homogeneous latexes L1, H2 and B) heterogeneous systems containing hydroplasticizable polymer (CS2 and Nano blends 2 with varying hydroplasticizable polymer content).

**III.II. Tensile properties of blends containing hydroplasticizable polymer with different molecular weights.**



**Figure S3-2.** Tensile properties of films of Blend 1, Blend 2, Blend CTAH1 and Blend CTAH2.

**III.III. Tensile properties of films made of core/shell particles and Nano Blend 1.**



**Figure S3-3.** Tensile properties of films of CS1 and Nano Blend 1 cast at 60 °C.



## Appendix IV. Supporting Information for Chapter 5

### IV.I. Characteristics of the soft polymers used to prepare the blends

Table S5-1 – Characteristics of the latexes used in latex blends

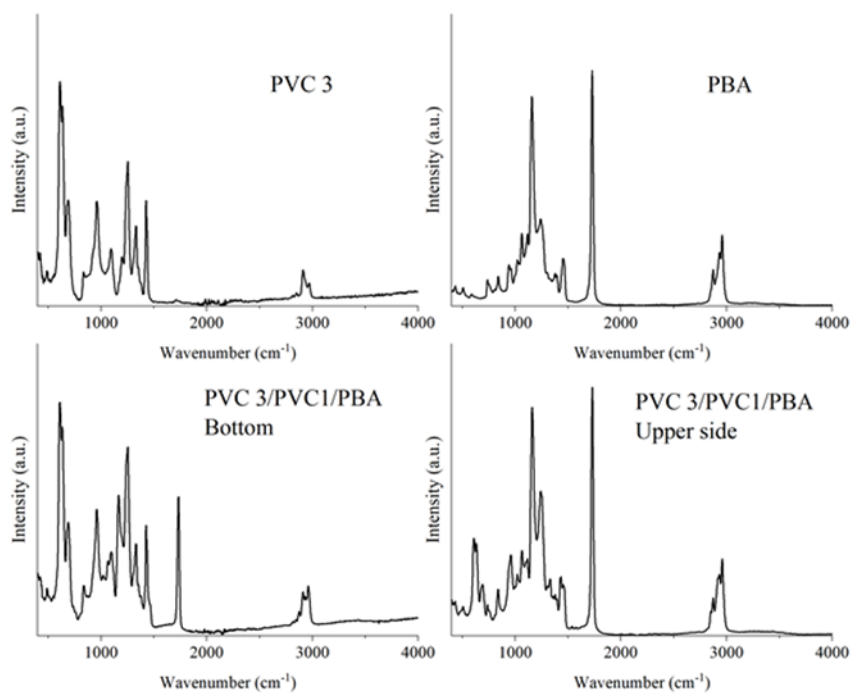
Sample	Particle size (nm)	PDI	M <sub>w</sub> (g/mol)	Đ	T <sub>g</sub> (°C)	MFFT (°C)
PBA	97	0.09	2.0×10 <sup>5</sup>	5.9	-45	<5
P(MMA-co-BA)	89	0.03	1.0 ×10 <sup>5</sup>	2.4	12	8

**IV.II. Phase separation in dried film containing PBA as film forming polymer.**



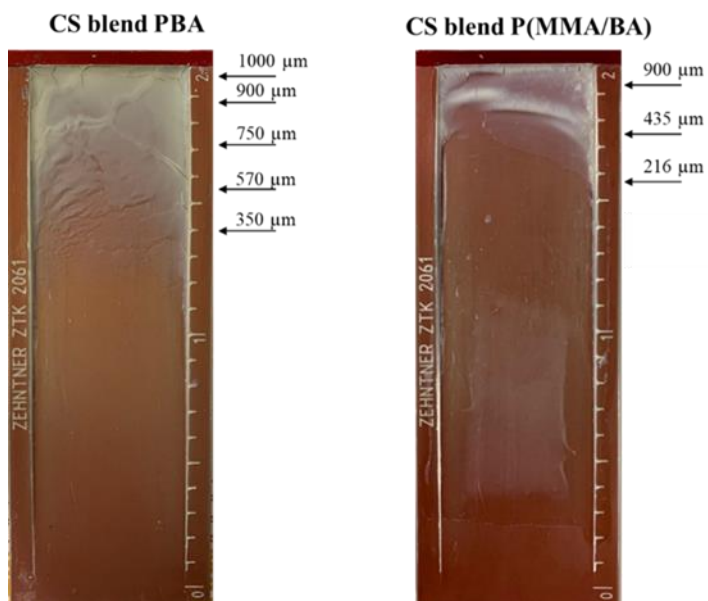
**Figure S5-1.** Dried film of a blend of PVC-1/PBA and PVC-3/PBA with 25 % of smaller particles in the composition after 5 days drying at 22 °C and 55 % humidity.





**Figure S5-2** – FTIR of upper and lower surfaces of blends of PVC-1/PBA and PVC-3/PBA with 25 % of smaller particles in the composition.

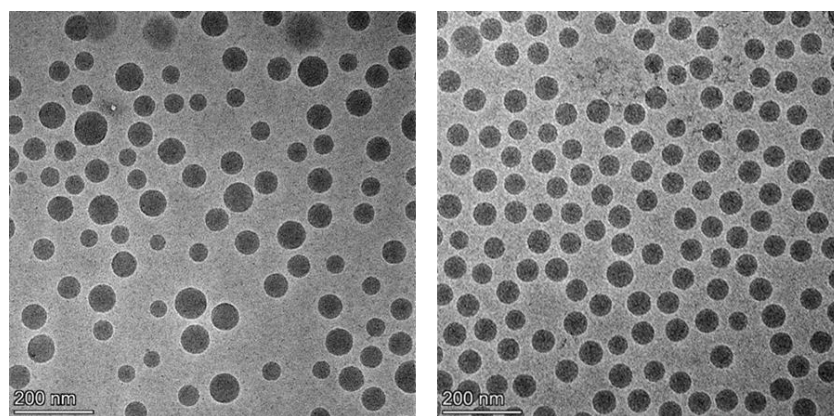
### IV.III. Critical film formation thickness of the Core/shell latex blends



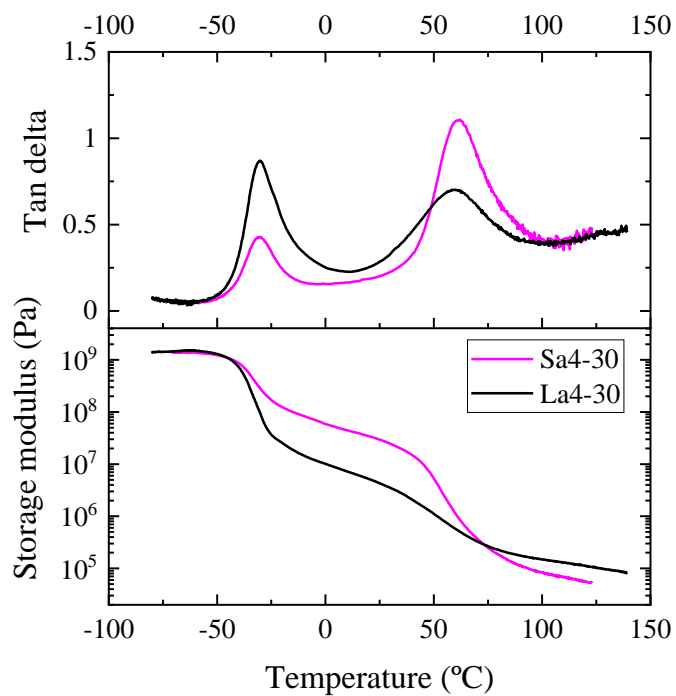
**Figure S5-3.** Critical cracking thickness for CS blend PBA and CS blend P(MMA/BA).

## Appendix V. Supporting Information for Chapter 6

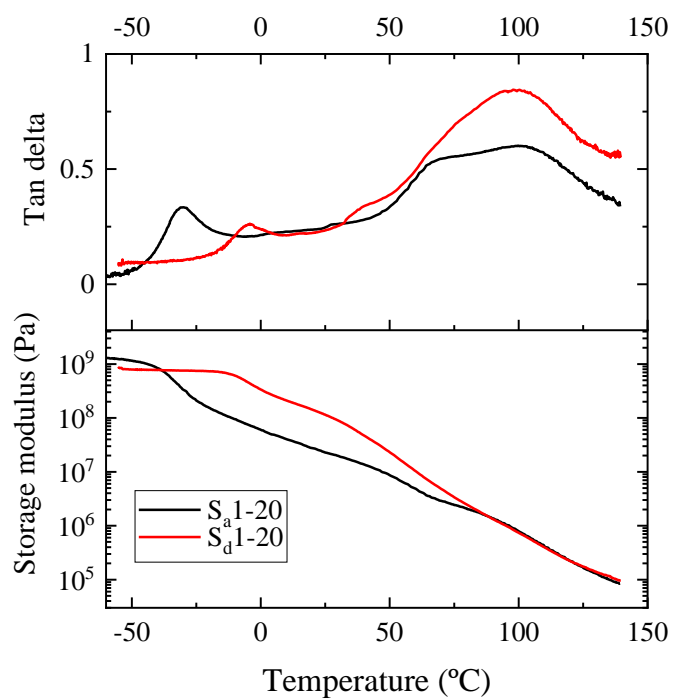
V.I. Images of two-stage latex particles obtained using crosslinked and non-crosslinked cores.



**Figure S6-1.** TEM images of (left) two stage latex particles with a non-cross-linked core (S<sub>b</sub>1-20) and (right) two stage latex particles with a cross-linked core (S<sub>c</sub>1-20)

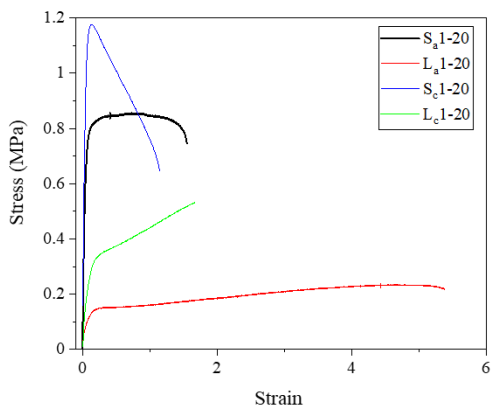
**V.II. Mechanical properties of samples S<sub>a</sub>4-30 and L<sub>a</sub>4-30.****Figure S6-2** – DMTA curves of S<sub>a</sub>4-30 and L<sub>a</sub>4-30

**V.III. Thermomechanical behaviour of the two-stage latex films with different seed composition.**

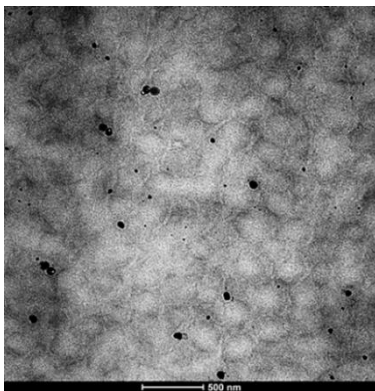


**Figure S6-3** – DMTA curves of S<sub>a</sub>1-20 and S<sub>d</sub>1-20.

**V.IV. Tensile properties and morphology of two-stage latex films with different seed composition.**



**Figure S6-4** – Stress-strain curves of two-stage latexes containing cross-linked ( $S_c1-20$  and  $L_c1-20$ ) and non-cross-linked ( $S_a1-20$  and  $L_a1-20$ ) seeds.



**Figure S6-5** – TEM image of cross-section of film cast from  $S_b1-20$  dried at 22 °C.

## List of acronyms and abbreviations

A	interfacial area
ASR	aAlkali soluble resin
MAA	methacrylic acid
AFM	atomic force microscopy
BA	butyl acrylate
EA	Ethyl acrylate
EHTG	2-Ethylhexyl thioglycolate
cryo-TEM	cryogenic transmission electron microscopy
DWS	diffusive wave spectroscopy
DMTA	dynamic mechanical thermal analysis
Đ	polydispersity index
DLS	dynamic light scattering

List of acronyms and abbreviations

---

DSC	differential scanning calorimetry
GPC	gel permeation chromatography
KOH	potassium hydroxide
KPS	potassium persulfate
M	monomer
PVC	Polyvinyl Chloride
MFFT	minimum film formation temperature
MMA	methyl methacrylate
$M_w$	weight average molecular weight
Pa	Pascal
PBA	poly (butyl acrylate)
PMMA	poly (methyl methacrylate)
PS	polystyrene
PSD	particle size distribution



S	styrene
SC	solids content
SDS	sodium dodecyl sulfate
SEM	scanning electron microscope
T	temperature
TEM	transmission electron microscope
T <sub>g</sub>	glass transition temperature
THF	tetrahydrofuran
VOC	volatile organic compound
wbm	weight based on monomer
wbp	weight bases on polymer
wt	weight
X	conversion
γ	interfacial tension